SUPPLEMENTARY INFORMATION

doi:10.1038/nature26157

Supplementary Tables and Supplementary Video Legends

Supplementary tables

Supplementary Table 1 | Compound libraries screened and the number of identified compounds in a primary screen for *C. elegans* survival

Compound library	Compounds screened	Hits	Hit rate (%)
Asinex 1	12378	65	0.53
Biomol 4	640	42	6.56
Chembridge 3	10560	24	0.23
Chembridge GPCR	250	0	0.00
ChemBridge Ion Channel Core	250	4	1.60
ChemBridge Kinase-Based Core	250	0	0.00
ChemBridge NHRB Core	250	1	0.40
ICBG 16 Fungal	1408	25	1.78
LOPAC 1	1280	0	0.00
MMV 7	704	18	2.56
Microsource 1	1040	70	6.73
MSDiscovery 1	270	0	0.00
NCDDG 8	352	0	0.00
NCDDG 9	704	0	0.00
ChemDiv 4	14677	34	0.23
Eamine 2	26576	40	0.15
Life Chemicals 1	3893	36	0.92
Maybridge 5	3212	27	0.84
Bionet 2	1700	3	0.18
I.F. Lab 2	292	1	0.34
Biomol ICCBL-2012	480	5	1.04
TocriscreenMini Library 2	1120	30	2.68
SUM	**82286**	**425**	**0.52**

Supplementary Table 2 | Minimum inhibitory concentration (μg/ml) of synthetic retinoids against a panel of bacterial strains

Strain	CD437	CD1530	Adar[1]	Van[1]	Dap[1]	Oxa[1]	Gm[1]	Cipro[1]
S. aureus MW2	1	1	2	1	1	64	1	0.25
S. aureus BF1	2	2	4	1	2	>64	1	0.5
S. aureus BF2	1	1	2	1	8	>64	1	1
S. aureus BF3	1	1	2	1	8	32	1	1
S. aureus BF4	2	1	2	0.5	0.5	16	1	0.5
S. aureus BF5	1	1	2	0.5	0.5	>64	1	0.5
S. aureus BF6	1	1	2	0.5	0.5	1	1	0.5
S. aureus BF7	1	1	2	0.5	1	>64	1	0.5
S. aureus BF8	1	1	2	0.5	0.5	>64	1	0.5
S. aureus BF9	1	2	2	0.5	0.5	0.25	1	0.5
S. aureus BF10	1	1	2	0.5	2	>64	1	0.25
S. aureus BF11	1	1	2	1	0.5	>64	1	0.25
S. aureus VRS1	1	1	2	>64	1	>64	64	64
E. faecium E007	2	2	4	1	16	>64	>64	64
E. faecium C68	2	2	4	64	8	>64	>64	>64
E. faecium D14	2	2	4	2	16	>64	32	4
E. faecium D24	1	1	2	1	32	>64	>64	1
E. faecium D25	1	1	4	1	16	>64	32	1
E. faecium D29	1	1	2	2	16	>64	64	0.5
E. faecium WB312	1	1	2	16	16	>64	32	32
E. faecium WC196	2	2	4	64	16	>64	64	1
K. pneumonia WGLW2	>64	>64	>64	>64	>64	>64	1	0.063
A. baumannii ATCC 17978	>64	>64	>64	>64	>64	>64	1	0.25
P. aeruginosa PA14	>64	>64	>64	>64	>64	>64	2	0.063
E. aerogenes ATCC 13048	>64	>64	>64	>64	>64	>64	2	0.031

[1]Adar: adarotene, Van: vancomycin, Dap: daptomycin, Oxa: oxacillin, Gm: gentamicin, Cipro: ciprofloxacin

Supplementary Table 3 | Amino acid changes located in open reading frames after *in vitro* selection with CD437

Culture	Day of passage	Mutated gene	Function	Base change	Amino acid change
SP1	8	MW_RS03385 (*graS*)	Two-component sensor histidine kinase, GraS	851C>T	Ser284Leu[1]
SP1	48	MW_RS11255 (*manA*)	Mannose-6-phosphate isomerase, ManA	182G>A	Trp61Stop codon
SP1	74	MW_RS13405	Hypothetical protein, TetR family regulatory protein	347G>A	Cys116Tyr
SP2	13	MW_RS04750 (*yjbH*)	Hypothetical protein, YjbH	730Cdeletion	Gln244frame shift
SP2	52	MW_RS04415 (*dltB*)	D-alanyl transfer protein	Insertion of TTAATTGCT between 30T and 31T	Insertion of LeuIleAla between Phe10 and Leu11
SP2	59	MW_RS11255 (*manA*)	Mannose-6-phosphate isomerase, ManA	777G>T	Lys259Asn
SP2	65	MW_RS09015	Hypothetical protein, tRNA-binding protein	359A>G	Asp120Gly

[1]Ser284 is located in the C-terminal ATP-binding domain.

Supplementary Table 4 | Antimicrobial susceptibility of *S. aureus* MW2 mutants isolated by serial passage for 100 days

		MIC (μg/ml)				
Mutant "strain"[1]	**Mutated gene**	**CD1530**	**Adarotene**	**Vancomycin**	**Gentamicin**	**Defensin 1**
SP1-1		1	2	1	1	16
SP1-8	*graS*	1.5	3	0.5	0.25	8
SP1-48	*graS*, *manA*	2	4	0.5	0.25	8
SP1-74	*graS*, *manA*, MW2474	2	4	0.5	0.25	8
SP1-100	*graS*, *manA*, MW2474	2	4	0.5	0.25	8
SP2-1		1	2	1	1	16
SP2-13	*yjbH*	1.5	3	1	1	16
SP2-52	*yjbH*, *dltB*	1.5	3	0.5	0.25	8
SP2-59	*yjbH*, *dltB*, *manA*	2	4	0.5	0.25	8
SP2-65	*yjbH*, *dltB*, *manA*, MW1685	2	4	0.5	0.25	8
SP2-100	*yjbH*, *dltB*, *manA*, MW1685	2	4	0.5	0.25	8

[1]The culture from each day during serial passage was named as 'the replicate number – day of passage.' For example, SP1-100 refers to the culture from the first biological replicate on day 100.

Supplementary Table 5 | MIC (µg/ml) of *S. aureus* JE2 *graS*, *manA*, or *yjbH* transposon insertion mutants and corresponding complemented strains

***S. aureus* strain**	**CD437**	**CD1530**	**Adarotene**
JE2 (wild-type)	1.5	1.5	2.5
NE1756 (JE2 *graS*::ΦNΞ)	2	2	4
NE1645 (JE2 *manA*::ΦNΞ)	3	3	4
NE896 (JE2 *yjbH*::ΦNΞ)	2	2	4
[1]JE2 (wild-type)	1	1	2
[1]NE1756/pBK123	1.5	1.5	2.5
[1]NE1756/pBK123 Ω *graS*	1	1	1.5
[1]NE1645/pBK123	1.5	1.5	2.5
[1]NE1645/pBK123 Ω *manA*	1	1	2
[1]NE896/pBK123	1.5	1.5	2.5
[1]NE896/pBK123 Ω *yjbH*	0.75	0.75	2

[1]2.5 µM $CdCl_2$ was added.

Extended Data Table 6 | Characteristic parameters derived from free energy profiles of retinoids penetrating the lipid bilayer[1]

Compound	Transfer Energy (k_BT)	Energy Barrier (k_BT)
CD437	-8.91	1.68
CD1530	-7.83	1.85
Adarotene	-2.59	3.63
Adapalene	3.16	11.22

[1]Lipid bilayer consists of 108 PG, 72 Lys-PG, and 10 DPG lipids

Supplementary Table 7 | Fractional inhibitory concentration index (FICI)[1] against MRSA MW2

	Defensin 1	Gentamicin	Vancomycin	Ciprofloxacin	Rifampicin	Tetracycline
CD437	0.5	0.375	1	0.625	0.625	1
CD1530	1	0.5	1	0.75	0.75	1.062
Adarotene	1	0.5	1.016	0.75	1	0.625

[1]Synergy, FICI≤0.5; no interaction, 0.5<FICI≤4; antagonism, FICI>4

Supplementary Table 8 | Ames test for evaluating genotoxicity of synthetic retinoids

Compound[1] (μg/plate)	Number of revertants			
	Without S9		With S9	
	T1535	T1538	T1535	T1538
NaN_3 (5)	2010±395	N.D.[2]	N.D.[2]	N.D.[2]
4NOP (5)	N.D.[2]	231±22	N.D.[2]	N.D.[2]
2AA (5)	N.D.[2]	N.D.[2]	263±15	2568±108
DMSO	11±1	5±1	6±2	7±3
CD437 (5)	6±2	5±2	6±3	9±3
CD437 (25)	5±2	4±1	8±3	10±2
CD437 (100)	8±2	3±3	8±3	6±1
CD1530 (5)	7±3	3±3	7±3	7±3
CD1530 (25)	7±2	4±2	7±2	10±4
CD1530 (100)	8±4	4±2	8±2	8±2
Adarotene (5)	6±1	6±1	6±2	8±4
Adarotene (25)	7±3	4±3	7±3	8±1
Adarotene (100)	6±2	5±2	7±1	7±3

[1]NaN3: sodium azide, 4NOP: 4-nitro-o-phenylenediame, 2AA: 2-Aminoanthracene.
[2]N.D.: not determined. All values are means ± s.d. of triplicate.

Supplementary Table 9 | Primers used in this study

Primer	5'-3' sequence
[1]graS-F	ACACCTGTGACAGCCATGAA
[1]graS-R	ACAGTCGACGTGACTTGCAG
[1]manA-F (for CD1)	AAAATTATGGGGCGGTCAAC
[1]manA-R (for CD1)	CGATTGCATCGTTTCGTATG
[1]MW2474-F	AAGCATTGTCGAGTAGCTTGC
[1]MW2472-R	CCCAGGCCAGTCAATTTTT
[1]yjbH-F	AAATCGAACAAGCCCCTTCT
[1]yjbH-R	CGAACTGGTTAAATTCGGAAA
[1]dltB-F	TGCCAACGACTGAAGTTACG
[1]dltB-R	TCTGATGTCCACCTAACCATGT
[1]manA-F (for CD2)	ATCATGTTCAACACGGAACG
[1]manA-R (for CD2)	TGAAATCGCCTTCAAAGACA
[1]MW1685-F	CGCATTTTTACAAATTGAACCA
[1]MW1685-R	ATCATACCGCTTGAGGCAAC
[2]graS-CF	CGCTCTAGAGGATATATGGCTCATGAAT
[2]graS-CR	CGCGGATCCCATGTTTAAAATGACAAATTTG
[2]manA-CF	CGCCTGCAGGTGCAACAATGCCATTATT
[2]manA-CR	CGCGGATCCCACTATTACACATAGCTAATC
[2]yjbH-CF	CGCTCTAGAGGTGAATAAACATGGCTGG
[2]yjbH-CR	CGCGGATCCGGTGTACGAGGTCTTTAATTT

[1]Primers used for identifying mutations, [2]Primers used for making complementary strains

Supplementary video legends

Supplementary Videos 1-5 | CD437, CD1530, and adarotene disrupt GUVs. GUVs consisting of DOPC/DOPG (7:3) labeled with 18:1 Liss Rhod PE (0.05%) were treated with 10 μg/ml (10X MIC) CD437 (**Supplementary Video 1**), 10 μg/ml (10X MIC) CD1530 (**Supplementary Video 2**), 20 μg/ml (10X MIC) adarotene (**Supplementary Video 3**), 20 μg/ml adapalene (**Supplementary Video 4)**, or 0.1% DMSO (**Supplementary Video 5**). After adding compounds at t=0 sec, changes in each GUV were recorded using a fluorescent microscope (63x objective, Ex=460 nm, Em=483 nm). Experiments were repeated 3 times with similar results.

Supplementary Videos 6-9 | Molecular dynamics of CD437 (**Supplementary Video 6**), CD1530 (**Supplementary Video 7**), adarotene (**Supplementary Video 8**) and adapalene (**Supplementary Video 9**) interacting with mixed 108PG/72lys PG/10DPG lipid bilayers. In the videos of MD simulations, the retinoids and sodium ions are depicted as large spheres, and phospholipids are represented as chains. The atoms in retinoids, phospholipids and sodium ions are colored as follows: hydrogen, white; oxygen, red; nitrogen, dark blue; carbon, cyan; phosphorus, orange; sodium, lavender. Water molecules are set to be transparent for clarity. The outer blue lines indicate the period boundaries of the simulation boxes. Simulations were repeated 5 times with similar results.

Supplementary videos 10-13 | Molecular dynamics of CD437 (**Supplementary Video 10**), CD1530 (**Supplementary Video 11**), adarotene (**Supplementary Video 12**) and adapalene (**Supplementary Video 13**) interacting with mixed lipid bilayers at a DOPC:DOPG ratio of 7:3. In the videos of MD simulations, the retinoids and sodium ions are depicted as large spheres, and phospholipids are represented as chains. The atoms in retinoids, phospholipids and sodium ions are colored as follows: hydrogen, white; oxygen, red; nitrogen, dark blue; carbon, cyan; phosphorus, orange; sodium, lavender. Water molecules are set to be transparent for clarity.

The outer blue lines indicate the period boundaries of the simulation boxes. Simulations were repeated 5 times with similar results.

Supplementary Videos 14-15 | Molecular dynamics of CD437 carboxylic glucuronide (**Supplementary Data Video 14**) and phenolic hydroxyl glucuronide (**Supplementary Data Video 15**) interacting with mixed lipid bilayers at a DOPC:DOPG ratio of 7:3. In the videos of MD simulations, the CD437-glucuronides and sodium ions are depicted as large spheres, and phospholipids are represented as chains. The atoms in CD437-glucuronides, phospholipids and sodium ions are colored as follows: hydrogen, white; oxygen, red; nitrogen, dark blue; carbon, cyan; phosphorus, orange; sodium, lavender. Water molecules are set to be transparent for clarity. The outer blue lines indicate the period boundaries of the simulation boxes. Simulations were repeated 5 times with similar results.

Supplementary Video 16 | Molecular dynamics of Analog 2 interacting with mixed 108PG/72lys PG/10DPG lipid bilayers. In the videos of MD simulations, Analog 2 and sodium ions are depicted as large spheres, and phospholipids are represented as chains. The atoms in Analog 2, phospholipids and sodium ions are colored as follows: hydrogen, white; oxygen, red; nitrogen, dark blue; carbon, cyan; phosphorus, orange; sodium, lavender. Water molecules are set to be transparent for clarity. The outer blue lines indicate the period boundaries of the simulation boxes. Simulations were repeated 5 times with similar results.

Supplementary Video 17 | Molecular dynamics of Analog 3 interacting with mixed lipid bilayers at a DOPC:DOPG ratio of 7:3. In the videos of MD simulations, Analog 3 and sodium ions are depicted as large spheres, and phospholipids are represented as chains. The atoms in Analog 3, phospholipids and sodium ions are colored as follows: hydrogen, white; oxygen, red; nitrogen, dark blue; carbon, cyan; phosphorus, orange; sodium, lavender. Water molecules are set to be transparent for clarity. The outer blue lines indicate the period boundaries of the simulation boxes. Simulations were repeated 5 times with similar results.

Supplementary Discussion

Identification of retinoid-resistant MRSA mutants

To generate CD437-resistant mutants, we serially passaged two independent cultures of MW2 (SP1 and SP2) for 100 days in sub-MIC levels of CD437 (details in METHODS). MW2 cells were also serially passaged in sub-MIC levels of ciprofloxacin as a control. Serial passage of MW2 in ciprofloxacin generated a mutant that was 256-fold more resistant than the starting culture (MIC from 0.25 to 64 μg/ml), whereas with CD437, we obtained putative mutants that were only 2-fold more resistant (MIC from 1 to 2 μg/ml) than the starting strain in two parallel cultures (SP1 and SP2; Fig. 1e). These putative mutants also exhibited 2-fold increased resistance to CD1530 and adarotene. The slight change in resistance to CD437 was confirmed by re-measuring MICs using three colonies from aliquots of each passage stored at -80°C (Fig. 1f). These results demonstrate that *S. aureus* cannot easily develop resistance to the retinoid compounds.

Next, we determined the correlation between the accumulation of mutations during 100 days of serial passage and decreases in susceptibility to CD437. To identify mutations in the SP1 and SP2 cultures, we compared whole genome sequences of day 100 cultures to day 1 cultures. A total of 36 mutations were identified in the day 100 culture of SP1, including 12 mutations in annotated genes, while 38 mutations were identified in the day 100 cultures of SP2, 10 of which were in annotated genes. Among the mutated genes, a limited number of mutations caused amino acid changes in the corresponding proteins. These mutations were in MW0622 (*graS*), MW2067 (*manA*), and MW2474 in SP1, and in MW0883 (*yjbH*), MW0815 (*dltB*), MW2067 (*manA*), and MW1685 in SP2 (Supplementary Table 3). PCR analysis showed that the mutations in *graS* and *yjbH* in SP1 and SP2 appeared at an early stage of the serial transfer experiment and resulted in a 1.5-fold increase in resistance to CD437 (Fig. 1f). Two independent mutations in *manA* in SP1 and SP2 were correlated with an increase in resistance to 2-fold above the MIC about halfway through the experiment (Fig. 1f). The mutations in *graS*, *yjbH*, and *manA* also resulted in a 1.5-fold increase in resistance to CD1530 and adarotene (Supplementary Table 4). A correlation between mutations in *graS*, *yjbH* and *manA* and increased resistance to

retinoids was also observed in *S. aureus* strain JE2 mutants containing transposon insertion in these 3 genes[1] and their complemented strains (Supplementary Table 5).

GraS is a sensor histidine kinase and constitutes the GraRS (Glycopeptide Resistance Associated) two-component system with its cognate response regulator, GraR[2]. The GraRS system is known to play an important role in resistance to cationic antimicrobial peptides (CAMPs), daptomycin, and vancomycin by increasing the net bacterial surface positive charge, which causes electrostatic repulsion[3-5]. Deletion of *graS* has been shown to increase susceptibility to vancomycin and cationic antimicrobial peptides[3,4], which is consistent with our result that SP1 exhibited increased susceptibility to vancomycin and defensin 1 after the *graS* mutation appeared on day 8 (Supplementary Table 4).

ManA is a mannose phosphate isomerase that belongs to the GraRS regulon and plays an important role in cell wall construction[6,7]. Deletion of *manA* leads to decreased cell wall integrity[6,7]. It is noteworthy that *manA*, MW2474 and *dltB* are part of the GraRS regulon, which, as stated above, is known to play an important role in resistance to cationic antimicrobial peptides (CAMPs)[3,4,7], although mutations in MW2474 and *dltB* alone did not appear to result in measurable increases in resistance to CD437 (Fig. 1f).

YjbH is an adaptor protein that enhances the degradation of the stress response transcriptional regulator, Spx[8]. Inactivation of YjbH results in increased peptidoglycan cross-linking and moderately increased resistance to beta-lactam antibiotics[9]. The common feature of GraS, ManA, and YjbH is that they all affect cell membrane physiology, suggesting that the retinoids target the bacterial membranes.

Membrane activity of CD437 glucuronide metabolites

Retinoids can be metabolized by glucuroconjugation in the presence of a glucuronyl transferases[10]. For example, adarotene was found to undergo glucuronidation on its carboxylic group or a phenolic hydroxyl group, which is responsible for its relatively rapid clearance[10,11]. To test if CD437 glucuronides still have membrane-activity, we conducted all-atom molecular dynamics (MD) simulations of the interactions between two CD437 glucuronides, such as a carboxylic-glucuronide and a phenolic hydroxyl-glucuronide and a 7DOPC/3DOPG lipid bilayer (Extended Data Fig. 2a). The simulation results revealed that both the carboxylic-glucuronide and

the phenolic hydroxyl-glucuronide of CD437 penetrated into lipid bilayers, exhibiting a similar penetration mechanism as CD437 (Extended Data Fig. 2a, Supplementary Videos 14, 15). The two CD437 glucuronides attach to the surface of lipid bilayers by both hydroxyl groups of a conjugated glucuronic moiety and the carboxylic acid or phenolic hydroxyl groups of CD437 binding to the hydrophilic lipid heads. The CD437 glucuronides then penetrate into the lipid bilayers by CD437's backbone providing hydrophobic interaction with lipid tail groups (Extended Data Fig. 2a, Supplementary Videos 14, 15). The energy calculations (Extended Data Fig. 2c) also showed that the membrane penetrations of both the carboxylic-glucuronide and the phenolic hydroxyl-glucuronide are energetically favorable, associated with transfer energies of -3.73 k_BT and -2.02 k_BT, and energy barriers of 5.01 k_BT and 7.40 k_BT, respectively. Since we have shown above that the membrane-activity of retinoids is correlated with their antibiotic activity (Fig. 2, Extended Data Fig. 1a), it is most likely that the two CD437-glucuroconjugated metabolites would retain their antimicrobial activity.

Next, we estimated the antimicrobial activity of the two CD437-glucuronided metabolites compared to CD437 based on MD simulations. First, in a comparison between the two CD437 glucuronides, it appears that the carboxylic-glucuronide may have higher antimicrobial activity than the hydroxyl-glucuronide because the carboxylic-glucuronide exhibits lower transfer energies and energy barriers than the phenolic hydroxyl-glucuronide (Extended Data Fig. 2c). Indeed, the carboxylic-glucuronide has a linear amphipathic structure, with the glucuronic moiety functioning as a hydrophilic head and the CD437 backbone functioning as a hydrophobic tail (Extended Data Fig. 2a, Supplementary Video 14). In contrast, the phenolic hydroxyl-glucuronide does not have a linear amphipathic structure due to the closely-located glucuronic moiety and the adamantane moiety (Extended Data Fig. 2a). Although it binds to the lipid heads by the carboxylic and glucuronic moieties, the highly polar glucuronic moiety prevents the penetration of the lipophilic adamantane moiety deep into the hydrophobic core of the membranes (Extended Data Fig. 2a, Supplementary Video 15). In any case, the two CD437-glucuronide metabolites may have lower antimicrobial activity than CD437 because of their higher transfer energies and energy barriers than those of CD437 (-8.92 k_BT and 1.42 k_BT, respectively in Extended Data Fig. 2c).

The mode of action of CD437 and CD1530 is different from ionophores

Although CD437 and CD1530 act synergistically with gentamicin, the mechanism of this synergism is different from the one between ionophores and gentamicin. Ionophores dissipate either membrane potential ($\Delta\Psi$) or the transmembrane proton gradient (ΔpH), two key elements of the proton motive force (PMF)[12]. Bacteria normally maintain a constant level of proton motive force. Thus, if $\Delta\Psi$ is dissipated, ΔpH increases, and *vice versa*. The uptake of gentamicin is facilitated by $\Delta\Psi$[13]. Thus, ionophores such as nigericin that dissipate ΔpH, which leads to an increase in $\Delta\Psi$, facilitate uptake of gentamicin. In contrast to CD437 and CD1530, however, dissipation of PMF by an ionophore does not disrupt the physical integrity of the membranes or cause bactericidal activity[12,14,15]. Besides, the proton ionophore carbonyl cyanide m-chlorophenyl hydrazine (CCCP) combined with gentamicin was found to have no effect on persister viability[16]. Consistent with these observations, nigericin had an MIC of 0.125 μg/ml and exhibited synergism with aminoglycosides against MRSA MW2 (Extended Data Fig. 5a). However, nigericin as well as two additional ionophores (valinomycin and monensin), did not induce SYTOX Green membrane permeabilization, or kill MRSA MW2 persisters (Extended Data Figs. 5b,c). In addition, neither 10X MIC of nigerician nor 10X MIC of monensin combined with 10X MIC of gentamicin killed MRSA persisters (Extended Data Figs. 5d,e). In contrast to gentamicin, the uptake of tetracycline is driven by ΔpH[17]. Therefore, ionophores such as nigericin exhibit antagonism with tetracycline[12]. However, CD437 and CD1530 did not show antagonism with tetracycline (CD437's FICI: 1, CD1530's FICI: 1.062 in Supplementary Table 7). These results suggest that dissipation of PMF *per se* does not lead to the killing of MRSA persisters and that the ionophores such as nigerician, on the one hand, and the retinoids CD437 and CD1530 studied here, on the other hand, have different modes of action.

Structure-activity relationship (SAR) 1: Effects of branch groups

We synthesized 16 analogs of CD437 to further explore the structure-activity relationships (SAR) (Extended Data Fig. 7a) with respect to antimicrobial activity, membrane permeability, and toxicity (Fig. 4, Extended Data Figs. 7-9). Our SAR design sought to further refine our bioactivity model by examining three key structural features of CD437: 1) the necessity of the carboxylic acid, 2) the location and number of phenols, and 3) the

importance of the adamantane moiety. Generally, we found that the replacement of the carboxylic acid abolished activity except when replaced by the corresponding benzylic alcohol (Analog 2, Fig. 4, Extended Data Fig. 7). As described in the main text, Analog 2, having a less polar primary alcohol substituted for a carboxylic acid, shows a similar level of anti-persister activity as CD437 but exhibits significantly reduced hemolytic activity, cytotoxicity, and anticancer activity (Fig. 4, Extended Data Fig. 7). Consistent with the structure/activity of adapalene, the replacement of the phenol group of Analog 2, which has a methoxy group (Analog 6 in Extended Data Fig. 7a), eliminated both antimicrobial activity and membrane permeability (Extended Data Fig. 7b). These results support the conclusion that two polar branch groups, for example a carboxylic group and a hydroxyl group, which contribute to persistent membrane attachment necessary for subsequent membrane penetration of the retinoids, play important roles in antimicrobial activity and provide evidence that retinoid toxicity can be lowered by structural modifications.

We next examined the *para*-substituted phenol of CD437. Analog 10, the *ortho*-phenol derivative, was >30-fold less active that the parent compound (Extended Data Fig. 7), indicating that the hydroxyl group location in close proximity to the bulky hydrophobic adamantane is important to facilitate penetration of the retinoid into lipid bilayers.

Finally, Analog 9, which has a benzyl group substituted for the adamantane group, has a 2-fold higher MIC (2 μg/ml) against growing MRSA MW2 cells (Extended Data Fig. 7), as well as against MRSA persisters (16 μg/ml; Extended Data Fig. 8c). Importantly, Analog 9 demonstrated similar hemolytic activity and hepatotoxicity as CD437 (Extended Data Fig. 8a), indicating that the substitution of a planar benzyl group does not reduce toxicity. These findings indicate that the bulky hydrophobic nature of the adamantane moiety in CD437 is advantageous for antimicrobial activity. Taken together, the SAR studies support the putative mode of action of synthetic retinoids described above and demonstrate that the antimicrobial activity and toxicity of synthetic retinoids can be modulated by the polarity of the branch groups.

SAR 2: Effects of negative charges

We substituted the carboxylic acid of CD437 for an amide (Analog 3 in Extended Data Fig. 7a). Like carboxylic acids, amides form hydrogen bonds. However, the nitrogen in the amide is known to have a higher negative charge than the carboxylic acid's oxygen[18-23] because the nitrogen in the primary resonance form of the amide attracts shared electrons from two N-H bonds[24,25] and is consistent with our calculations of partial atomic charges (Extended Data Fig. 9a). Analog 3 neither exhibited antimicrobial activity nor membrane permeability (Extended Data Fig. 7b), indicating that an increase in negative charge causes adverse effects on the antimicrobial activity of the retinoids. To further explore why Analog 3 does not exhibit antimicrobial activity, we conducted MD simulations of Analog 3 with lipid bilayers consisting of 7DOPC/3DOPG. As mentioned in the main text, the 7DOPC/3DOPG composition has been widely used to mimic anionic charged bacterial membranes and to elucidate the mechanism of action of membrane-active antimicrobials, including daptomycin in *S. aureus*[26-29]. Consistent with these *in vitro* results, MD simulation revealed that Analog 3 could not penetrate, and instead was repelled away from the membrane due to electrostatic repulsion (Extended Data Fig. 9b, Supplementary Video. 17), with a high energy barrier and an unfavorable transfer energy (Extended Data Fig. 9c). To further explore effects of negative charges on antimicrobial activity, we simulated the interaction between CD437 and lipid bilayers with an increasing proportion of negatively charged DOPG lipids. We found that a higher proportion of negative lipids leads to a higher energy barrier for CD437 penetration into the lipid bilayer, due to electrostatic repulsion between the carboxyl group of CD437 and the negatively-charged DOPG head groups (Extended Data Fig. 9d). Interestingly, this simulation suggests that resistance to retinoids is opposite to the resistance mechanism for cationic antimicrobials. That is, an increase in the net positive surface charge repels cationic antimicrobials[3,4], but would attract retinoids due to electrostatic interactions. Consistent with this simulation, we found that all 3 retinoids showed excellent antimicrobial activity against vancomycin- or daptomycin-resistant *S. aureus* or *E. faecium* strains (Supplementary Table 2). Furthermore, the mutation in *graS*, known to cause an increase of net negative charge of the *S. aureus* envelope[4] resulted in a 1.5-fold increase in resistance to CD437 (Supplementary Tables 4, 5).

SAR 3: Effect of additional hydroxyl groups

As shown in Extended Data Fig. 7, Analog 11, which has an additional hydroxyl group, showed a 4-fold decrease in antimicrobial activity (MIC 4 μg/ml vs. 1 μg/ml for CD437). Further, the MIC of Analog 14, which has two additional hydroxyl groups, was 16 μg/ml, which is another 4-fold decrease in antimicrobial activity. These data clearly demonstrate a trend where additional hydroxyl groups decrease antimicrobial activity. This trend was also observed in Analog 9, which has a benzyl group substituted for an adamantane, Analog 12, has one more hydroxyl group than Analog 9, and Analog 15, which has two more hydroxyl groups than Analog 9 (Extended Data Fig. 7). The MD simulations using the 7DOPC/3DOPG lipid bilayers showed that the attachment energies of Analogs 11 and 14 are -5.29 k_BT, and -6.82 k_BT, respectively, which are better than the -3.61 k_BT of CD437 (Extended Data Fig. 9e). However, Analogs 11 and 14 have higher transfer energies of -2.79 k_BT and -1.58 k_BT, respectively, than the -8.92 k_BT of CD437 (Extended Data Fig. 9e), and their energy barriers are also higher (3.36 k_BT for Analog 11, and 4.32 k_BT for Analog 14 vs. 1.42 k_BT for CD437 in Extended Data Fig. 9e). These results demonstrate that the addition of hydroxyl groups on CD437 can provide stronger binding to lipid head groups, but the increased hydrophilicity prevents penetration deep into hydrophobic core of membranes, which may be why additional hydroxyl groups decreases antimicrobial activity. Although Analog 13, which has an additional hydroxyl group on Analog 10, showed an 8-fold increase in antimicrobial activity (4 μg/ml for Analog 13 vs. 32 μg/ml for Analog 10), the attachment of one more hydroxyl group on Analog 13 led to a decrease in antimicrobial activity (8 μg/ml for Analog 16 vs. 4 μg/ml for Analog 13 in Extended Data Fig. 7).

References

1. Fey, P. D. *et al.* A genetic resource for rapid and comprehensive phenotype screening of nonessential *Staphylococcus aureus* genes. *MBio* **4,** e00537–12–e00537–12 (2013).
2. Cui, L., Lian, J.-Q., Neoh, H.-M., Reyes, E. & Hiramatsu, K. DNA microarray-based identification of genes associated with glycopeptide resistance in *Staphylococcus aureus*. *Antimicrob. Agents Chemother.* **49,** 3404–3413 (2005).
3. Yang, S.-J. *et al.* The *Staphylococcus aureus* two-component regulatory system, GraRS, senses and confers resistance to selected cationic antimicrobial peptides. *Infect. Immun.* **80,** 74–81 (2012).
4. Meehl, M., Herbert, S., Götz, F. & Cheung, A. Interaction of the GraRS two-component system with the VraFG ABC transporter to support vancomycin-intermediate resistance in *Staphylococcus aureus*. *Antimicrob. Agents Chemother.* **51,** 2679–2689 (2007).
5. Neoh, H.-M. *et al.* Mutated response regulator *graR* is responsible for phenotypic conversion of *Staphylococcus aureus* from heterogeneous vancomycin-intermediate resistance to vancomycin-intermediate resistance. *Antimicrob. Agents Chemother.* **52,** 45–53 (2008).

6. Elbaz, M. & Ben-Yehuda, S. The metabolic enzyme ManA reveals a link between cell wall integrity and chromosome morphology. *PLoS Genet.* **6,** e1001119 (2010).
7. Falord, M., Mäder, U., Hiron, A., Débarbouillé, M. & Msadek, T. Investigation of the *Staphylococcus aureus* GraSR regulon reveals novel links to virulence, stress response and cell wall signal transduction pathways. *PLoS ONE* **6,** e21323 (2011).
8. Engman, J., Rogstam, A., Frees, D., Ingmer, H. & Wachenfeldt, von, C. The YjbH adaptor protein enhances proteolysis of the transcriptional regulator Spx in *Staphylococcus aureus*. *J. Bacteriol.* **194,** 1186–1194 (2012).
9. Göhring, N. *et al.* New role of the disulfide stress effector YjbH in β-lactam susceptibility of *Staphylococcus aureus*. *Antimicrob. Agents Chemother.* **55,** 5452–5458 (2011).
10. Sala, F. *et al.* Development and validation of a liquid chromatography-tandem mass spectrometry method for the determination of ST1926, a novel oral antitumor agent, adamantyl retinoid derivative, in plasma of patients in a Phase I study. *J. Chromatogr. B* **877,** 3118–3126 (2009).
11. Basma, H. *et al.* The synthetic retinoid ST1926 as a novel therapeutic agent in rhabdomyosarcoma. *Int. J. Cancer* **138,** 1528–1537 (2016).
12. Farha, M. A., Verschoor, C. P., Bowdish, D. & Brown, E. D. Collapsing the proton motive force to identify synergistic combinations against *Staphylococcus aureus*. *Chem. Biol.* **20,** 1168–1178 (2013).
13. Taber, H. W., Mueller, J. P., Miller, P. F. & Arrow, A. S. Bacterial uptake of aminoglycoside antibiotics. *Microbiol. Rev.* **51,** 439–457 (1987).
14. Nagaraja, T. G. & Taylor, M. B. Susceptibility and resistance of ruminal bacteria to antimicrobial feed additives. *Appl. Environ. Microbiol.* **53,** 1620–1625 (1987).
15. Hurdle, J. G., O'Neill, A. J., Chopra, I. & Lee, R. E. Targeting bacterial membrane function: an underexploited mechanism for treating persistent infections. *Nat. Rev. Microbiol.* **9,** 62–75 (2011).
16. Allison, K. R., Brynildsen, M. P. & Collins, J. J. Metabolite-enabled eradication of bacterial persisters by aminoglycosides. *Nature* **473,** 216–220 (2011).
17. Yamaguchi, A., Ohmori, H., Kaneko-Ohdera, M., Nomura, T. & Sawai, T. Delta pH-dependent accumulation of tetracycline in *Escherichia coli*. *Antimicrob. Agents Chemother.* **35,** 53–56 (1991).
18. la Cour Jansen, T., Dijkstra, A. G., Watson, T. M., Hirst, J. D. & Knoester, J. Modeling the amide I bands of small peptides. *J Chem Phys* **125,** 044312 (2006).
19. Cieplak, P., Caldwell, J. & Kollman, P. Molecular mechanical models for organic and biological systems going beyond the atom centered two body additive approximation: aqueous solution free energies of methanol and N-methyl acetamide, nucleic acid base, and amide hydrogen bonding and chloroform/water partition coefficients of the nucleic acid bases. *J Comput Chem* **22,** 1048–1057 (2001).
20. Rizzo, R. C. & Jorgensen, W. L. OPLS all-atom model for amines: resolution of the amine hydration problem. *J. Am. Chem. Soc.* **121,** 4827–4836 (1999).
21. Oostenbrink, C., Villa, A., Mark, A. E. & van Gunsteren, W. F. A biomolecular force field based on the free enthalpy of hydration and solvation: The GROMOS force-field parameter sets 53A5 and 53A6. *J Comput Chem* **25,** 1656–1676 (2004).
22. Wang, J., Wolf, R. M., Caldwell, J. W., Kollman, P. A. & Case, D. A. Development and testing of a general amber force field. *J Comput Chem* **25,** 1157–1174 (2004).
23. Vanommeslaeghe, K. *et al.* CHARMM general force field: A force field for drug-like molecules compatible with the CHARMM all-atom additive biological force fields. *J Comput Chem* **31,** 671–690 (2010).
24. Kemnitz, C. R. & Loewen, M. J. 'Amide Resonance' correlates with a breadth of C−N rotation barriers. *J Am Chem Soc* **129,** 2521–2528 (2007).
25. Milner-White, E. J. The partial charge of the nitrogen atom in peptide bonds. *Protein Sci.* **6,** 2477–2482 (1997).
26. Lee, M.-T., Sun, T.-L., Hung, W.-C. & Huang, H. W. Process of inducing pores in membranes by melittin. *Proc. Natl. Acad. Sci. U. S. A.* **110,** 14243–14248 (2013).
27. Ganewatta, M. S. *et al.* Bio-inspired resin acid-derived materials as anti-bacterial resistance agents with

unexpected activities. *Chem Sci* **5,** 2011–2016 (2014).
28. Chen, Y.-F., Sun, T.-L., Sun, Y. & Huang, H. W. Interaction of daptomycin with lipid bilayers: a lipid extracting effect. *Biochemistry* **53,** 5384–5392 (2014).
29. Joshi, S., Dewangan, R. P., Yar, M. S., Rawat, D. S. & Pasha, S. N-terminal aromatic tag induced self assembly of tryptophan–arginine rich ultra short sequences and their potent antibacterial activity. *RSC Advances* **5,** 68610–68620 (2015).

Methods

Bacterial strains, growth conditions and persister isolation. Methicillin-resistant *S. aureus* (MRSA) strain MW2 BAA-1707[1], the VanA-type vancomycin-resistant *S. aureus* strain VRS1[2], 11 clinical *S. aureus* isolates[3], 8 clinical *Enterococcus faecium* isolates[4,5] (including VanB-type VRE isolates, C68[6,7] and WB312[8], and a VanA-type VRE isolate WC196[8]), *Klebsiella pneumoniae* WGLW2 (BEI Resources, Manassas, VA, USA), *Acinetobacter baumannii* ATCC 17978[9], *Pseudomonas aeruginosa* PA14[10], and *Enterobacter aerogenes* ATCC 13048 were used to test antimicrobial activity (Supplementary Table 2). *S. aureus* and *E. faecium* strains were grown in tryptic soy broth (TSB) (BD, Franklin Lakes, NJ, USA) or brain-heart infusion (BHI) broth (BD, Franklin Lakes, NJ, USA), respectively at 37°C. *K. pneumoniae*, *A. baumannii*, *P. aeruginosa*, and *E. aerogenes* were grown in Luria Bertani (LB) broth (BD, Franklin Lakes, NJ, USA).

Antimicrobial agents and chemicals. Vancomycin, oxacillin, gentamicin, ciprofloxacin, rifampicin, tetracycline, and adapalene were purchased from Sigma-Aldrich (St Louis, MO, USA). CD437, CD1530, linezolid, and daptomycin were purchased from R&D Systems (Minneapolis, MN, USA), and adarotene was purchased from MedChem Express (Monmouth Junction, NJ, USA). 10 mg/ml stocks of all compounds were made in DMSO or ddH_2O. For assays with daptomycin, media or buffer were supplemented with 50 μg/ml $CaCl_2$.

High-throughput *C. elegans*-MRSA liquid infection assay for compound screening. The *C. elegans*-MRSA liquid infection assay was performed as described previously[11]. Briefly, sterile and immune-compromised *C. elegans glp-4(bn2);sek-1(km4)* animals were maintained at 15°C on 10 cm slow kill (SK) agar plates seeded with *Escherichia coli* HB101[12]. The *glp-4(bn2)* mutation causes *C. elegans* to lose its capacity to produce progeny at 25°C[13], and the *sek-1(km4)* mutation increases the sensitivity of *C. elegans* to infection, which reduces the assay time[14]. Eggs isolated from gravid adults by hypochlorite isolation were resuspended in M9 buffer and incubated with gentle rocking at 15°C for 48 h. Approximately 4,500 L1 hatchlings were placed on each 10 cm SK plate seeded with HB101 for 52 h at 25°C until the animals grew into sterile young adults. *S. aureus* MW2 was statically grown in TSB at 37°C for 24 h, and then was adjusted to OD_{600nm} = 0.08 with 20%

TSB diluted into M9 buffer. Black, clear-bottom 384-well plates (Corning no. 3712, Corning, NY, USA) were used for the screening assay. 100 nl of small molecules dissolved in DMSO were pinned into the 384-well plates including 19.9 µl M9 buffer by the Institute of Chemistry and Cell Biology (ICCB) at Harvard Medical School. Vancomycin and DMSO were added into at least one column of each 384-well plate as positive and negative controls, respectively. 15 young adult worms were transferred into the 384-well plates containing the compounds by a COPAS large particle sorter (Union Biometrica, MA, USA), and then 35 µl of the diluted *S. aureus* MW2 culture (OD_{600nm} = 0.08) was added to each well of the 384-well plates. The final volume in each well was 70 µl and consisted of 70% M9 buffer, 19% sheath solution (Union Biometrica Part no. 300-5101-00), 10% TSB, and 1% DMSO. The assay plates were sealed with a gas-permeable membrane (Breathe-Easy, Diversified Biotech, Dedham, MA, USA) and were incubated at 25°C with 80% to 85% humidity for 5 days. Afterwards, the bacteria and other debris were removed from the worms by washing with M9 buffer using a microplate washer (BioTek ELx405, BioTek, Winooski, VT, USA). After leaving 10 µl M9 buffer including worms in each well, the assay plates were filled with 60 µl of 0.9 µM SYTOX Orange (Molecular Probes, Waltham, MA, USA) in M9 buffer. The assay plates were incubated at 25°C with 80% to 85% humidity overnight. Transmitted light and TRITC (535 nm excitation, 610 nm emission) fluorescent images of *C. elegans* in each well were obtained using an Image Xpress Micro automated microscope (Molecular Devices, CA, USA). To score worm survivability, the obtained worm images were analyzed by CellProfiler analysis software[15,16]. Hits were identified by calculating a Z score: $Z=(x-\mu)/\sigma$, where x is the survivability score of each well, μ is the mean of the survivability scores from the all wells, and σ is the standard deviation of the survivability scores from all wells. Hits were defined with $Z>3\sigma$.

In the primary screen, 82,286 small molecules and natural product extracts from multiple compound collections were screened in duplicate, and 425 compounds were identified as 'hits' (Supplementary Table 1). Among the primary hits, the top 200 compounds with the highest z scores were retested in a secondary screen. The anti-infective activity of all 200 compounds was confirmed by retesting them in duplicate in the *C. elegans*-MRSA assay. Because some of the 200 compounds were duplicates, a total of 185 unique compounds were identified as potential anti-infective agents.

Minimal inhibitory concentration (MIC) assay. The MICs of antibiotics were determined by the standard micro-dilution method recommended by the Clinical and Laboratory Standards Institute[17]. The assay was conducted in triplicate.

Killing kinetics assay. An overnight culture of *S. aureus* MW2 was diluted 1:10,000 in 25ml fresh TSB in a 250 ml flask. In order to obtain exponential-phase cells, the diluted cell suspension was incubated at 37°C, with shaking at 225 rpm for 4 h until the OD_{600nm} was 0.4 (~2×10^7 CFU/ml). 1 ml of the exponential phase cell culture was added to the wells of a 96-well assay block (Corning Costar 3960, Corning, NY, USA) containing 1 ml of pre-warmed TSB with twice the desired concentrations of compounds. The assay block was sealed with a gas-permeable Breathe-Easy membrane and incubated at 37°C shaking at 225 rpm. At specific times, 400 µl samples were removed and washed once with PBS to remove the antibiotic. The samples were serially diluted 10^5 fold with PBS and spot-plated onto TSA plates. After incubating the plates overnight (~18h) at 37°C, the colonies were counted to enumerate the number of cells. These experiments were conducted in triplicate. To determine bacterial lysis, 5 ml of exponential-phase MW2 culture (OD_{600nm} ~0.4) was treated with 10X MIC of CD437, CD1530, or benzalkonium chloride (BAC) for 4 h. Anti-infective detergent BAC was used as a positive control to cause bacterial lysis. Every hour, 1 ml of each sample was added to an optical cuvette with a 1 cm path length. OD_{600nm} was measured using an Eppendorf BioPhotometer plus (Eppendorf, Hamburg, Germany). The experiments were conducted in triplicate.

Persister killing assay. As has been previously demonstrated, stationary-phase cells of *S. aureus* can be used to model persister cells[18-21], and we have shown previously that MW2 and the 11 clinical *S. aureus* isolates (BF1 – BF11) become persisters that when grown to stationary phase are tolerant to conventional antibiotics such as gentamicin, ciprofloxacin and vancomycin[3,22]. Persistency of stationary-phase *S. aureus* VRS1 was evaluated by treating with 100X MIC daptomycin and 100X MIC linezolid, because the strain is resistant to vancomycin, gentamicin, ciprofloxacin, and rifampicin. We prepared persister cells of the 13 *S. aureus* strains by growing cultures overnight to stationary phase at 37°C at 225 rpm. The overnight cultures were washed three times with PBS and diluted to ~5×10^7 CFU/ml with the same buffer. 2 ml of the persister suspension containing

appropriate concentrations of antibiotics was added to the wells of a 96-well assay block (Corning Costar 3960) and incubated at 37°C, with shaking at 225 rpm. At specific times, 400 µl samples were removed and washed once with PBS to remove the antibiotic. The samples were serially diluted 10^5 fold with PBS and spot-plated onto TSA plates. After incubating the plates overnight (~18h) at 37°C, the colonies were counted to enumerate the number of cells. These experiments were conducted in triplicate.

Biofilm persister killing assay. An overnight culture of *S. aureus* MW2 was diluted 1:200 with TSB supplemented with 0.2% glucose and 3% NaCl[23]. A 13 mm diameter Millipore mixed cellulose ester membrane (GSWP01300, EMD Millipore, Billerica, MA, USA) was placed at the bottom of each well of a 12-well plate (Falcon 353043, Corning, NY, USA). 1 mL of the diluted culture was added to each well and incubated statically at 37°C for 24 h. The membranes were washed 3-times with PBS and transferred to a fresh 12-well plate. 1 mL of PBS containing the desired concentration of antibiotics or the synthetic retinoids was added to each well, and then the plate was incubated statically at 37°C for 24 h. The membranes were washed 3 times with PBS, placed in 2-ml microcentrifuge tubes containing 1 mL PBS, and sonicated in an ultrasonic bath (Fisher Scientific FS 30) for 10 min. The sonicated samples were serially diluted and spot-plated on TSA plates. After incubating the plates overnight (~18h) at 37°C, the colonies were counted to enumerate the number of cells. The experiment was conducted in triplicate.

Resistance selection. To attempt to select retinoid-resistant mutants, ~10^{10} CFU of an *S. aureus* MW2 culture were first plated onto TSA plates containing 2.5X, 5X, or 10X MICs of CD437, CD1530, or adarotene. When this approach proved unsuccessful, development of resistant mutants by serial passage in liquid medium was conducted as previously described[24]. Briefly, 50 µl of ~10^6 CFU *S. aureus* MW2 were added to the wells of a 96-well plate containing 50 µl of an extended concentration gradient of CD437. The extended gradient was created by 2-fold serial dilutions with cation-adjusted Mueller Hinton (CaMH) broth from three different starting concentrations: 80, 96, and 128 µg/ml. The plate contained final antibiotic concentrations of 0, 0.375, 0.5, 0.625, 0.75, 1, 1.25, 1.5, 2, 2.5, 3, 4, 5, 6, 8, 10, 12, 16, 20, 24, 32, 40, 48, and 64 µg/ml. After incubating the plate at 37°C for 24h, OD_{600nm} was measured by a spectrophotometer (SpectraMax M2, Molecular Devices).

Bacterial growth was defined as $OD_{600nm} \geq 0.1$. 2 µl of the bacterial culture at the highest drug concentration that permitted bacterial growth was diluted 1,000-fold in CaMH, and the diluted culture was used as inoculum for the next passage. The rest of the culture was stored in 16% glycerol at -80°C. Serial passage was performed on two independent cultures (SP1 and SP2) for 100 days, and a separate ciprofloxacin selection served as a control. Confirmation of decreased susceptibility to retinoids was conducted by re-measuring MICs of retinoids against the resistant mutants from each glycerol freezer stock. In a separate experiment, daptomycin was used as the control instead of ciprofloxacin and the cultures were passaged for 15 days instead of 100 days.

Genomic DNA extraction, library preparation, and genome sequencing. Genomic DNAs from days 1, 75, and 100 from SP1 and days 1, 55, and 100 from SP2 were isolated using a DNeasy kit (Qiagen, Valencia, CA, USA). A standard Gram-positive DNA isolation protocol was preceded by treatment of the bacterial pellet with 10 mg/ml lysozyme and 5 ng/ml lysostaphin and incubation at 37°C for 30 min. Genomic DNA was quantified using a Qubit fluorometric assay (Invitrogen, Carlsbad, CA, USA), and a paired-end sequencing library (2×250 bp) was prepared for each sample using a Nexttera XT DNA sample preparation kit (Illumina, San Diego, CA, USA). The quality and quantity of each sequencing library were determined using an Agilent 2100 Bioanalyzer (Santa Clara, CA, USA), and libraries were pooled and sequenced using an Illumina MiSeq (MEEI Ocular Genomics Institute, Boston, MA, USA).

Genome assembly, annotation, and variant calling. Genomes of the starting strain for each selection were assembled *de novo* using CLC Genomics Workbench version 7.0 (CLC bio, Cambridge, MA, USA). Assemblies were annotated using RAST (http://rast.nmpdr.org), and the annotated assembly of each starting strain was used as a reference to call genetic variants in subsequent samples. Single nucleotide polymorphisms (SNPs) and insertion/deletion (indel) variants were identified by mapping sequencing reads to the annotated reference assembly using default parameters. Variants supported by at least 50 sequencing reads and present at >50% frequency were examined further.

Correlation of mutations with decreased susceptibility to retinoids. Mutations causing amino acid changes

were confirmed by sequencing of PCR amplified regions (~500 bp) surrounding each altered nucleotide. The primers are listed in Supplementary Table 9. PCR products were sequenced by GENEWIZ (South Plainfield, NJ, USA). The passage day when the mutations occurred was identified by colony PCR using three colonies from each glycerol freezer stock, followed by sequencing of the PCR products. The passage day when susceptibility to the retinoids changed was identified by repeating MIC determinations using overnight cultures from three colonies from each glycerol freezer stock. Altered genes causing decreased retinoid susceptibility were identified by comparing the day of mutation with the day of change in retinoid susceptibility. The correlation between mutations in *graS*, *manA*, and *yjbH* and decreased susceptibility to retinoids was confirmed by comparing the susceptibility of *S. aureus* JE2 (wild-type, parent strain) to mutant strains: NE1756 (*graS*::ΦNΞ), NE1645 (*manA*::ΦNΞ), and NE896 (*yjbH*::ΦNΞ) from the Nebraska Transposon Mutant Library[25]. Transposon mutants in *graS*, *manA*, and *yjbH* were complemented with the wild-type copy of each mutated gene cloned in pBK123[26]. The primers shown in Supplementary Table 9 were used to amplify each gene. Plasmids were propagated in the *E. coli* strain DC10B[27] prior to transformation into *S. aureus*. Transposon mutant strains were made electrocompetent following the protocol of Grosser and Richardson[28], and were transformed with the corresponding complementation plasmid or the pBK123 empty plasmid. Plasmid-containing strains were selected with 5 μg/ml (*E. coli*) or 10 μg/ml (*S. aureus*) chloramphenicol, and gene expression was induced by adding 2.5 μM cadmium chloride.

SYTOX Green membrane permeability assay. Black, clear-bottom, 96-well plates (Corning no. 3904, Corning, NY, USA) were filled with 50 μl of phosphate buffered saline (PBS)/well containing the indicated concentration of antibiotics. Exponential-phase *S. aureus* MW2 cells prepared as described in the *Killing kinetics assay* were washed 3 times with the same volume of PBS. The washed cells were adjusted to OD_{600} = 0.4 (~2×10^7 CFU/ml) with PBS. For persister membrane permeability study, overnight stationary-phase *S. aureus* MW2 cells were washed 3 times with PBS and then adjusted to ~10^8 CFU/ml. SYTOX Green (Molecular Probes, Waltham, MA, USA) was added to 10 ml of the diluted bacterial suspension to a final concentration of 5 μM and incubated for 30 min at room temperature in the dark. 50 μl of the bacteria/SYTOX

Green mixture was added to each well of the 96-well plates containing antibiotics and fluorescence was measured at room temperature using a spectrophotometer (SpectraMax M2, Molecular Devices, Sunnyvale, CA, USA), with excitation and emission wavelengths of 485 nm and 525 nm, respectively. All experiments were conducted in duplicate or triplicate.

Transmission electron microscopy. *S. aureus* MW2 was grown to the exponential phase (OD_{600} = ~0.4) at 37°C. Bacterial cultures were then treated with 10X MIC of CD437, CD1530 or 0.1% DMSO (control) at 37°C for 30 minutes. 1 ml of the retinoid treated cells was fixed with the same volume of a 2X fixative, a mixture of 5% glutaraldehyde, 2.5% paraformaldehyde and 0.06% picric acid in 0.2 M sodium cacodylate buffer (pH 7.4). After spinning down, a pellet of cells were incubated for at least 2 h at room temperature and then stored at 4°C. Fixed cells were washed in 0.1 M cacodylate buffer and post-fixed with 1% Osmium tetroxide (OsO_4)/1.5% Potassium ferrocyanide ($KFeCN_6$) for 1 h, washed twice in water, once in maleate buffer (MB), and incubated in 1% uranyl acetate in MB for 1h. Cells were then washed twice in water and subsequently dehydrated in an alcohol gradient series (10 min each; 50%, 70%, 90%, 2x10min 100%). The cells were then put in propyleneoxide for 1 h and infiltrated overnight in a 1:1 mixture of propyleneoxide and Spurr's low viscosity resin (Electron Microscopy sciences, Hatfield, PA). The cells were embedded in Spurr's resin and polymerized at 60°C for 48 h. Ultrathin sections (about 60 nm) were cut on a Reichert Ultracut-S microtome (Leica Microsystem, Wetzlar, Germany), picked up onto copper grids, and stained with lead citrate. Micrographs of the cells were taken using a JEOL 1200EX transmission electron microscope (Harvard Medical School EM facility).

Preparation of giant unilamellar vesicles (GUVs) and observation of effects of compounds on GUVs. GUVs were prepared by the electroformation method described previously[3]. Dioleoyl-glycero-phosphocholine (DOPC), Dioleoyl-glycero-phosphoglycerol (DOPG) and Dioleoyl-glycero-phosphoethanolamine-N-lissamine rhodamine B sulfonyl (18:1 Liss Rhod PE) were purchased from Avanti Polar Lipids (Alabaster, AL, USA). 4 mM of a lipid mixture consisting of DOPC/DOPG/18:1 Liss Rhod PE (7:3:0.005) was dissolved in chloroform, and 40 µl of this mixture was then spread onto indium tin oxide (ITO)-coated slides (50 × 75 × 1.1mm, Delta

Technologies, Loveland, CO, USA). In order to remove chloroform, the ITO slides were dried in a vacuum chamber for 2 h. To make an elecroformation chamber, a 2 mm thick Teflon spacer was inserted between the lipid-applied surfaces of two ITO slides. 2 ml of 100 mM sucrose was added into the electroformation chamber, followed by sealing with binder clips. The swelling of the lipid bilayers was facilitated by applying an electric AC-field (10 Hz). The field strength was gradually increased from 0 to 0.5 kV/m for 30 min, and then was maintained constantly for 30 min. GUVs were detached from surfaces by reducing the AC-field from 10 Hz to 5 Hz for 20 min. The GUV suspension was diluted (1:30) in a 100 mM glucose solution. 49 µl of the diluted GUV suspension (~100 vesicles) was transferred to a black, clear-bottom 384-well plate (Corning no. 3712, Corning, NY, USA). The plate was left in the dark at room temperature for 30 min until all GUVs settled on the bottom of the plates. After adding 1 µl of compound solution to a well (final compound concentration: 10X MIC or 1X MIC), the GUVs were observed and imaged with an optical microscope equipped with a fluorescence contrast and a digital camera (40x or 63x objectives, Axio Observer. A1 & AxioCam MRm, Zeiss, Germany). Images and videos are representative of three independent experiments.

All-atom molecular dynamics (MD) simulations. All-atom MD simulations based on the GROMACS package (version 4.6.7)[29] were performed to investigate the interactions between selected retinoids (CD437, CD1530, adarotene, adapalene, other analogs, and glucuronided metabolites) and a simulated plasma membrane of *S. aureus*. The Gromos54a7 force field[30] with Automated Topology Builder[31] was employed for the partial atomic charges and the non-bonded and bonded parameters of the retinoid molecules in the simulations. Two membrane models of different lipid compositions were adopted to represent the plasma membrane of *S. aureus*. One was a mixed lipid bilayer composed of 88 neutral-charged DOPC and 40 negatively-charged DOPG lipids (~7:3 ratio) with dimensions of 5.96 nm × 5.96 nm. This mixture of lipids is widely used to mimic anionic bacterial membranes and to investigate the mechanisms of action of membrane-active antimicrobials, such as daptomycin and antimicrobial peptides on *S. aureus* membranes[32-35]. Lipid bilayers at different lipid ratios of 6:4 (80 DOPC and 48 DOPG lipids) and 5:5 (64 DOPC and 64 DOPG lipids) were also constructed to study the effects of membrane surface charges on the antimicrobial activity of retinoids. The DOPC and DOPG lipids

were modeled with Berger's lipid force field[36], which is an extensively validated all-atom lipid model for membrane-related simulations[37,38]. The other membrane model was a mixed lipid bilayer composed of 108 PG lipids, 72 Lys-PG lipids, and 10 DPG (Cardiolipin) lipids with dimensions of 8.50 nm × 7.36 nm, which was used previously to more specifically mimic *S. aureus* membranes[39]. Repetitions of simulations with these two different membrane compositions were performed to verify the robustness of results and mechanisms. Sodium ions were added into the simulation system to neutralize the negative charge of membranes. For enhanced computational efficiency, water molecules were represented by a polarization corrected simple point-charge SPC/E model[40]. A geometric combining rule of Lennard-Jones potential was adopted for non-bonded interactions of retinoid molecules with lipids, ions and water. The fast smooth particle-mesh Ewald[41] was used to calculate the long-rang electrostatic interactions. The system was modeled as an NPT ensemble, with periodic boundary conditions in all directions, under constant pressure P (1 atm) and constant temperature T (300 K). The simulation box had an initial height of 12.3 nm, which was large enough to prevent the membrane and retinoid molecules from interacting with their periodic images. The time step was fixed at 2 fs. After a 500 ns initial equilibration of solvated lipid systems, the retinoid molecules were introduced into the water phase above the membrane. After 100 ns of re-equilibration, the retinoid molecules were released and their interactions with the membrane including attachment, penetration and equilibrium configurations were further simulated for 500-1000 ns[42]. The free energy profiles for the translocations of retinoid molecules were calculated by steered molecular dynamics[43], umbrella sampling, and weighted histogram analysis method[44,45], with the output giving the transfer energies and energy barriers that describe the feasibility (favorability and rate, respectively) of membrane penetration. The energy profile of penetration is a theoretical representation of an energetic pathway, as the retinoids are translocated into membrane, with two independent parameters: transfer energy and energy barrier. The transfer energy of penetration, which is defined as the energy conversion of two equilibrium states from outside to inside the membrane, describes the direction of translocation. The negative value of transfer energy that represents the energy decrease for penetration indicates that the embedment of retinoids inside the membrane is energetically favorable. The energy barrier is calculated as the height of the peak along the pathway relative to the equilibrium state outside the membrane. The energy

barrier is the least energy the retinoids must possess to cross over the membrane surface which governs the rate of penetration. A lower energy barrier corresponds to a faster and easier penetration. The thermal energy k_BT was used as the unit of energy in the simulations with the T corresponding to the room temperature (300 K). In equilibrium, the probability of a system being in the state with energy E is proportional to e^{-E/k_BT}. By using the k_BT as the measurement, the system stability could be explicitly compared at different equilibrium states. To visualize the membrane attachment and penetration, the retinoids and sodium ions are depicted as large spheres, and phospholipids are represented as chains. The atoms in retinoids, phospholipids and sodium ions are colored as follows: hydrogen, white; oxygen, red; nitrogen, dark blue; carbon, cyan; phosphorus, orange; sodium, lavender. Water molecules are set to be transparent for clarity. The outer blue lines in the MD videos indicate the period boundaries of the simulation boxes.

Human blood hemolysis. Hemolytic activity of retinoids on human erythrocytes was evaluated using a previously described method with modifications[46]. 10% human erythrocytes were purchased from Rockland Immunochemicals (Limerick, PA, USA). The erythrocytes were diluted to 4% with PBS, and 100 µl was added to 100 µl of two-fold serial dilutions of compounds in PBS, 0.2% DMSO (negative control), or 2% Triton-X 100 (positive control) in a 96-well plate. The plate was incubated at 37°C for 1 h and then centrifuged at 500×g for 5 min. 100 µl of the supernatant was transferred to a fresh 96-well plate and absorbance of supernatants was measured at 540 nm. Percent hemolysis was calculated using the following equation: (A_{540nm} of compound treated sample − A_{540nm} of 0.1% DMSO treated sample) / (A_{540nm} of 1% Triton X-100 treated sample − A_{540nm} of 0.1% DMSO treated sample) × 100. HC_{50} (concentration of compound causing 50% hemolysis) was determined using SigmaPlot 10.0 (Systat Software Inc., San Jose, CA, USA).

Cytotoxicity. Cryopreserved rat and human primary hepatocytes were purchased from the Cell Resource Core at Massachusetts General Hospital (Boston, MA, USA). The hepatocytes were cultured in a collagen sandwiched configuration in 24-well plates, as described previously[47-49]. Briefly, 4×10^5 live cells were seeded in 24-well plates coated with rat tail collagen type I. Plates were incubated in a humidified 5% CO_2 incubator at 37°C for 4 h to allow cells to attach to the collagen gel. The cells were washed and then cultured in 0.5 ml

standard hepatocyte culture medium consisting of pre-warmed Dulbecco's modified Eagle's medium (DMEM) media supplemented with 10% FBS, 0.5 U/ml insulin, 14 ng/ml glucagon, 20 ng/ml EGF, 7.5 µg/ml hydrocortisone and 200 U/ml penicillin-streptomycin. The cell cultures were incubated in a humidified 5% CO_2 incubator at 37°C. At 24 h after seeding the cells, a top layer of collagen gel was deposited on the hepatocytes attached to the bottom collagen layer and incubated for additional 24 h.

Human hepatoma, HepG2 (ATCC HB-8065) cells were maintained in DMEM containing 10% fetal bovine serum and antibiotics penicillin–streptomycin (100 units/ml). Normal human primary renal proximal tubular epithelial cells (RPTEC, Lonza catalog # CC-2553, Walkersville, MD, USA) and adult normal human epidermal keratinocytes (NHEK, Lonza catalog # 192627) were maintained in renal cell growth media with growth supplements (REGM, Lonza catalog # CC-3190) and in keratinocyte growth media 2 with growth supplements (KGM-2, Lonza catalog # CC-3107), respectively in a humidified 5% CO_2 incubator at 37°C.

For cytotoxicity tests, HepG2, RPTEC, and NHEK were cultured at 70–80% confluence in tissue culture treated 96-well plates in a volume of 100 µl/well corresponding culture media. To test cytotoxicity in the absence of serum, all cells were washed twice with PBS and then once with the serum-free corresponding culture media. The cells were then treated with a range of concentrations of retinoids in the serum-free culture media for 24 h. For the last 4 h of the 24 h period, 50 µl and 10 µl of WST-1 (Roche, Mannheim, Germany) were added in each well of the 24-well and the 96-well plates, respectively. WST-1 reduction was measured at 450 nm. The percent fluorescence relative to that of the no-treatment control was calculated. The assay was done in triplicate.

Evaluation of human ether-a-go-go-related gene (hERG) potassium channel inhibition potential. The inhibitory potential of CD437, CD1530, and adarotene on the cardiac voltage-gated potassium channel hERG was evaluated by Cyprotex (Watertown, MA, USA). Electrophysiology measurements were conducted using an IonWorks^{TM} HT instrument (Molecular Devices Corporation, Sunnyvale, CA, USA) and 384-well planar PatChPlate^{TM} (Molecular Devices Corporation). Briefly, Chinese hamster ovary (CHO) cells expressing the hERG potassium channel were dispensed into 384-well planar arrays, and hERG tail currents were measured by

whole-cell voltage clamping. A range of concentrations (0.008 µM to 25 µM) of each retinoid were then added to the cells, and a second recording of the hERG current was made. The percent change in the hERG current was calculated. Quinidine, an established hERG inhibitor was used as a positive control, and 0.25% DMSO was used as a negative control.

Genotoxicity. The mutagenic potentials of CD437, CD1530, and adarotene were evaluated by the Ames test[50] using histidine auxotrophic *Salmonella typhimurium* strains TA 1535 and TA 1538 in the presence and absence of 4% rat liver S9 fraction (Moltox, Boone, NC, USA). Briefly, 100 µl of bacterial overnight cultures was added into 500 µl of phosphate buffer containing a range of concentrations of the retinoids dissolved in 10 µl DMSO. After incubation at 37°C for 1 h, the samples were added into 2 ml of soft agar including 0.5 mM of histidine/biotin, mixed, and poured onto minimal glucose agar plates. The plates were incubated at 37°C for 48 h, and revertant colonies counted. 10 µl DMSO was used as a negative control. 5 µg/plate sodium azide for TA1535 and 5 µg/plate 4-Nitro-o-phenylenediamine (4NOP) for TA1538 were used as positive controls in the non-metabolic activation system. 5 µg/plate 2-aminoanthracene was used as a positive control for both strains in the metabolic activation system. The test was performed in triplicate.

Antibiotic synergy test. The checkerboard method was used for determining synergy of the synthetic retinoids with conventional antibiotics[46]. Briefly, 2-fold serial dilutions of each retinoid were combined with 2-fold serial dilutions of each conventional antibiotic, creating an 8×8 matrix in a 96-well microtiter plate. The fractional inhibitory concentration index (FICI) was calculated as follows: FICI = MIC of compound A in combination / MIC of compound A alone + MIC of compound B in combination / MIC of compound B alone. The interaction between two compounds was defined, as follows: synergy if $FICI \leq 0.5$, no interaction if $0.5 < FICI \leq 4$, antagonism if $FICI > 4$[51].

Pharmacokinetic analysis. Pharmacokinetic experiments were conducted by SAI Life Sciences Ltd. (Pune, India) in accordance with guidelines provided by the Committee for the Purpose of Control and Supervision of Experiments on Animals (CPCSEA). The Institutional Animal Ethics Committee (IAEC) approved the

experimental protocol. In brief, healthy female CD1 mice (6 weeks old) weighing between 20 to 25 g were procured from Hylasco (Hyderabad, India). Analog 2 was dissolved in a 1:1 solution of Kolliphor EL (Sigma-Aldrich, St Louis, MO, USA) and ethanol and then diluted 1:10 in saline to a final concentration of 2 mg/ml. Groups of mice (n=3) were treated with 20 mg/kg Analog 2 (i.p.). Blood samples were collected as terminal a bleed under light isoflurane anesthesia through a cardiac puncture such that samples were obtained at pre-dose, 0.08, 0.25, 0.5, 1, 2, 4, 8 & 24 h. Immediately after collection, plasma was harvested by centrifugation and stored at -70 ºC until analysis. All samples were processed for analysis by protein precipitation using acetonitrile and analyzed with fit-for-purpose LC/MS/MS method (LLOQ = 4.90 ng/mL for plasma). Pharmacokinetic parameters were calculated using the non-compartmental analysis tool of Phoenix WinNonlin (Version 6.3). No statistical methods were used to predetermine samples size. The experiments were not randomized, and investigators were not blinded to allocation during experiments and outcome assessment. Outliers were determined based on Grubb's test using GraphPad Prism 7 (GraphPad Software, La Jolla, CA, USA).

Maximum tolerated dose. Six-week-old female CD1 ICR outbred mice (20-25 g) were obtained from Charles River Laboratories (Wilmington, MA, USA). Analog 2 was dissolved in a 1:1 solution of Kolliphor EL (Sigma-Aldrich, St Louis, MO, USA) and ethanol and then diluted 1:10 in saline to a final concentration of 4 mg/ml. Groups of mice (n=6) were treated with 10, 20, 40, 80 mg/kg Analog 2 i.p. or vancomycin (25 mg/kg) every 12 h for 3 days. Control mice were injected with 400 µl of 10% Kolliphor EL/ethanol in saline i.p. every 12 h for 3 days. Mice were closely monitored until they were euthanized at 72 h from the first infection. After euthanizing mice, blood was collected by cardiac puncture. All samples were stored at 4°C until for analysis. Serum was analyzed for alanine aminotransferase and urea nitrogen content with commercially available kits, following the manufacturer's protocol (Pointe Scientific, Canton, MI, USA). No statistical methods were used to predetermine samples size. The experiments were not randomized, and investigators were not blinded to allocation during experiments and outcome assessment. This study and all experimental protocols were approved by the Rhode Island Hospital Institutional Animal Care and Use Committee (RIH IACUC) and

conducted in accordance with the Animal Welfare Act and National Institutes of Health guidelines for animal care and use. Statistical significance among each group was analyzed by one-way ANOVA with post-hoc Tukey test using PASW Statistics 18 (SPSS Inc. Chicago, IL, USA) and GraphPad Prism 7 (GraphPad Software, La Jolla, CA, USA).

Deep-seated mouse thigh infection model for evaluating drug efficacy. A previously described[20] protocol to mimic a chronic, deep-tissue infection was used with modifications. Six-week-old female CD1 ICR outbred mice (20-25 g) were obtained from Charles River Laboratories (Wilmington, MA, USA). To make mice neutropenic, 150 mg/kg and 100 mg/kg of cyclophosphamide were administered via i.p. injection at 4 days and 1 day before infection, respectively. On the day of infection, ~10^5 cells of stationary-phase *S. aureus* MW2 suspended in 50 µl of saline were injected to the right thigh of each mouse. To test the efficacy of CD437, the compound was dissolved in a 1:1 solution of Kolliphor EL (Sigma-Aldrich, St Louis, MO, USA) and ethanol and then diluted 1:10 in saline to a final concentration of 20 mg/kg. Because CD437 shows *in vivo* efficacy in the mouse xenograft cancer models at 10-30 mg/kg up to 3 weeks without showing detectable toxicity[52-54], we tested it at 20 mg/kg in the MRSA mouse deep-seated thigh infection model. At 24 h post-infection, groups of mice (n=10) were treated with 30 mg/kg gentamicin subcutaneously (s.c.), 25 mg/kg vancomycin i.p., 20 mg/kg CD437 i.p., or a combination of 20 mg/kg CD437 i.p. and 30 mg/kg gentamicin s.c. every 12 h for 3 days. Control mice were injected with 200 µl of 10% Kolliphor EL/ethanol in saline i.p. every 12 h for 3 days. For testing the efficacy of Analog 2, the compound was dissolved in a 1:1 solution of Kolliphor EL (Sigma-Aldrich, St Louis, MO, USA) and ethanol and then diluted 1:10 in saline to a final concentration of 4 mg/ml. Groups of mice (n=10) were treated with 40 or 80 mg/kg Analog 2 i.p. or in combination with 30 mg/kg gentamicin s.c., or a combination of 25 mg/kg vancomycin i.p. and 30 mg/kg gentamicin s.c. every 12 h for 3 days. Control mice were injected with 400 µl of 10% Kolliphor EL/ethanol in saline i.p. every 12 h for 3 days. After euthanizing mice at 96 h post-infection, blood was collected by cardiac puncture and the infected thighs were aseptically excised. All samples were stored at 4°C until use. Serum was analyzed for alanine aminotransferase and urea nitrogen content with commercially available kits, following the manufacturer's protocol (Pointe

Scientific, Canton, MI, USA). Thigh tissue was homogenized in PBS and the number of MRSA in homogenates was enumerated by serial dilution and spot-plating on TSA plates. The bacterial burden was recorded as CFU/g tissue. A sample size of 10 mice per group was calculated for a single-tailed power analysis using a standard deviation based on our historical data and the literature[20] in consultation with the Rhode Island Hospital Biostatistics Core. The experiments were not randomized, and investigators were not blinded to allocation during experiments and outcome assessment. This study and all experimental protocols were approved by the Rhode Island Hospital Institutional Animal Care and Use Committee (RIH IACUC) and conducted in accordance with the Animal Welfare Act and National Institutes of Health guidelines for animal care and use. Statistical significance among each group was analyzed by one-way ANOVA with post-hoc Tukey test using PASW Statistics 18 (SPSS Inc. Chicago, IL, USA) and GraphPad Prism 7 (GraphPad Software, La Jolla, CA, USA).

Synthesis of CD437 analogs. NMR spectra were recorded using the following spectrometers: Bruker Avance 500 (500 MHz – ^{1}H /125 MHz – ^{13}C) or Bruker Avance 400 (400 MHz – ^{1}H/100 MHz – ^{13}C). Chemical shifts are quoted in ppm relative to tetramethylsilane and with the indicated solvent as an internal reference. The following abbreviations are used to describe signal multiplicities: s (singlet), d (doublet), t (triplet), q (quartet), m (multiplet), br (broad), dd (doublet of doublets), dt (doublet of triplets), etc. Accurate mass spectra were recorded on an Agilent 6520 Accurate-Mass Q-TOF LC/MS, infrared spectra were obtained using a Thermo Nicolet Nexus 670 FTIR spectrophotometer.

Non-aqueous reactions were performed under an atmosphere of argon, in flame-dried glassware, with HPLC-grade solvents purified on a Pure Process Technology solvent purification system. Brine refers to a saturated aqueous solution of sodium chloride, sat. $NaHCO_3$ refers to a saturated aqueous solution of sodium bicarbonate, sat. NH_4Cl refers to a saturated aqueous solution of ammonium chloride, etc “Column chromatography”, unless otherwise indicated, refers to purification in a gradient of increasing EtOAc concentration in hexanes on a Biotage® flash chromatography purification system. All chemicals were used as received from Oakwood, TCI America, Sigma-Aldrich, Alfa Aesar, or AK Scientific.

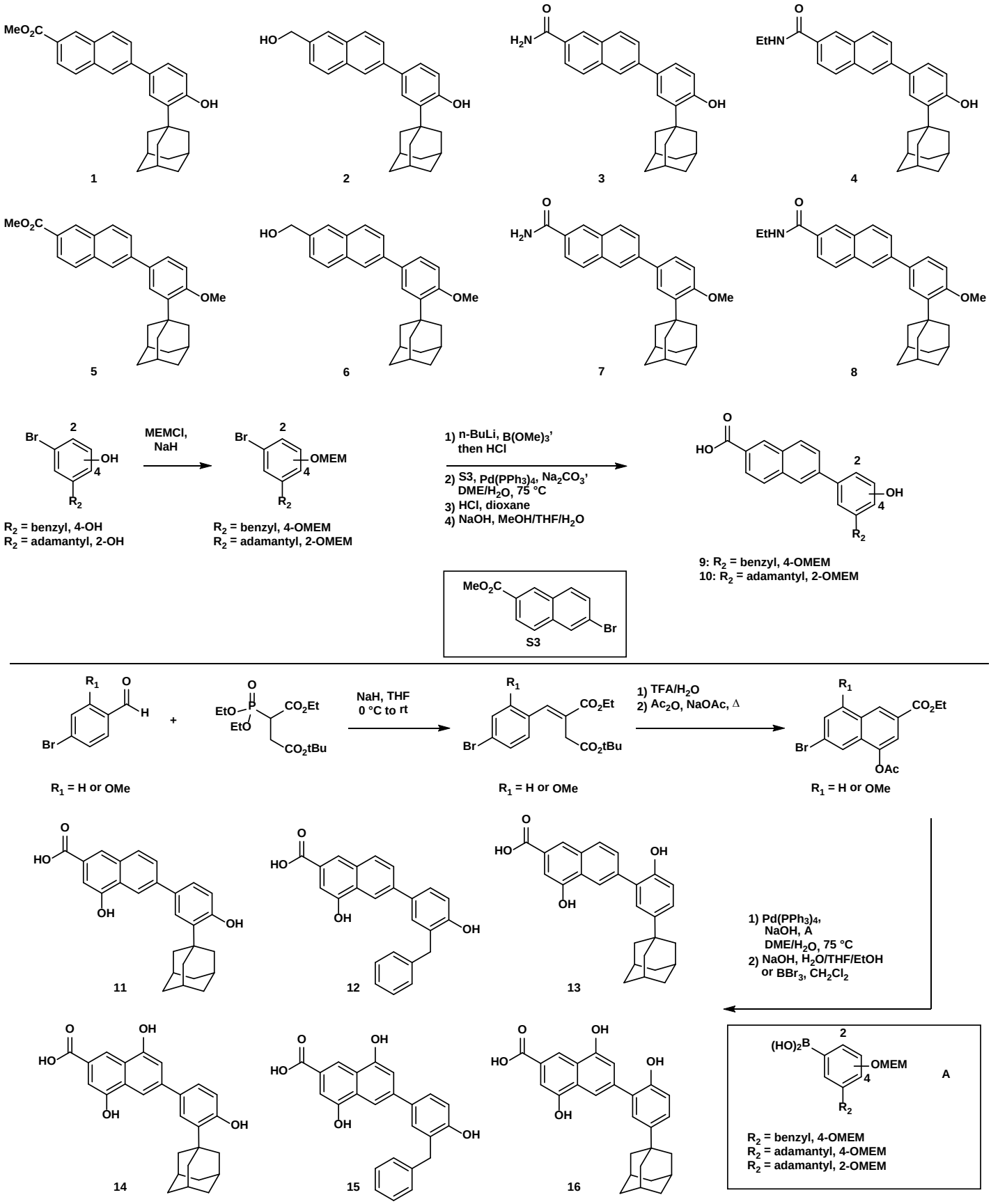

Supplementary Figure 1. Structures of first-generation adapalene analogs **1** – **8** and synthesis of second-generation adapalene analogs **11** – **16**.

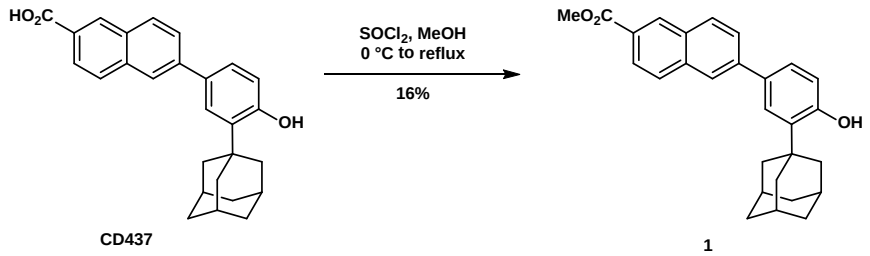

CD437 1

Methyl 6-(3-(adamantan-1-yl)-4-hydroxyphenyl)-2-naphthoate (1). To a solution of CD437 (20 mg, 0.047 mmol) in MeOH (0.5 mL) was added $SOCl_2$ (0.01 mL, 0.12 mmol) at 0°C, the reaction was heated to reflux and stirred for 2 hours. The reaction was cooled to room temperature and concentrated. The yellow solid was purified by HPLC, yielding the title compound as a white solid (3.1 mg, 16% yield). **^{1}H NMR** (500 MHz, DMSO) δ 9.60 (s, 1H), 8.62 (s, 1H), 8.22 – 8.12 (m, 2H), 8.08 (d, *J* = 8.8 Hz, 1H), 7.97 (dd, *J* = 8.6, 1.7 Hz, 1H), 7.88 (dd, *J* = 8.6, 1.8 Hz, 1H), 7.55 – 7.46 (m, 2H), 6.92 (d, *J* = 8.2 Hz, 1H), 3.92 (s, 3H), 2.17 (s, 6H), 2.07 (s, 3H), 1.76 (s, 6H); **^{13}C NMR** (125 MHz, DMSO) δ 166.39, 156.55, 140.89, 136.09, 135.66, 130.68, 130.27, 129.91, 129.83, 128.50, 126.24, 126.06, 125.44, 125.26, 125.03, 123.65, 117.02, 52.19, 36.64, 36.37, 28.41; **HRMS** Accurate mass (ES+): Found 413.2115, $C_{28}H_{29}O_3$ (M+H+) requires 413.2117.

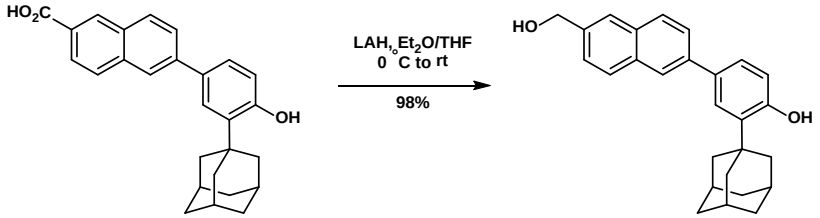

CD437 2

2-(adamantan-1-yl)-4-(6-(hydroxymethyl)naphthalen-2-yl)phenol (2). Lithium aluminum hydride (LAH) (44 mg, 1.154 mmol) was added to a solution of CD437 (230 mg, 0.577 mmol) in 2:1 Et_2O:THF (15 mL) at 0 °C. The reaction was warmed to room temperature and stirred for 2 hours. The reaction was cooled to 0 °C and H_2O (10 mL) was added slowly followed by 2M NaOH (10 mL). The resulting slurry was filtered over Celite and washed with EtOAc. The aqueous layer was extracted with EtOAc 3x and the combined organics were washed with water and brine, dried over Na_2SO_4, filtered, and concentrated; yielding the title compound as a white solid (217 mg, 98% yield). **^{1}H NMR** (500 MHz, DMSO) δ 8.03 (s, 1H), 7.90 (t, J = 8.9 Hz, 2H), 7.79 (s, 1H), 7.73 (dd, J = 8.5, 1.8 Hz, 1H), 7.47 – 7.38 (m, 3H), 6.96 (d, J = 8.2 Hz, 1H), 4.66 (s, 2H), 2.17 (s, 6H), 2.06 (s, 3H), 1.76 (s, 6H); **^{13}C NMR** (150 MHz, CDCl3) δ 154.33, 139.11, 138.11, 136.91, 133.67, 133.44, 132.30, 128.66, 128.39, 126.51, 126.14, 125.75, 125.69, 125.42, 124.97, 117.42, 65.73, 40.72, 37.20, 29.19; **HRMS** Accurate mass (ES+): Found 385.2177, $C_{27}H_{29}O_2$ (M+H+) requires 385.2168.

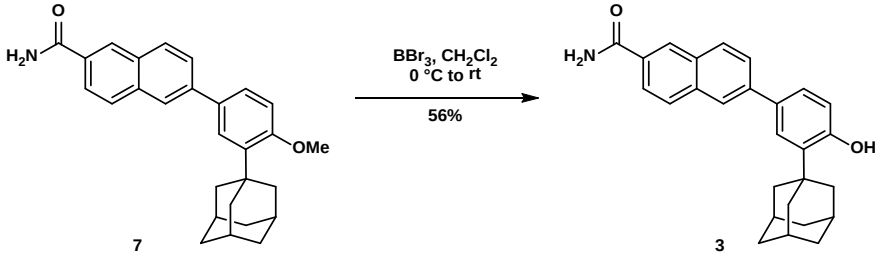

7 3

6-(3-(adamantan-1-yl)-4-hydroxyphenyl)-2-naphthamide (3). To a solution of amide **7** (25 mg, 0.061 mmol) in CH_2Cl_2 (2 mL) at 0°C was added BBr_3 (1M in CH_2Cl_2, 0.06 mL, 0.06 mmol), the reaction was warmed to room temperature and stirred overnight. The reaction was cooled to 0 °C and quenched with water and allowed to stir for 15 minutes, then extracted with EtOAc 3x. The combined organic layers were washed with water and brine, dried over Na_2SO_4, filtered, concentrated, and purified by HPLC, yielding the title compound as a white solid (13 mg, 56% yield). **^{1}H NMR** (500 MHz, DMSO) δ 9.68 (br s, 1H), 8.47 (s, 1H), 8.12 (d, J = 9.5 Hz, 2H), 8.02 (d, J = 8.6 Hz, 2H), 7.94 (dd, J = 8.6, 1.7 Hz, 1H), 7.84 (dd, J = 8.6, 1.8 Hz, 1H), 7.54 – 7.40 (m, 1H), 7.44 (br s, 1H) 6.92 (d, J = 8.2 Hz, 1H), 2.17 (s, 6H), 2.07 (s, 3H), 1.76 (s, 6H); **^{13}C NMR** (125 MHz, DMSO) δ 168.36, 156.84, 140.29, 136.44, 135.14, 131.45, 131.15, 130.47, 129.75, 128.28, 127.95, 126.13, 125.71,

125.52, 125.06, 123.99, 117.43, 37.06, 36.77, 28.83; **HRMS** Accurate mass (ES+): Found 398.2127, $C_{27}H_{28}NO_2$ (M+H+) requires 398.2120.

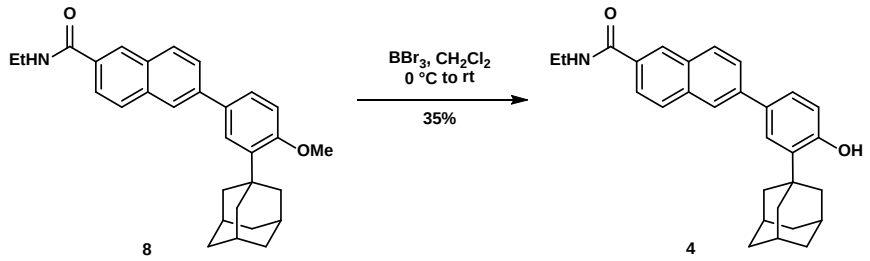

8 4

6-(3-(adamantan-1-yl)-4-hydroxyphenyl)-N-ethyl-2-naphthamide (4). To a solution of amide **8** (25 mg, 0.061 mmol) in CH_2Cl_2 (2 mL) at 0°C was added BBr_3 (1M in CH_2Cl_2, 0.12 mL, 0.122 mmol). The reaction was warmed to room temperature and stirred overnight. The reaction was cooled to 0 °C then quenched with water and allowed to stir for 15 minutes, then extracted with EtOAc 3x. The combined organic layers were washed with water and brine, dried over Na_2SO_4, filtered, concentrated, and purified by HPLC, yielding the title compound as a white solid (5.3 mg, 35% yield). **^{1}H NMR** (500 MHz, $CDCl_3$) δ 8.29 (s, 1H), 8.06 (br s, 1H), 7.98 (s, 1H), 7.93 (dd, *J* = 12.3, 8.7 Hz, 2H), 7.82 (dd, *J* = 8.5, 1.8 Hz, 1H), 7.77 (dd, *J* = 8.5, 1.8 Hz, 1H), 7.58 (d, *J* = 2.3 Hz, 1H), 7.41 (dd, *J* = 8.1, 2.3 Hz, 1H), 6.81 (d, *J* = 8.1 Hz, 1H), 3.59 (qd, *J* = 7.3, 5.6 Hz, 2H), 2.22 (s, 6H), 2.12 (s, 3H), 1.81 (s, 6H), 1.32 (t, *J* = 7.3 Hz, 3H); **^{13}C NMR** (125 MHz, $CDCl_3$) δ 168.03, 154.86, 140.92, 137.04, 135.28, 133.01, 131.51, 131.41, 129.39, 128.71, 127.29, 126.74, 126.54, 125.81, 124.82, 123.94, 117.51, 40.70, 37.20, 37.06, 29.19, 15.08; **HRMS** Accurate mass (ES+): Found 448.2247, $C_{29}H_{31}NO_2Na$ (M+Na+) requires 448.2252.

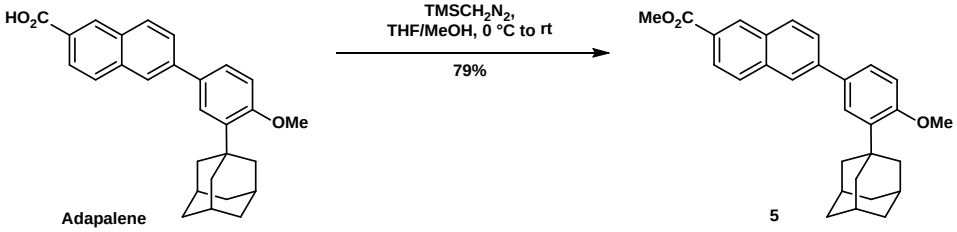

Adapalene 5

Methyl 6-(3-(adamantan-1-yl)-4-methoxyphenyl)-2-naphthoate (5). To a solution of adapalene (50 mg, 0.121 mmol) in 4:1 THF/MeOH (0.4 mL) at 0 °C was added $TMSCH_2N_2$ (0.15 mL, 0.290 mmol) and the reaction was warmed to room temperature over 1 hour. The reaction mixture was concentrated, 1N HCl was added, and was extracted with EtOAc 3x. The combined organic layers were washed with water and brine, dried over Na_2SO_4, filtered, and concentrated; yielding the title compound as a white solid (41 mg, 79% yield). **^{1}H NMR** (500 MHz, $CDCl_3$) δ 8.61 (s, 1H), 8.07 (dd, J = 8.6, 1.7 Hz, 1H), 8.03 – 7.96 (m, 2H), 7.92 (d, J = 8.6 Hz, 1H), 7.80 (dd, J = 8.5, 1.8 Hz, 1H), 7.60 (d, J = 2.4 Hz, 1H), 7.55 (dd, J = 8.4, 2.4 Hz, 1H), 7.00 (d, J = 8.5 Hz, 1H), 3.99 (s, 3H), 3.91 (s, 3H), 2.19 (s, 6H), 2.10 (s, 3H), 1.80 (s, 6H); **^{13}C NMR** (125 MHz, $CDCl_3$) δ 167.44, 159.03, 141.51, 139.11, 136.06, 132.67, 131.35, 130.95, 129.82, 128.33, 127.02, 126.59, 126.09, 125.84, 125.68, 124.84, 112.21, 55.27, 52.31, 40.72, 37.25, 29.23; **HRMS** Accurate mass (ES+): Found 427.2268, $C_{29}H_{31}O_3$ (M+H+) requires 427.2273.

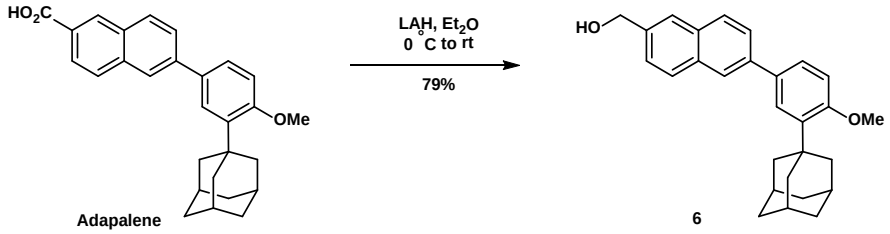

Adapalene 6

(6-(3-(adamantan-1-yl)-4-methoxyphenyl)naphthalen-2-yl)methanol (6). To a solution of lithium aluminum hydride (LAH) (5.05 mg, 0.133 mmol) in Et_2O (1 mL) at 0 °C was added adapalene (50 mg, 0.121 mmol) in Et_2O (0.5 mL). The reaction was warmed to room temperature and stirred for 2 hours. The reaction was cooled to 0 °C and H_2O (1 mL) was added slowly followed by 1N NaOH (1 mL). The resulting slurry was filtered over

Celite and washed with EtOAc. The aqueous layer was extracted with EtOAc 3x and the combined organics were washed with water and brine, dried over Na_2SO_4, filtered, and concentrated; yielding the title compound as a white solid (38 mg, 79% yield). **^{1}H NMR** (500 MHz, $CDCl_3$) δ 7.98 (d, J = 1.1 Hz, 1H), 7.88 (t, J = 8.5 Hz, 2H), 7.82 (s, 1H), 7.74 (dd, J = 8.5, 1.8 Hz, 1H), 7.60 (d, J = 2.3 Hz, 1H), 7.53 (dd, J = 8.4, 2.3 Hz, 1H), 7.50 (dd, J = 8.4, 1.6 Hz, 1H), 6.99 (d, J = 8.4 Hz, 1H), 4.87 (s, 2H), 3.90 (s, 3H), 2.20 (s, 6H), 2.11 (s, 3H), 1.81 (s, 6H); **^{13}C NMR** (125 MHz, $CDCl_3$) δ 158.72, 139.19, 139.01, 138.09, 133.44, 133.20, 132.29, 128.64, 128.36, 126.17, 126.01, 125.70, 125.65, 125.40, 124.98, 112.22, 65.69, 55.31, 40.76, 37.28, 29.26; **HRMS** Accurate mass (ES+): Found 421.2141, $C_{28}H_{31}O_2Na$ (M+Na+) requires 421.2143.

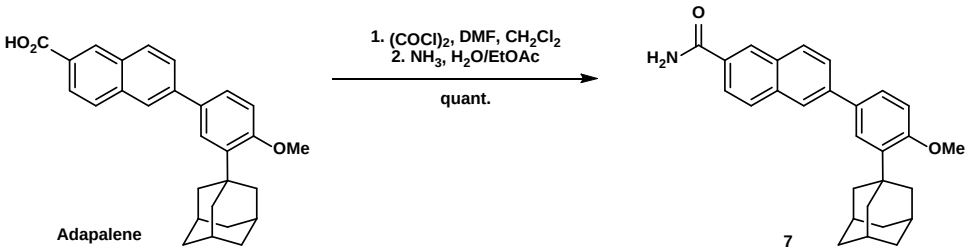

6-(3-(adamantan-1-yl)-4-methoxyphenyl)-2-naphthamide (7). To a solution of adapalene (50 mg, 0.121 mmol) in CH_2Cl_2 (3 mL) and DMF (one drop, cat.) was added oxalyl chloride (2M in CH_2Cl_2, 0.15 mL, 0.30 mmol), and the reaction was stirred at room temperature 2 hours. The reaction was concentrated and dissolved in 8:1 EtOAc/NH_4OH (5 mL) and stirred at 0°C for 30 minutes. The reaction was diluted with EtOAc and water, and the aqueous layer was extracted with EtOAc 3x. The combined organic layers were washed with water and brine, dried over Na_2SO_4, filtered, and concentrated, yielding the title compound as a white solid (49 mg, quant.). **^{1}H NMR** (500 MHz, $CDCl_3$) δ 8.36 (s, 1H), 8.02 (s, 1H), 8.00 – 7.93 (m, 2H), 7.87 (dd, J = 8.5, 1.8 Hz, 1H), 7.81 (dd, J = 8.5, 1.8 Hz, 1H), 7.60 (d, J = 2.4 Hz, 1H), 7.55 (dd, J = 8.4, 2.4 Hz, 1H), 7.00 (d, J = 8.5 Hz, 1H), 3.91 (s, 3H), 2.19 (s, 6H), 2.11 (s, 3H), 1.80 (s, 6H); **^{13}C NMR** (125 MHz, $CDCl_3$) δ 170.04, 159.00, 141.20, 139.11, 135.53, 132.60, 131.39, 129.97, 129.49, 128.68, 128.09, 126.77, 126.03, 125.79, 124.79, 124.11, 112.22, 55.26, 40.69, 37.20, 29.19; **HRMS** Accurate mass (ES+): Found 434.2085, $C_{28}H_{29}NO_2Na$ (M+Na+) requires 434.2096.

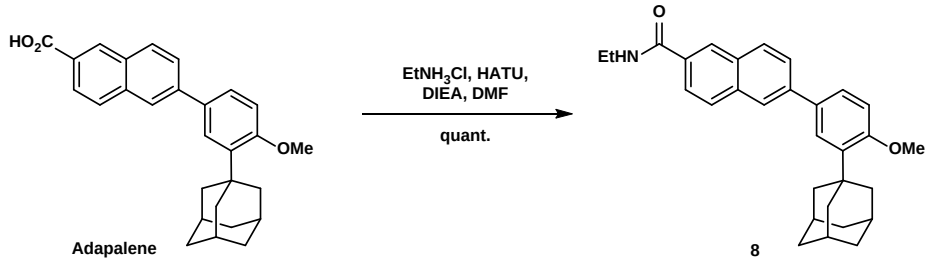

6-(3-(adamantan-1-yl)-4-methoxyphenyl)-N-ethyl-2-naphthamide (8). To a slurry of adapalene (50 mg, 0.121 mmol) in DMF (3 mL) was added DIEA (0.13 mL, 0.726 mmol) followed by HATU (50.6 mg, 0.133 mmol) and $EtNH_3Cl$ (30 mg, 0.363 mmol) and the reaction was stirred at room temperature overnight. The reaction poured into water and quenched with sat. $NaHCO_3$, then extracted with CH_2Cl_2 3x. The combined organic layers were washed with water and brine, dried over Na_2SO_4, filtered, concentrated, and purified by prep TLC (neat EtOAc), yielding the title compound as a white solid (53 mg, quant.). **^{1}H NMR** (500 MHz, $CDCl_3$) δ 8.28 (s, 1H), 8.00 (s, 1H), 7.94 (dd, J = 13.3, 8.6 Hz, 2H), 7.83 (dd, J = 8.5, 1.7 Hz, 1H), 7.79 (dd, J = 8.5, 1.8 Hz, 1H), 7.59 (d, J = 2.4 Hz, 1H), 7.54 (dd, J = 8.4, 2.4 Hz, 1H), 7.00 (d, J = 8.5 Hz, 1H), 6.24 (br s, 1H), 3.91 (s, 3H), 3.58 (qd, J = 7.3, 5.9 Hz, 2H), 2.19 (s, 6H), 2.10 (s, 3H), 1.80 (s, 6H), 1.32 (t, J = 7.3 Hz, 3H); **^{13}C NMR** (125 MHz, $CDCl_3$) δ 167.64, 158.98, 140.85, 139.12, 135.23, 132.76, 131.65, 131.53, 129.36, 128.64, 127.15, 126.70, 126.08, 125.81, 124.86, 124.01, 112.24, 55.30, 40.75, 37.27, 35.20, 29.25, 15.13; **HRMS** Accurate mass (ES+): Found 462.2404, $C_{30}H_{33}NO_2Na$ (M+Na+) requires 462.2409.

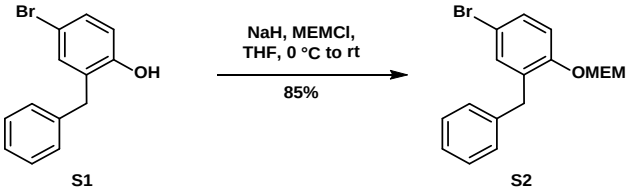

S1 S2

2-benzyl-4-bromo-1-((2-methoxyethoxy)methoxy)benzene (S2). Phenol **S1**[55] (1.500g, 5.701 mmol) dissolved in THF (5 mL) was added via cannula to a suspension of NaH (60% in mineral oil, 296 mg, 7.411 mmol) in THF (15 mL) at 0 °C. The solution was warmed to room temperature and stirred for 30 minutes, after which time MEMCl (1.04 mL, 9.12 mmol) was added, and the reaction was stirred for 2 hours at room temperature. The reaction was quenched with water and extracted with EtOAc 3x. The combined organic layers were washed with brine, dried over Na_2SO_4, filtered, concentrated, and purified by column chromatography, yielding the title compound as a clear oil (1.70g, 85% yield). **^{1}H NMR** (500 MHz, $CDCl_3$) δ 7.32 - 7.27 (m, 3H), 7.25 (d, J = 2.5 Hz, 1H), 7.21 (t, J = 6.6 Hz, 3H), 7.04 (d, J = 8.7 Hz, 1H), 5.25 (s, 2H), 3.96 (s, 2H), 3.66 (dd, J = 5.5, 3.7 Hz, 2H), 3.49 (dd, J = 5.5, 3.8 Hz, 2H), 3.37 (s, 3H); **^{13}C NMR** (125 MHz, $CDCl_3$) δ 153.91, 139.93, 132.99, 132.38, 130.09, 128.68, 128.22, 125.94, 115.60, 113.87, 93.04, 71.34, 67.49, 58.77, 35.92; **HRMS** Accurate mass (ES+): Found 375.0382, $C_{17}H_{19}{}^{81}BrO_3Na$ (M+Na+) requires 375.0382.

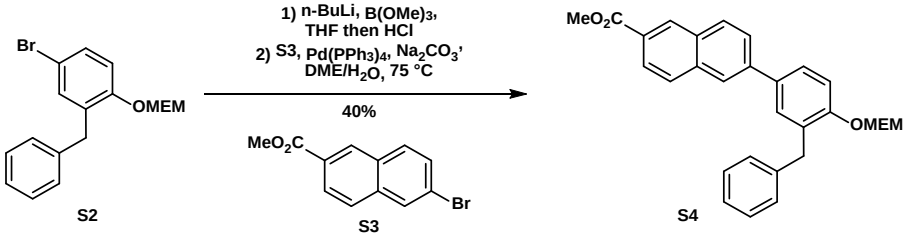

S2 S3 S4

Methyl 6-(3-benzyl-4-((2-methoxyethoxy)methoxy)phenyl)-2-naphthoate (S4). To a solution of bromide **S2** (198 mg, 0.56 mmol) in THF (5 mL) at -78 °C was added *n*-BuLi (2.40 M in hexanes, 0.26 mL, 0.62 mmol) dropwise. The reaction was stirred for 15 minutes at -78 °C. $B(OMe)_3$ was then added dropwise, and the reaction stirred for an additional hour at -78 °C, then warmed to room temperature. After one hour at room temperature, 0.1 M HCl was added (5 mL) and the reaction was stirred for an additional 30 minutes. Water was added, and the solution was extracted with EtOAc 3x. The combined organic layers were washed with brine, dried over Na_2SO_4, filtered, concentrated and purified by column chromatography (EtOAc/hexanes then MeOH/CH_2Cl_2). The intended boronic acid product also contained another similar compound, presumably a borate oligomer of the material (Rf = 0.75 in 5% MeOH/95% CH_2Cl_2, stains red in vanillin), both of which reacted in the following step. The boronic acid mixture was then dissolved in 9:1 DME:H_2O (5 mL), then methyl 6-bromo-2-naphthoate (**S3**) (126 mg, 0.47 mmol) and Na_2CO_3 (100 mg, 0.94 mmol) were added, then argon was bubbled through the mixture for 5 minutes. After degassing, $Pd(PPh_3)_4$ (16 mg, 0.014 mmol) was added, and the reaction was heated to 75 °C for 6 hours. Water and EtOAc were added, and the aqueous layer was extracted with EtOAc 3x. The combined organic layers were washed with brine, dried over Na_2SO_4, filtered, concentrated, and purified by column chromatography, yielding the title compound as a white foam (86 mg, 40% yield with respect to **S3**). **^{1}H NMR** (500 MHz, $CDCl_3$) δ 8.60 (s, 1H), 8.06 (dd, J = 8.6, 1.7 Hz, 1H), 7.98 - 7.97 (m, 2H), 7.90 (d, J = 8.7 Hz, 1H), 7.75 (dd, J = 8.5, 1.8 Hz, 1H), 7.56 (dd, J = 8.5, 2.4 Hz, 1H), 7.52 (d, J = 2.3 Hz, 1H), 7.30 – 7.24 (m, 5H), 7.20 – 7.16 (m, 1H), 5.32 (s, 2H), 4.08 (s, 2H), 3.99 (s, 3H), 3.70 – 3.65 (m, 2H), 3.52 – 3.47 (m, 2H), 3.37 (s, 3H); **^{13}C NMR** (125 MHz, $CDCl_3$) δ 167.33, 155.09, 140.88, 140.64, 135.94, 133.96, 131.42, 130.88, 130.76, 129.85, 129.79, 128.91, 128.40, 128.33, 127.15, 126.67, 126.35, 126.02, 125.71, 124.94, 114.47, 93.22, 71.64, 67.71, 59.10, 52.29, 36.59; **HRMS** Accurate mass (ES+): Found 457.2028, $C_{29}H_{29}O_5$ (M+H+) requires 457.2015.

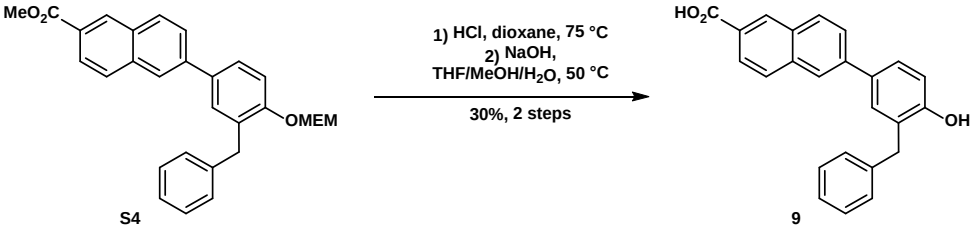

6-(3-benzyl-4-hydroxyphenyl)-2-naphthoic acid (9). MEM ether **S4** (78 mg, 0.17 mmol) was dissolved in dioxane (1.5 mL) and 4M HCl in dioxane (0.5 mL) was added. The reaction was heated to 75 °C for 2 hours. The solution was concentrated under reduced pressure, then dissolved in 1:1 THF:MeOH (2 mL) and 1M NaOH was added (0.34 mL, 0.34 mmol), and this reaction was heated to 50 °C overnight. The following day, the reaction was acidified with 1M HCl (pH 1) and filtered. The filter cake was washed with water, yielding the title compound as a white solid (20 mg, 30% yield over two steps). **^{1}H NMR** (500 MHz, CD_3CN) δ 9.51 (br s, 1H), 8.60 (s, 1H), 8.11 (s, 1H), 8.06 (d, J = 8.7 Hz, 1H), 8.02 (dd, J = 8.6, 1.6 Hz, 1H), 7.97 (d, J = 8.6 Hz, 1H), 7.83 (dd, J = 8.6, 1.8 Hz, 1H), 7.61 (d, J = 2.4 Hz, 1H), 7.53 (dd, J = 8.3, 2.4 Hz, 1H), 7.33 – 7.25 (m, 4H), 7.20 – 7.13 (m, 2H), 6.96 (d, J = 8.3 Hz, 1H), 4.03 (s, 2H); **^{13}C NMR** (125 MHz, DMSO) δ 167.51, 155.48, 141.24, 139.95, 135.49, 130.83, 130.30, 130.27, 129.81, 129.29, 128.67, 128.25, 128.22, 128.15, 127.56, 126.14, 125.71, 125.55, 123.65, 115.79, 35.53; **HRMS** Accurate mass (ES+): Found 355.1331, $C_{24}H_{19}O_3$ (M+H+) requires 355.1334.

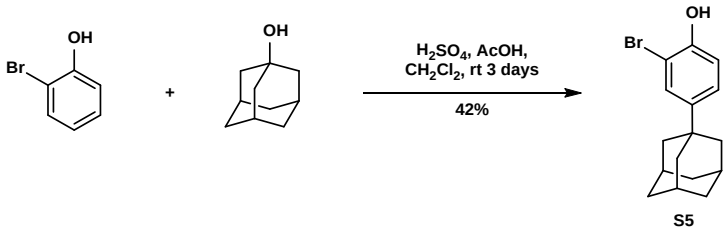

4-(adamantan-1-yl)-2-bromophenol (S5). To a mixture of 2-bromophenol (1.475g, 8.526 mmol) and 1-adamantol (1.298g, 8.526 mmol) in CH_2Cl_2 (4 mL) was added 5:1 AcOH:H_2SO_4 (3 mL), and the reaction was stirred at room temperature for 3 days. The reaction poured into water and quenched with sat. $NaHCO_3$, then extracted with CH_2Cl_2 3x. The combined organic layers were washed with water and brine, dried over Na_2SO_4, filtered, concentrated, and purified by column chromatography (loaded crude oil in hexanes, 0 → 2% EtOAc/hexanes), yielding the title compound as a white solid (1.100g, 42% yield). **^{1}H NMR** (500 MHz, $CDCl_3$) δ 7.41 (d, J = 2.3 Hz, 1H), 7.21 (dd, J = 8.5, 2.3 Hz, 1H), 6.98 – 6.95 (m, 1H), 5.34 (s, 1H), 2.08 (s, 3H), 1.85 (d, J = 2.6 Hz, 6H), 1.81 – 1.70 (m, 6H); **^{13}C NMR** (125 MHz, $CDCl_3$) δ 150.10, 145.54, 128.70, 125.83, 115.68, 110.16, 68.11, 43.40, 36.78, 35.83, 29.02, 25.74; **HRMS** Accurate mass (ES+): Found 307.0711, $C_{16}H_{20}{}^{79}BrO$ (M+H+) requires 307.0698.

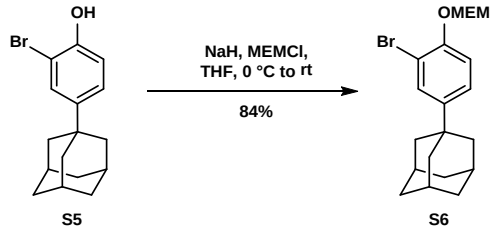

1-(3-bromo-4-((2-methoxyethoxy)methoxy)phenyl)adamantane (S6). To a suspension of sodium hydride (60% in mineral oil, 258 mg, 6.453 mmol) in THF (5 mL) at 0 °C was added a solution of phenol **S5** (1.525g, 4.964 mmol) in THF (3 mL) dropwise. The ice bath was removed and the reaction was stirred at room temperature for 30 minutes, at which time MEMCl (0.91 mL, 7.942 mmol) was added. After 2 hours at room temperature, the reaction was quenched with water and extracted with EtOAc 3x. The combined organic layers were washed with brine, dried over Na_2SO_4, filtered, concentrated, and purified by column chromatography, yielding the title compound as a clear oil (1.650g, 84% yield). **^{1}H NMR** (500 MHz, $CDCl_3$) δ 7.50 (d, J = 2.3 Hz, 1H), 7.22 (dd, J = 8.6, 2.3 Hz, 1H), 7.13 (d, J = 8.7 Hz, 1H), 5.30 (d, J = 5.2 Hz, 2H), 3.89 – 3.85 (m, 2H),

3.59 – 3.55 (m, 2H), 3.37 (s, 3H), 2.08 (s, 3H), 1.85 (d, J = 2.3 Hz, 6H), 1.75 (dd, J = 26.7, 12.1 Hz, 6H); **^{13}C NMR** (125 MHz, $CDCl_3$) δ 151.53, 146.85, 130.11, 125.04, 116.05, 112.65, 94.33, 71.62, 68.02, 59.12, 43.28, 36.74, 35.84, 28.96; **HRMS** Accurate mass (ES+): Found 417.1058, $C_{20}H_{27}{}^{79}BrO_3Na$ (M+Na+) requires 417.1041.

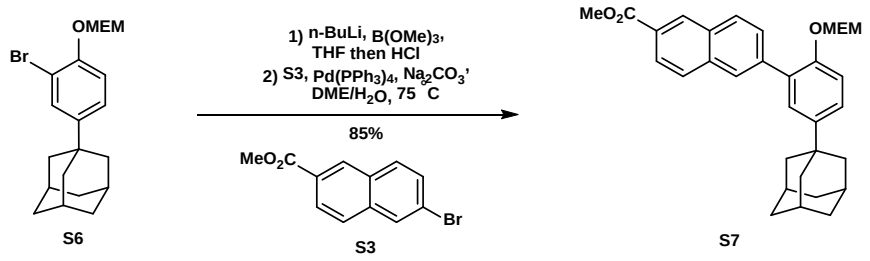

Methyl 6-(5-(adamantan-1-yl)-2-((2-methoxyethoxy)methoxy)phenyl)-2-naphthoate (S7). To a solution of bromide **S6** (31 mg, 0.079 mmol) in THF (2 mL) at -78 °C was added *n*-BuLi (2.40 M in hexanes, 0.036 mL, 0.087 mmol) dropwise and then stirred for 15 minutes at -78 °C, over which time the reaction turned blue. $B(OMe)_3$ was then added dropwise, and the reaction stirred for an additional hour at -78 °C, then warmed to room temperature, over which time the reaction turned maroon. After one hour at room temperature, 0.1 M HCl was added (2 mL) and the reaction was stirred for an additional 30 minutes. Water was added, and the solution was extracted with EtOAc 3x. The combined organic layers were washed with brine, dried over Na_2SO_4, filtered, concentrated and purified by column chromatography (EtOAc/hexanes then MeOH/CH_2Cl_2). The intended boronic acid product also contained another similar compound, presumably a borate oligomer of the material (Rf = 0.75 in 5% MeOH/ 95% CH_2Cl_2, stains red in vanillin), both of which reacted in the following step. The boronic acid mixture was then dissolved in 9:1 DME:H_2O (2 mL), then methyl 6-bromo-2-naphthoate (21 mg, 0.079 mmol), and Na_2CO_3 (17 mg, 0.158 mmol) were added, then argon was bubbled through the mixture for 5 minutes. After degassing, $Pd(PPh_3)_4$ (3 mg, 0.002 mmol) was added, and the reaction was heated to 75 °C for 6 hours. Water and EtOAc were added, and the aqueous layer was extracted with EtOAc 3x. The combined organic layers were washed with brine, dried over Na_2SO_4, filtered, concentrated, and purified by column chromatography, yielding the title compound as a white foam (34 mg, 85% yield with respect to naphthyl bromide). **^{1}H NMR** (500 MHz, $CDCl_3$) δ 8.63 (s, 1H), 8.07 (d, J = 8.6 Hz, 1H), 7.99 – 7.89 (m, 3H), 7.75 (d, J = 8.5 Hz, 1H), 7.40 (s, 1H), 7.34 (d, J = 8.6 Hz, 1H), 7.25 (d, J = 8.2 Hz, 1H), 5.21 (s, 2H), 3.99 (s, 3H), 3.72 – 3.65 (m, 2H), 3.49 – 3.42 (m, 2H), 3.32 (s, 3H), 2.10 (s, 3H), 1.95 (s, 6H), 1.77 (q, J = 12.2 Hz, 6H); **^{13}C NMR** (125 MHz, $CDCl_3$) δ 167.44, 152.34, 145.63, 139.61, 135.65, 131.47, 130.89, 130.71, 129.23, 128.68, 128.41, 127.99, 127.88, 127.31, 125.73, 125.46, 115.63, 94.46, 71.61, 67.82, 59.07, 52.32, 43.46, 36.87, 35.91, 29.07; **HRMS** Accurate mass (ES+): Found 523.2461, $C_{32}H_{36}O_5Na$ (M+Na+) requires 523.2460.

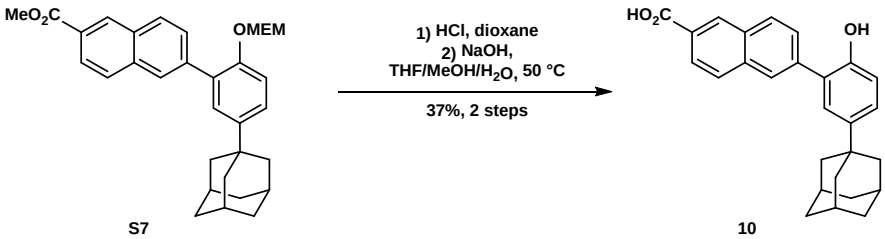

6-(5-(adamantan-1-yl)-2-hydroxyphenyl)-2-naphthoic acid (10). MEM ether **S7** (34 mg, 0.068 mmol) was dissolved in 4M HCl in dioxane (1 mL), and stirred for 2 hours at room temperature. The solution was concentrated under reduced pressure, then dissolved in 1:1 THF:MeOH (2 mL) and 1M NaOH was added (0.34 mL, 0.34 mmol), and this reaction was heated to 50 °C overnight. The following day, the reaction was acidified with 1M HCl (pH 1) and extracted with EtOAc 3x. The combined organic layers were washed with brine, dried over Na_2SO_4, filtered, concentrated, and purified by column chromatography (0 to 3% MeOH/0.1% AcOH/CH_2Cl_2, loaded in EtOAc), yielding the title compound as a white solid (10 mg, 37% yield over two steps). **^{1}H NMR** (500 MHz, DMSO) δ 13.06 (br s, 1H), 9.47 (br s, 1H), 8.60 (d, J = 0.7 Hz, 1H), 8.13 – 8.07 (m, 2H), 8.04 (d, J = 8.8 Hz, 1H), 7.97 (dd, J = 8.5, 1.6 Hz, 1H), 7.82 (dd, J = 8.5, 1.7 Hz, 1H), 7.32 (d, J = 2.5

Hz, 1H), 7.20 (dd, J = 8.5, 2.5 Hz, 1H), 6.93 (d, J = 8.5 Hz, 1H), 2.04 (s, 3H), 1.88 (d, J = 2.7 Hz, 6H), 1.72 (s, 6H); **^{13}C NMR** (100 MHz, DMSO) δ 167.56, 152.33, 142.08, 139.35, 135.05, 130.83, 130.18, 128.88, 128.46, 128.32, 127.73, 127.14, 126.89, 126.48, 125.35, 125.18, 115.82, 42.88, 36.23, 35.11, 28.41; **HRMS** Accurate mass (ES+): Found 399.1957, $C_{27}H_{27}O_3$ (M+H+) requires 399.1960.

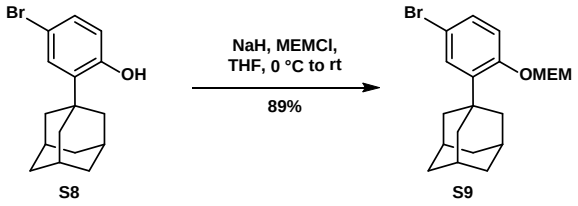

1-(5-bromo-2-((2-methoxyethoxy)methoxy)phenyl)adamantane (S9). To a suspension of sodium hydride (60% in mineral oil, 53 mg, 1.33 mmol) in THF (3 mL) at 0 °C was added phenol **S8**[56] (314 mg, 1.02 mmol) dissolved in THF (2 mL). The solution was warmed to room temperature and stirred for one hour, at which time MEMCl (0.19 mL, 1.64 mmol) was added dropwise, and the reaction was stirred for two hours at room temperature. The reaction was quenched with water, and extracted with EtOAc 3x. The combined organic layers were washed with water then brine, dried over Na_2SO_4, filtered, concentrated, and purified by column chromatography, yielding the title compound as a white solid (361 mg, 89% yield). **^{1}H NMR** (500 MHz, $CDCl_3$) δ 7.31 (d, J = 2.5 Hz, 1H), 7.23 (dd, J = 8.7, 2.5 Hz, 1H), 7.04 (d, J = 8.7 Hz, 1H), 5.28 (s, 2H), 3.87 – 3.79 (m, 2H), 3.59 – 3.56 (m, 2H), 3.39 (s, 3H), 2.06 (s, 9H), 1.76 (s, 6H); **^{13}C NMR** (125 MHz, $CDCl_3$) δ 155.68, 140.93, 129.95, 129.55, 116.49, 114.54, 93.51, 71.62, 67.91, 59.11, 40.52, 37.31, 37.02, 29.03; **HRMS** Accurate mass (ES+): Found 417.1036, $C_{20}H_{27}{}^{79}BrO_3Na$ (M+Na+) requires 417.1041.

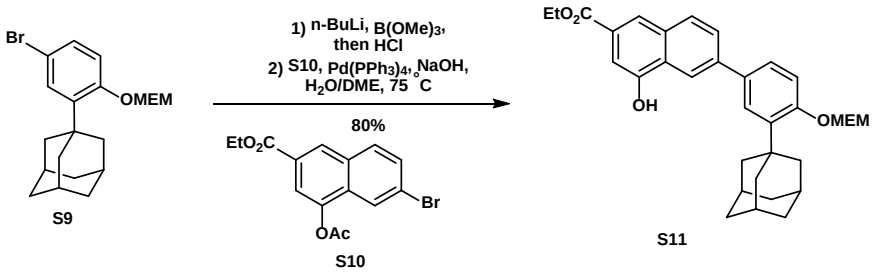

Ethyl 6-(3-(adamantan-1-yl)-4-((2-methoxyethoxy)methoxy)phenyl)-4-hydroxy-2-naphthoate (S11). *General procedure A:* To a solution of bromide **S9** (68 mg, 0.172 mmol) in THF (2 mL) at -78 °C was added *n*-BuLi (2.40 M in hexanes, 0.036 mL, 0.087 mmol) dropwise and then stirred for 15 minutes at -78 °C, over which time the reaction turned blue. $B(OMe)_3$ was then added dropwise, and the reaction stirred for an additional hour at -78 °C, then warmed to room temperature, over which time the reaction turned maroon. After one hour at room temperature, 0.1 M HCl was added (2 mL) and the reaction was stirred for an additional 30 minutes. Water was added, and the solution was extracted with EtOAc 3x. The combined organic layers were washed with brine, dried over Na_2SO_4, filtered, concentrated and purified by column chromatography (EtOAc/hexanes then MeOH/CH_2Cl_2). The intended boronic acid product also contained another similar compound, presumably a borate oligomer of the material (Rf = 0.75 in 5% MeOH/ 95% CH_2Cl_2, stains red in vanillin), both of which reacted in the following step. The boronic acid mixture was then dissolved in DME (2 mL), then naphthyl bromide **S10**[57] (53 mg, 0.143 mmol), and 1M NaOH (0.72 mL, 0.72 mmol) were added, then argon was bubbled through the mixture for 5 minutes. After degassing, $Pd(PPh_3)_4$ (5 mg, 0.004 mmol) was added, and the reaction was heated to 75 °C for 4 hours, at which time another portion of 1M NaOH (0.72 mL, 0.72 mmol) was added, to ensure complete acetate hydrolysis. After 2 additional hours, the reaction was complete by TLC and **S10** was consumed. Water and EtOAc were added, and the aqueous layer was extracted with EtOAc 3x. The combined organic layers were washed with brine, dried over Na_2SO_4, filtered, concentrated, and purified by column chromatography, yielding the title compound as a white foam (64 mg, 80% yield with respect to **S10**). **^{1}H NMR** (500 MHz, $CDCl_3$) δ 8.40 (s, 1H), 8.21 (s, 1H), 7.95 (d, J = 8.6 Hz, 1H), 7.79 (dd, J = 8.5, 1.8 Hz, 1H), 7.65 – 7.60 (m, 2H), 7.53 (dd, J = 8.5, 2.3 Hz, 1H), 7.27 (d, J = 8.4 Hz, 1H),

6.64 (br s, 1H), 5.38 (s, 2H), 4.46 (q, J = 7.1 Hz, 2H), 3.95 – 3.88 (m, 2H), 3.69 – 3.62 (m, 2H), 3.44 (s, 3H), 2.19 (d, J = 2.0 Hz, 6H), 2.10 (s, 3H), 1.80 (s, 6H), 1.46 (t, J = 7.1 Hz, 3H); **^{13}C NMR** (125 MHz, $CDCl_3$) δ 167.41, 156.59, 152.38, 140.70, 139.06, 134.07, 132.71, 129.68, 127.39, 126.96, 126.23, 126.08, 123.35, 119.37, 115.19, 108.12, 93.51, 71.80, 67.97, 61.48, 59.21, 40.85, 37.40, 37.23, 29.23, 14.51; **HRMS** Accurate mass (ES+): Found 531.2758, $C_{33}H_{39}O_6$ (M+H+) requires 531.2747.

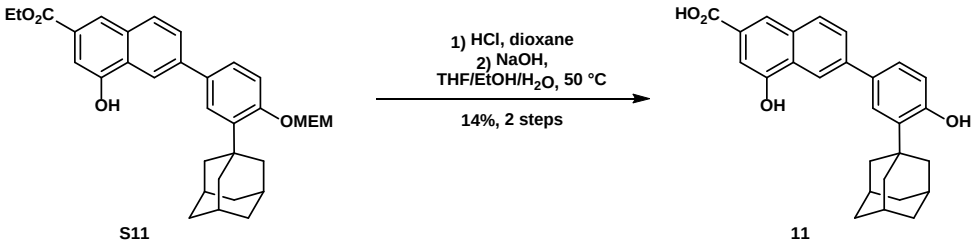

S11 11

6-(3-(adamantan-1-yl)-4-hydroxyphenyl)-4-hydroxy-2-naphthoic acid (11). *General procedure B:* MEM ether **S11** (20 mg, 0.038 mmol) was dissolved in 4M HCl in dioxane (2 mL) and the reaction was stirred at room temperature overnight. The reaction was quenched with water and extracted with EtOAc 3x. The combined organic layers were washed with brine, dried over Na_2SO_4, filtered, and concentrated. The crude intermediate was dissolved in 2:1 EtOH/THF (1.5 mL) and 1N NaOH was added (0.2 mL), the mixture was heated to 50°C and stirred overnight. The reaction was cooled to room temperature, acidified (pH 1) with 1M HCl and extracted with EtOAc 3x. The combined organic layers were washed with brine, dried over Na_2SO_4, filtered, concentrated, and purified by column chromatography (0→6% MeOH/0.1%AcOH/CH_2Cl_2) yielding the title compound as a white solid (2.1 mg, 14% over two steps). **^{1}H NMR** (500 MHz, CD_3CN) δ 8.33 (d, J = 1.9 Hz, 1H), 8.14 (s, 1H), 8.00 (d, J = 8.5 Hz, 1H), 7.84 (dd, J = 8.6, 1.9 Hz, 1H), 7.58 (d, J = 2.4 Hz, 1H), 7.47 (dd, J = 8.2, 2.4 Hz, 1H), 7.37 (d, J = 1.4 Hz, 1H), 6.88 (d, J = 8.2 Hz, 1H), 2.22 – 2.19 (m, 6H), 2.10 – 2.07 (m, 3H), 1.81 (t, J = 2.8 Hz, 6H); **^{13}C NMR** (100 MHz, CD_3CN) δ 167.87, 156.85, 153.83, 141.36, 137.78, 133.46, 132.88, 130.63, 128.30, 128.17, 127.45, 126.85, 126.61, 123.50, 119.26, 108.29, 41.05, 37.74, 30.04; **HRMS** Accurate mass (ES+): Found 415.1906, $C_{27}H_{27}O_4$ (M+H+) requires 415.1909.

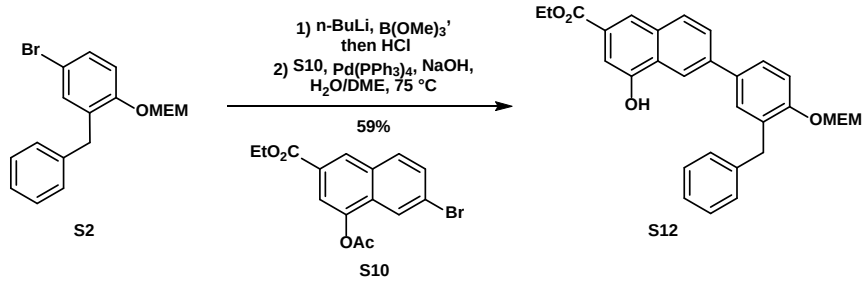

S2 S10 S12

Ethyl 6-(3-benzyl-4-((2-methoxyethoxy)methoxy)phenyl)-4-hydroxy-2-naphthoate (S12). Following general procedure A, bromide **S2** (40 mg, 0.114 mmol) and naphthyl bromide **S10** (32 mg, 0.095 mmol) yielded the title compound as a clear oil (26 mg, 59% yield with respect to **S10**). **^{1}H NMR** (400 MHz, $CDCl_3$) δ 8.35 (s, 1H), 8.20 (s, 1H), 7.93 (d, J = 8.5 Hz, 1H), 7.75 (dd, J = 8.5, 1.8 Hz, 1H), 7.60 – 7.54 (m, 2H), 7.48 (d, J = 1.2 Hz, 1H), 7.26 – 7.23 (m, 5H), 7.20 – 7.14 (m, 1H), 5.80 (br s, 1H), 5.30 (s, 2H), 4.43 (q, J = 7.1 Hz, 2H), 4.07 (s, 2H), 3.69 – 3.61 (m, 2H), 3.53 – 3.45 (m, 2H), 3.36 (s, 3H), 1.44 (t, J = 7.1 Hz, 3H); **^{13}C NMR** (125 MHz, $CDCl_3$) δ 167.48, 155.01, 152.52, 141.04, 139.89, 134.27, 132.74, 130.62, 129.92, 129.71, 128.90, 128.39, 127.45, 126.79, 126.70, 125.98, 123.20, 119.40, 114.45, 108.12, 93.20, 71.70, 67.67, 61.52, 59.12, 36.70, 29.84, 14.49; **HRMS** Accurate mass (ES+): Found 487.2126, $C_{30}H_{31}O_6$ (M+H+) requires 487.2121.

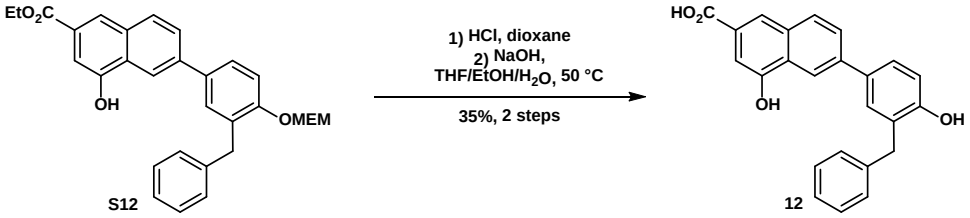

6-(3-benzyl-4-hydroxyphenyl)-4-hydroxy-2-naphthoic acid (12). Following general procedure B, MEM ether **S12** (25 mg, .055 mmol) yielded the title compound as a yellow residue (7.0 mg, 35% yield over two steps). **^{1}H NMR** (500 MHz, CD_3CN) δ 8.31 (s, 1H), 8.15 (d, J = 14.7 Hz, 1H), 8.01 – 7.93 (m, 1H), 7.83 – 7.77 (m, 1H), 7.58 (d, J = 1.9 Hz, 1H), 7.54 – 7.50 (m, 1H), 7.37 (s, 1H), 7.28 (q, J = 8.1 Hz, 4H), 7.18 (t, J = 6.9 Hz, 1H), 6.95 (d, J = 8.3 Hz, 1H), 4.02 (s, 2H); **^{13}C NMR** (125 MHz, CD_3CN) δ 172.55, 167.98, 155.76, 153.85, 142.27, 140.70, 133.53, 133.20, 130.65, 129.69, 129.46, 129.31, 128.27, 127.40, 127.29, 126.85, 123.49, 119.33, 116.72, 108.35, 36.52; **HRMS** Accurate mass (ES+): Found 393.1093, $C_{24}H_{18}O_4Na$ (M+Na+) requires 393.1103.

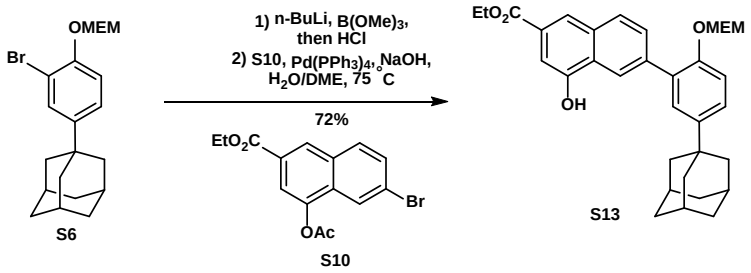

Ethyl 6-(5-(adamantan-1-yl)-2-((2-methoxyethoxy)methoxy)phenyl)-4-hydroxy-2-naphthoate (S13). Following general procedure A, bromide **S6** (66 mg, 0.167 mmol) and naphthyl bromide **S10** (47 mg, 0.139 mmol) yielded the title compound as a clear oil (53 mg, 72% yield with respect to **S10**). **^{1}H NMR** (500 MHz, $CDCl_3$) δ 8.37 (s, 1H), 8.22 (s, 1H), 7.93 (d, J = 8.4 Hz, 1H), 7.75 (d, J = 8.2 Hz, 1H), 7.58 (s, 1H), 7.42 (s, 1H), 7.31 (t, J = 11.5 Hz, 1H), 7.23 (d, J = 8.6 Hz, 1H), 6.76 (br s, 1H), 5.22 (s, 2H), 4.46 (dd, J = 13.7, 6.7 Hz, 2H), 3.73 (s, 2H), 3.50 (s, 2H), 3.34 (s, 3H), 2.10 (s, 3H), 1.94 (s, 6H), 1.77 (q, J = 11.6 Hz, 6H), 1.46 (t, J = 7.0 Hz, 3H); **^{13}C NMR** (125 MHz, $CDCl_3$) δ 167.42, 152.23, 145.60, 138.77, 132.77, 131.05, 129.56, 128.60, 127.97, 127.64, 127.03, 125.61, 123.23, 122.38, 115.46, 108.00, 94.35, 71.70, 67.88, 61.49, 59.10, 43.45, 36.88, 35.90, 29.09, 14.51; **HRMS** Accurate mass (ES+): Found 553.2562, $C_{33}H_{38}O_6Na$ (M+Na+) requires 553.2566.

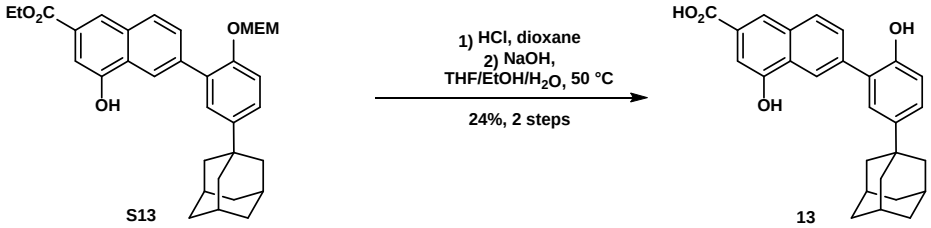

6-(5-(adamantan-1-yl)-2-hydroxyphenyl)-4-hydroxy-2-naphthoic acid (13). Following general procedure B, MEM ether **S13** (39 mg, .073 mmol) yielded the title compound as a yellow residue (7.2 mg, 24% yield over two steps). **^{1}H NMR** (500 MHz, CD_3CN) δ 8.31 (s, 1H), 8.17 (s, 1H), 7.98 (d, J = 8.5 Hz, 1H), 7.78 (dd, J = 8.5, 1.7 Hz, 1H), 7.40 – 7.35 (m, 2H), 7.24 (dd, J = 8.5, 2.5 Hz, 1H), 6.90 (d, J = 8.5 Hz, 1H), 1.97 – 1.95 (m, 6H), 1.93 – 1.90 (m, 3H), 1.81 – 1.75 (m, 6H); **^{13}C NMR** (125 MHz, CD_3CN) δ 172.64, 168.08, 153.93, 152.55, 144.70, 139.34, 133.62, 130.15, 129.69, 128.49, 128.44, 128.35, 127.93, 126.55, 123.48, 122.82, 116.84, 108.17, 44.04, 37.37, 30.04; **HRMS** Accurate mass (ES+): Found 415.1905, $C_{27}H_{27}O_4$ (M+H+) requires 415.1909.

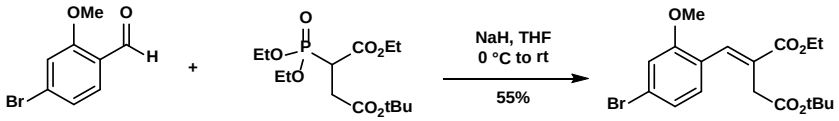

S14 S15

4-(tert-butyl) 1-ethyl (E)-2-(4-bromo-2-methoxybenzylidene)succinate (S15). To a suspension of NaH (60% in mineral oil, 176 mg, 4.6 mmol) in THF (10 mL) at 0 °C was added phosphonate **S14**[58] (1.56g, 4.6 mmol), and the solution was warmed to room temperature and stirred for 1 hour. The solution was cooled back down to 0 °C and 4-bromo-2-methoxybenzaldehyde dissolved in THF (2 mL) was added dropwise. The resulting orange suspension was allowed to warm to room temperature and stirred overnight. The following day, the solvent was concentrated and diluted with EtOAc, then washed with water 3x and brine, dried over Na_2SO_4, filtered, concentrated, and purified by column chromatography, yielding the title compound as a clear oil (731 mg, 55% yield). **^{1}H NMR** (500 MHz, $CDCl_3$) δ 7.83 (s, 1H), 7.15 (dd, J = 8.1, 0.6 Hz, 1H), 7.10 (dd, J = 8.1, 1.7 Hz, 1H), 7.04 (d, J = 1.7 Hz, 1H), 4.27 (q, J = 7.1 Hz, 2H), 3.84 (s, 3H), 3.34 (d, J = 0.6 Hz, 2H), 1.46 (s, 9H), 1.33 (t, J = 7.1 Hz, 3H); **^{13}C NMR** (100 MHz, $CDCl_3$) δ 170.52, 167.38, 158.19, 136.60, 130.77, 127.51, 123.88, 123.65, 123.44, 114.42, 81.09, 61.16, 55.92, 35.37, 28.15, 14.40; **HRMS** Accurate mass (ES+): Found 365.0007, $C_{14}H_{15}{}^{79}BrO_5Na$ (M+Na+) requires 365.0001.

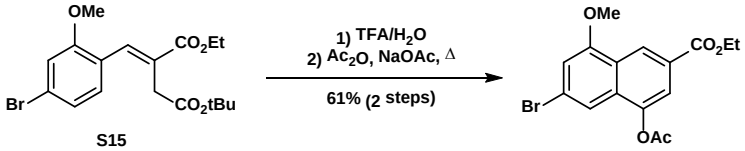

S15 S16

Ethyl 4-acetoxy-6-bromo-8-methoxy-2-naphthoate (S16). Ester **S15** (1.02g, 2.55 mmol) was dissolved in 9:1 TFA:H_2O (3 mL) and stirred at room temperature for 3.5 hours. The reaction was concentrated under reduced pressure and azeotropically dried twice with toluene. The crude oil was cooled to 0 °C and saturated $NaHCO_3$ was added (3 mL), then the mixture was acidified with 1M HCl (pH 1). The aqueous layer was extracted with EtOAc 3x, and the combined organic layers were washed with brine, dried over Na_2SO_4, filtered and concentrated, yielding the crude acid as a clear oil. The crude acid was dissolved in Ac_2O (13 mL) and sodium acetate (227 mg, 2.77 mmol) was added, and the mixture turned from pink to yellow. The reaction was refluxed for 2 hours, cooled to room temperature, and then poured into water. The yellow precipitate was filtered and washed with water. The solids were dissolved in CH_2Cl_2, washed with brine, and dried over Na_2SO_4, filtered and concentrated, yielding the title compound as a yellow solid (568 mg, 61% yield over two steps). **^{1}H NMR** (500 MHz, $CDCl_3$) δ 8.84 (dd, *J* = 1.5, 0.9 Hz, 1H), 7.86 (d, *J* = 1.6 Hz, 1H), 7.59 (dd, *J* = 1.5, 0.9 Hz, 1H), 6.97 (d, *J* = 1.6 Hz, 1H), 4.43 (q, *J* = 7.1 Hz, 1H), 4.03 (s, 1H), 2.48 (s, 1H), 1.43 (t, *J* = 7.1 Hz, 1H); **^{13}C NMR** (125 MHz, CDCl3) δ 169.12, 165.80, 157.05, 145.38, 130.60, 127.18, 124.77, 123.72, 123.23, 119.56, 115.85, 109.31, 61.41, 56.08, 21.01, 14.43; **HRMS** Accurate mass (ES+): Found 367.0162, $C_{16}H_{16}{}^{79}BrO_5$ (M+H+) requires 367.0181.

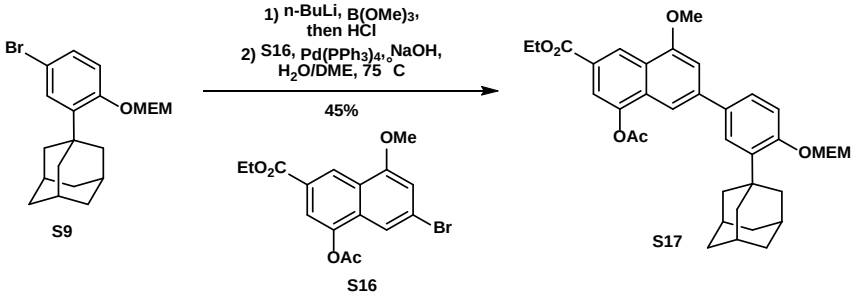

S9 S16 S17

Ethyl 4-acetoxy-6-(3-(adamantan-1-yl)-4-((2-methoxyethoxy)methoxy)phenyl)-8-methoxy-2-naphthoate (S17). Following general procedure A, bromide **S9** (43 mg, 0.109 mmol) and naphthyl bromide **S16** (30 mg, 0.090 mmol) yielded the title compound as a clear oil (21 mg, 45% yield with respect to **S16**). **^{1}H NMR** (500 MHz, $CDCl_3$) δ 8.92 (s, 1H), 7.86 (s, 1H), 7.53 (d, J = 8.4 Hz, 2H), 7.47 (d, J = 8.4 Hz, 1H), 7.29 (d, J = 8.4 Hz,

1H), 7.08 (s, 1H), 5.40 (s, 2H), 4.44 (q, J = 7.1 Hz, 2H), 4.10 (s, 3H), 3.94 – 3.86 (m, 2H), 3.67 – 3.60 (m, 2H), 3.42 (s, 3H), 2.47 (s, 3H), 2.19 (s, 6H), 2.11 (s, 3H), 1.81 (s, 6H), 1.45 (t, J = 7.1 Hz, 3H); **^{13}C NMR** (125 MHz, $CDCl_3$) δ 169.44, 166.29, 157.00, 156.80, 146.60, 143.00, 139.11, 134.51, 130.47, 126.45, 126.28, 126.18, 125.12, 123.43, 118.85, 115.16, 111.03, 105.42, 93.49, 71.74, 68.01, 61.31, 59.21, 55.94, 40.80, 37.39, 37.19, 29.82, 29.19, 21.11, 14.55; **HRMS** Accurate mass (ES+): Found 625.2781, $C_{36}H_{42}O_8Na$ (M+Na+) requires 625.2777.

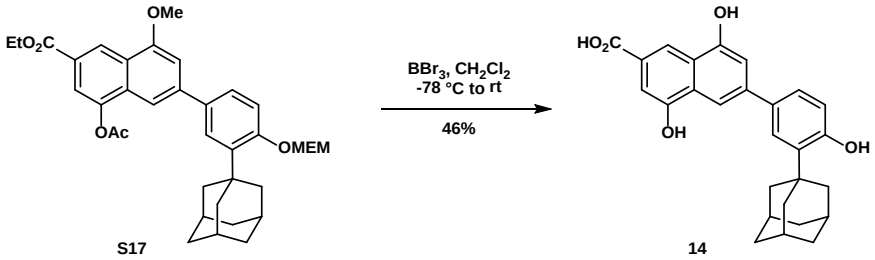

S17 14

6-(3-(adamantan-1-yl)-4-hydroxyphenyl)-4,8-dihydroxy-2-naphthoic acid (14). *General procedure C:* To a solution of MEM ether **S17** (18 mg, 0.03 mmol) dissolved in CH_2Cl_2 (2 mL) at -78 °C was added BBr_3 (1M in CH_2Cl_2, 0.24 mL, 0.24 mmol) dropwise, and the mixture was allowed to warm to room temperature and stir overnight. The reaction was quenched with water and extracted with EtOAc 3x. The combined organic layers were washed with brine, dried over Na_2SO_4, filtered, concentrated, and purified by column chromatography (0→6% MeOH/0.1%AcOH/DCM) yielding the title compound as an orange oil (7 mg, 46% yield). **^{1}H NMR** (400 MHz, CD_3CN) δ 8.37 (s, 1H), 7.85 (s, 1H), 7.55 (d, J = 2.2 Hz, 1H), 7.43 (dd, J = 8.3, 2.3 Hz, 1H), 7.34 (s, 1H), 7.23 (s, 1H), 6.87 (d, J = 8.1 Hz, 1H), 2.22 – 2.17 (m, 6H), 2.11 – 2.05 (m, 3H), 1.83 – 1.79 (m, 6H); **^{13}C NMR** (125 MHz, CD_3CN) δ 168.03, 156.86, 155.13, 153.73, 142.15, 137.68, 133.00, 129.59, 126.92, 126.69, 126.44, 124.74, 111.14, 109.72, 108.71, 41.07, 37.75, 30.07; **HRMS** Accurate mass (ES+): Found 431.1856, $C_{27}H_{27}O_5$ (M+H+) requires 431.1859.

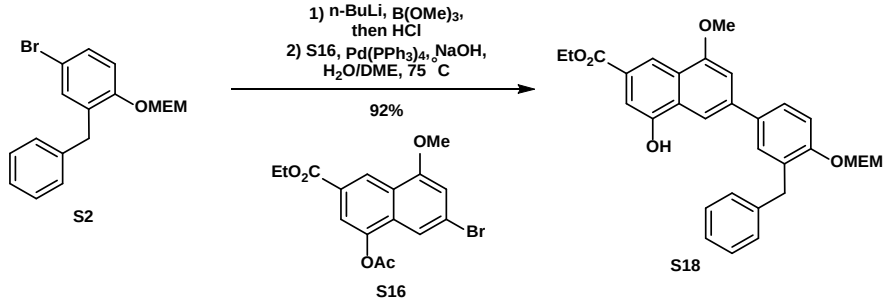

S2 S16 S18

Ethyl 6-(3-benzyl-4-((2-methoxyethoxy)methoxy)phenyl)-4-hydroxy-8-methoxy-2-naphthoate (S18). Following general procedure A, bromide **S2** (60 mg, 0.171 mmol) and naphthyl bromide **S16** (50 mg, 0.136 mmol) yielded the title compound as a clear oil (66 mg, 92% yield with respect to **S16**). **^{1}H NMR** (500 MHz, $CDCl_3$) δ 8.72 (s, 1H), 8.11 (s, 1H), 7.80 (s, 1H), 7.70 (s, 2H), 7.45 – 7.36 (m, 5H), 7.31 (s, 1H), 7.18 (s, 1H), 6.98 (br s, 1H), 5.44 (s, 2H), 4.61 (dd, J = 13.9, 6.8 Hz, 2H), 4.23 (s, 2H), 4.20 (s, 3H), 3.81 (s, 2H), 3.65 (s, 2H), 3.53 (s, 3H), 1.60 (t, J = 6.9 Hz, 3H); **^{13}C NMR** (125 MHz, $CDCl_3$) δ 167.73, 156.74, 154.97, 152.42, 141.03, 140.46, 134.80, 130.48, 129.92, 128.85, 128.34, 126.74, 126.54, 125.93, 125.04, 117.50, 114.33, 111.85, 108.96, 104.82, 93.14, 71.69, 67.62, 61.46, 59.08, 55.74, 36.69, 29.82, 14.50; **HRMS** Accurate mass (ES+): Found 517.2227, $C_{31}H_{33}O_7$ (M+H+) requires 517.2226.

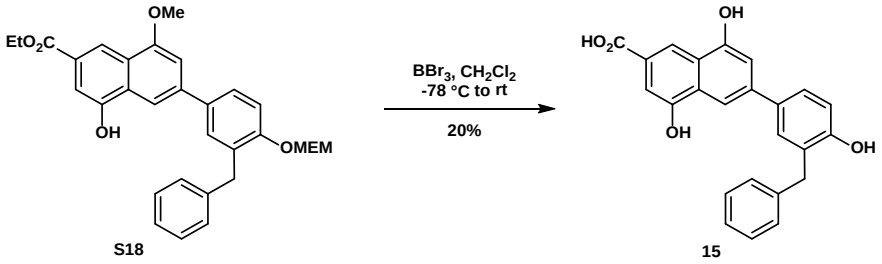

S18 15

6-(3-benzyl-4-hydroxyphenyl)-4,8-dihydroxy-2-naphthoic acid (15). Following general procedure C, MEM ether **S18** (20 mg, 0.039 mmol) yielded the title compound as an orange oil (3.0 mg, 20% yield). **^{1}H NMR** (400 MHz, CD_3CN) δ 8.36 (s, 1H), 7.82 (s, 1H), 7.76 (br s, 1H), 7.52 (d, J = 2.4 Hz, 1H), 7.47 (dd, J = 8.3, 2.4 Hz, 1H), 7.34 (d, J = 1.4 Hz, 1H), 7.33 – 7.25 (m, 5H), 7.22 – 7.11 (m, 2H), 6.94 (d, J = 8.3 Hz, 1H), 4.02 (s, 2H); **^{13}C NMR** (125 MHz, CD_3CN) δ 168.08, 155.74, 155.12, 153.74, 142.28, 141.51, 133.36, 130.48, 129.67, 129.52, 129.30, 127.26, 127.02, 126.84, 124.79, 117.86, 116.62, 111.23, 109.59, 108.71, 36.48; **HRMS** Accurate mass (ES+): Found 387.1241, $C_{24}H_{19}O_5$ (M+H+) requires 387.1233.

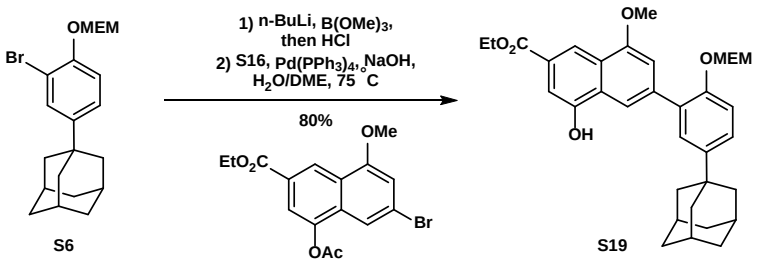

S6 S16 S19

Ethyl 6-(5-(adamantan-1-yl)-2-((2-methoxyethoxy)methoxy)phenyl)-4-hydroxy-8-methoxy-2-naphthoate (S19). Following general procedure A, bromide **S6** (68 mg, 0.172 mmol) and naphthyl bromide **S16** (53 mg, 0.143 mmol) yielded the title compound as a white foam (64 mg, 80% yield with respect to **S16**). **^{1}H NMR** (500 MHz, $CDCl_3$) δ 8.60 (s, 1H), 7.89 (s, 1H), 7.60 (s, 1H), 7.42 (d, J = 2.2 Hz, 1H), 7.33 (dd, J = 8.6, 2.1 Hz, 1H), 7.22 (d, J = 8.7 Hz, 1H), 7.10 (s, 1H), 6.49 (br s, 1H), 5.22 (s, 2H), 4.46 (q, J = 7.0 Hz, 2H), 4.03 (s, 3H), 3.75 – 3.70 (m, 2H), 3.52 – 3.48 (m, 2H), 3.34 (s, 3H), 2.10 (s, 3H), 1.94 (s, 6H), 1.77 (q, J = 12.2 Hz, 6H), 1.46 (t, J = 7.1 Hz, 3H); **^{13}C NMR** (125 MHz, $CDCl_3$) δ 167.74, 155.67, 152.48, 152.09, 145.57, 139.24, 131.66, 128.06, 127.79, 126.72, 125.54, 125.07, 117.40, 115.65, 114.67, 108.74, 107.83, 94.42, 71.65, 67.84, 61.41, 59.02, 55.73, 43.40, 36.84, 35.85, 29.05, 14.49; **HRMS** Accurate mass (ES+): Found 583.2653, $C_{34}H_{40}O_7Na$ (M+Na+) requires 583.2672.

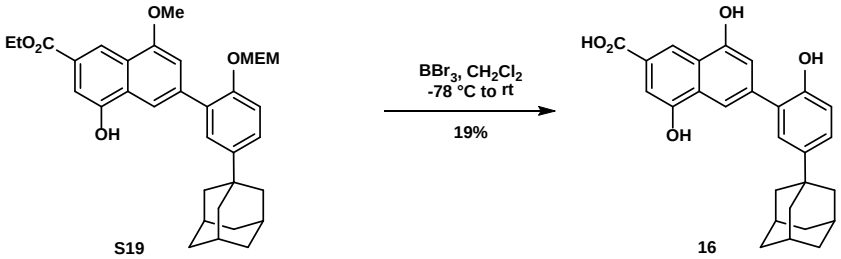

S19 16

6-(5-(adamantan-1-yl)-2-hydroxyphenyl)-4,8-dihydroxy-2-naphthoic acid (16). Following general procedure C, MEM ether **S19** (19 mg, 0.034 mmol) yielded the title compound as an orange oil (2.8 mg, 19% yield). **^{1}H NMR** (500 MHz, CD_3CN) δ 8.40 (s, 1H), 7.80 (s, 1H), 7.74 (br s, 1H), 7.35 (s, 2H), 7.29 – 7.22 (m, 1H), 7.18 (s, 1H), 6.90 (d, J = 8.4 Hz, 1H), 6.74 (br s, 1H), 2.10 – 2.03 (m, 3H), 1.96 – 1.89 (m, 6H *overlaps with CD_3CN signal*), 1.83 – 1.75 (m, 6H); **^{13}C NMR** (125 MHz, CD_3CN) δ 168.06, 154.35, 153.77, 152.45, 144.59, 139.97, 129.19, 128.52, 128.12, 127.20, 126.50, 124.90, 117.85, 116.84, 114.63, 112.47, 108.54, 44.03, 37.35, 30.02; **HRMS** Accurate mass (ES+): Found 453.1673, $C_{27}H_{26}O_5Na$ (M+Na+) requires 453.1678.

References

1. Baba, T. *et al.* Genome and virulence determinants of high virulence community-acquired MRSA. *Lancet* **359,** 1819–1827 (2002).
2. Weigel, L. M. *et al.* Genetic analysis of a high-level vancomycin-resistant isolate of *Staphylococcus aureus*. *Science* **302,** 1569–1571 (2003).
3. Kim, W. *et al.* NH125 kills methicillin-resistant *Staphylococcus aureus* persisters by lipid bilayer disruption. *Future Med. Chem.* **8,** 257–269 (2016).
4. Garsin, D. A. *et al.* A simple model host for identifying Gram-positive virulence factors. *Proc. Natl. Acad. Sci. U. S. A.* **98,** 10892–10897 (2001).
5. Rice, L. B. *et al. Enterococcus faecium* low-affinity pbp5 is a transferable determinant. *Antimicrob. Agents Chemother.* **49,** 5007–5012 (2005).
6. Carias, L. L., Rudin, S. D., Donskey, C. J. & Rice, L. B. Genetic linkage and cotransfer of a novel, *vanB*-containing transposon (Tn5382) and a low-affinity penicillin-binding protein 5 gene in a clinical vancomycin-resistant *Enterococcus faecium* isolate. *J. Bacteriol.* **180,** 4426–4434 (1998).
7. García-Solache, M. & Rice, L. B. Genome sequence of the multiantibiotic-resistant *Enterococcus faecium* Strain C68 and insights on the pLRM23 colonization plasmid. *Genome Announc.* **4,** e01719–15 (2016).
8. Thorisdottir, A. S. *et al.* IS6770, an enterococcal insertion-like sequence useful for determining the clonal relationship of clinical enterococcal isolates. *J. Infect. Dis.* **170,** 1539–1548 (1994).
9. Smith, M. G. *et al.* New insights into *Acinetobacter baumannii* pathogenesis revealed by high-density pyrosequencing and transposon mutagenesis. *Genes Dev.* **21,** 601–614 (2007).
10. Rahme, L. G. *et al.* Common virulence factors for bacterial pathogenicity in plants and animals. *Science* **268,** 1899–1902 (1995).
11. Rajamuthiah, R. *et al.* Whole animal automated platform for drug discovery against multi-drug resistant *Staphylococcus aureus*. *PLoS ONE* **9,** e89189 (2014).
12. Tan, M. W., Mahajan-Miklos, S. & Ausubel, F. M. Killing of *Caenorhabditis elegans* by *Pseudomonas aeruginosa* used to model mammalian bacterial pathogenesis. *Proc. Natl. Acad. Sci. U. S. A.* **96,** 715–720 (1999).
13. Beanan, M. J. & Strome, S. Characterization of a germ-line proliferation mutation in *C. elegans*. *Development* **116,** 755–766 (1992).
14. Hino, M. T. *et al.* SEK-1 MAPKK mediates Ca2+ signaling to determine neuronal asymmetric development in *Caenorhabditis elegans*. *EMBO reports* **3,** 56–62 (2002).
15. Moy, T. I. *et al.* High-throughput screen for novel antimicrobials using a whole animal infection model. *ACS Chem. Biol.* **4,** 527–533 (2009).
16. Kamentsky, L. *et al.* Improved structure, function and compatibility for CellProfiler: modular high-throughput image analysis software. *Bioinformatics* **27,** 1179–1180 (2011).
17. Clinical and Laboratory Standards Institute. *Methods for dilution antimicrobial susceptibility tests for bacteria that grow aerobically; approved standard-ninth edition. CLSI document M07-A9.* 1–88 (2012).
18. Keren, I., Kaldalu, N., Spoering, A., Wang, Y. & Lewis, K. Persister cells and tolerance to antimicrobials. *FEMS Microbiol. Lett.* **230,** 13–18 (2004).
19. Allison, K. R., Brynildsen, M. P. & Collins, J. J. Metabolite-enabled eradication of bacterial persisters by aminoglycosides. *Nature* **473,** 216–220 (2011).
20. Conlon, B. P. *et al.* Activated ClpP kills persisters and eradicates a chronic biofilm infection. *Nature* **503,** 365–370 (2013).
21. Conlon, B. P. *et al.* Persister formation in *Staphylococcus aureus* is associated with ATP depletion. *Nat. Microbiol.* **1,** 16051 (2016).
22. Kim, W. *et al.* Identification of an antimicrobial agent effective against methicillin-resistant *Staphylococcus aureus* persisters using a fluorescence-based screening strategy. *PLoS ONE* **10,** e0127640 (2015).
23. Cassat, J. E., Lee, C. Y. & Smeltzer, M. S. Investigation of biofilm formation in clinical isolates of *Staphylococcus aureus*. *Methods Mol. Biol.* **391,** 127–144 (2007).

24. Friedman, L., Alder, J. D. & Silverman, J. A. Genetic changes that correlate with reduced susceptibility to daptomycin in *Staphylococcus aureus*. *Antimicrob. Agents Chemother.* **50,** 2137–2145 (2006).
25. Fey, P. D. *et al.* A genetic resource for rapid and comprehensive phenotype screening of nonessential *Staphylococcus aureus* genes. *MBio* **4,** e00537–12–e00537–12 (2013).
26. Sharma-Kuinkel, B. K. *et al.* The *Staphylococcus aureus* LytSR two-component regulatory system affects biofilm formation. *J. Bacteriol.* **191,** 4767–4775 (2009).
27. Monk, I. R., Shah, I. M., Xu, M., Tan, M.-W. & Foster, T. J. Transforming the untransformable: application of direct transformation to manipulate genetically *Staphylococcus aureus* and *Staphylococcus epidermidis*. *MBio* **3,** e00277–11–e00277–11 (2012).
28. Grosser, M. R. & Richardson, A. R. in *The Genetic Manipulation of Staphylococci* **1373,** 51–57 (Springer, 2016).
29. Hess, B., Kutzner, C., van der Spoel, D. & Lindahl, E. GROMACS 4: algorithms for highly efficient, load-balanced, and scalable molecular simulation. *J. Chem. Theory Comput.* **4,** 435–447 (2008).
30. Schmid, N. *et al.* Definition and testing of the GROMOS force-field versions 54A7 and 54B7. *Eur. Biophys. J.* **40,** 843–856 (2011).
31. Malde, A. K. *et al.* An automated force field topology builder (ATB) and repository: version 1.0. *J. Chem. Theory Comput.* **7,** 4026–4037 (2011).
32. Lee, M.-T., Sun, T.-L., Hung, W.-C. & Huang, H. W. Process of inducing pores in membranes by melittin. *Proc. Natl. Acad. Sci. U. S. A.* **110,** 14243–14248 (2013).
33. Ganewatta, M. S. *et al.* Bio-inspired resin acid-derived materials as anti-bacterial resistance agents with unexpected activities. *Chem. Sci.* **5,** 2011–2016 (2014).
34. Chen, Y.-F., Sun, T.-L., Sun, Y. & Huang, H. W. Interaction of daptomycin with lipid bilayers: a lipid extracting effect. *Biochemistry* **53,** 5384–5392 (2014).
35. Joshi, S., Dewangan, R. P., Yar, M. S., Rawat, D. S. & Pasha, S. N-terminal aromatic tag induced self assembly of tryptophan–arginine rich ultra short sequences and their potent antibacterial activity. *RSC Advances* **5,** 68610–68620 (2015).
36. Berger, O., Edholm, O. & Jähnig, F. Molecular dynamics simulations of a fluid bilayer of dipalmitoylphosphatidylcholine at full hydration, constant pressure, and constant temperature. *Biophys. J.* **72,** 2002–2013 (1997).
37. Tu, Y. *et al.* Destructive extraction of phospholipids from *Escherichia coli* membranes by graphene nanosheets. *Nat. Nanotechnol.* **8,** 594–601 (2013).
38. Zhu, W. *et al.* Nanomechanical mechanism for lipid bilayer damage induced by carbon nanotubes confined in intracellular vesicles. *Proc. Natl. Acad. Sci. U. S. A.* **113,** 12374–12379 (2016).
39. Piggot, T. J., Holdbrook, D. A. & Khalid, S. Electroporation of the *E. coli* and *S. aureus* membranes: molecular dynamics simulations of complex bacterial membranes. *J. Phys. Chem. B* **115,** 13381–13388 (2011).
40. Berendsen, H. J. C., Grigera, J. R. & Straatsma, T. P. The missing term in effective pair potentials. *J. Phys. Chem.* **91,** 6269–6271 (1987).
41. Essmann, U. *et al.* A smooth particle mesh Ewald method. *J Chem Phys* **103,** 8577–8593 (1995).
42. Creighton, M. A. *et al.* Three-dimensional graphene-based microbarriers for controlling release and reactivity in colloidal liquid phases. *ACS Nano* **10,** 2268–2276 (2016).
43. Isralewitz, B., Gao, M. & Schulten, K. Steered molecular dynamics and mechanical functions of proteins. *Curr. Opin. Struct. Biol.* **11,** 224–230 (2001).
44. Kumar, S., Rosenberg, J. M., Bouzida, D., Swendsen, R. H. & Kollman, P. A. The weighted histogram analysis method for free-energy calculations on biomolecules. I. The method. *J. Comput. Chem.* **13,** 1011–1021 (1992).
45. Hub, J. S., de Groot, B. L. & van der Spoel, D. g_wham—a free weighted histogram analysis implementation including robust error and autocorrelation estimates. *J. Chem. Theory Comput.* **6,** 3713–3720 (2010).
46. Rajamuthiah, R. *et al.* A defensin from the model beetle *Tribolium castaneum* acts synergistically with telavancin and daptomycin against multidrug resistant *Staphylococcus aureus*. *PLoS ONE* **10,** e0128576

(2015).
47. Dunn, J. C., Yarmush, M. L., Koebe, H. G. & Tompkins, R. G. Hepatocyte function and extracellular matrix geometry: long-term culture in a sandwich configuration. *FASEB J.* **3,** 174–177 (1989).
48. Dunn, J. C., Tompkins, R. G. & Yarmush, M. L. Hepatocytes in collagen sandwich: evidence for transcriptional and translational regulation. *J. Cell Biol.* **116,** 1043–1053 (1992).
49. Sharma, N. S., Nagrath, D. & Yarmush, M. L. Metabolic profiling based quantitative evaluation of hepatocellular metabolism in presence of adipocyte derived extracellular matrix. *PLoS ONE* **6,** e20137 (2011).
50. Maron, D. M. & Ames, B. N. Revised methods for the *Salmonella* mutagenicity test. *Mutat. Res.* **113,** 173–215 (1983).
51. Odds, F. C. Synergy, antagonism, and what the chequerboard puts between them. *J. Antimicrob. Chemother.* **52,** 1–1 (2003).
52. Schadendorf, D. *et al.* Treatment of melanoma cells with the synthetic retinoid CD437 induces apoptosis via activation of AP-1 *in vitro*, and causes growth inhibition in xenografts *in vivo*. *J. Cell Biol.* **135,** 1889–1898 (1996).
53. Langdon, S. P. *et al.* Growth-inhibitory effects of the synthetic retinoid CD437 against ovarian carcinoma models *in vitro* and *in vivo*. *Cancer Chemother. Pharmacol.* **42,** 429–432 (1998).
54. Ponzanelli, I. *et al.* Isolation and characterization of an acute promyelocytic leukemia cell line selectively resistant to the novel antileukemic and apoptogenic retinoid 6-[3-adamantyl-4-hydroxyphenyl]-2-naphthalene carboxylic acid. *Blood* **95,** 2672–2682 (2000).
55. Williams, A. B. & Hanson, R. N. Synthesis of substituted asymmetrical biphenyl amino esters as alpha helix mimetics. *Tetrahedron* **68,** 5406–5414 (2012).
56. Liu, Z. & Xiang, J. A high yield and pilot-scale process for the preparation of adapalene. *Org Process Res Dev* **10,** 285–288 (2006).
57. Tietze, L. F., Panknin, O., Major, F. & Krewer, B. Synthesis of a novel pentagastrin-drug conjugate for a targeted tumor therapy. *Chem Eur J* **14,** 2811–2818 (2008).
58. Owton, W. M., Gallagher, P. T. & Juan-Montesinos, A. tert-Butyl 3-Carboxyethyl-3-phosphonodiethylpropionate. A novel reagent for stobbe-like condensations. *Synth. Commun.* **23,** 2119–2125 (1993).

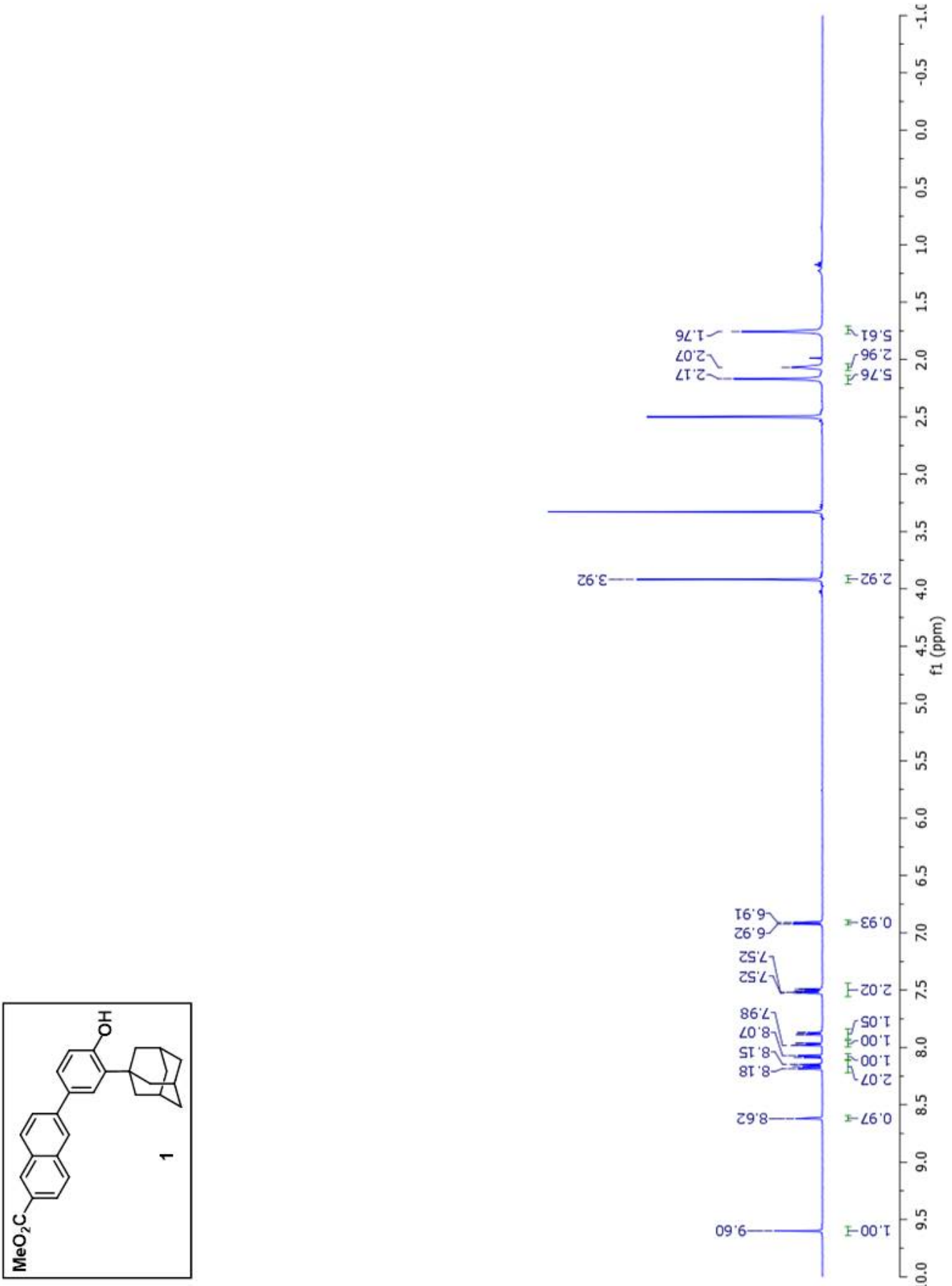

Supplementary Figure 2. ^{1}H NMR spectrum of **1** recorded in DMSO-d_6 at 500 MHz.

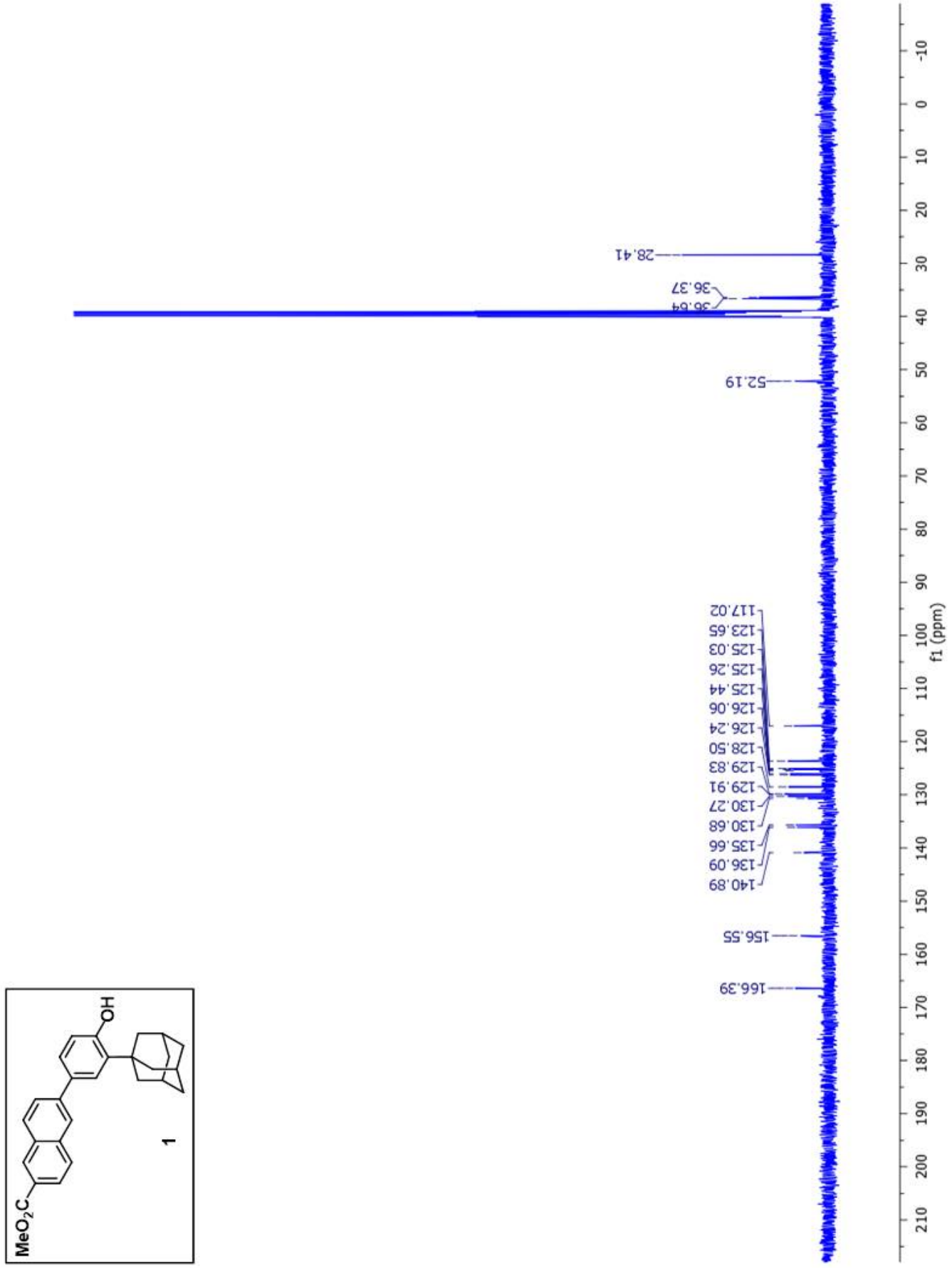

Supplementary Figure 3. ^{13}C NMR spectrum of **1** recorded in DMSO-d_6 at 125 MHz.

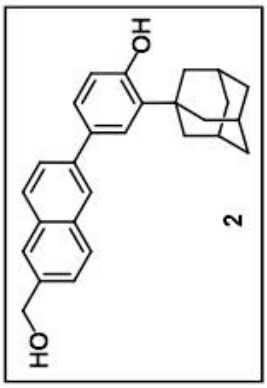

Supplementary Figure 4. ^{1}H NMR spectrum of **2** recorded in DMSO-d_6 at 500 MHz.

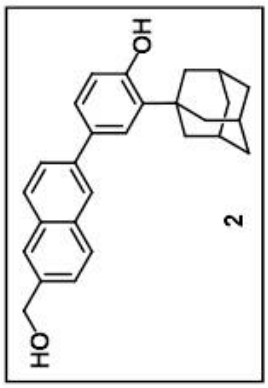

Supplementary Figure 5. ^{13}C NMR spectrum of **2** recorded in $CDCl_3$ at 150 MHz.

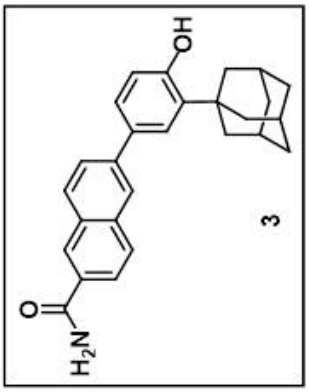

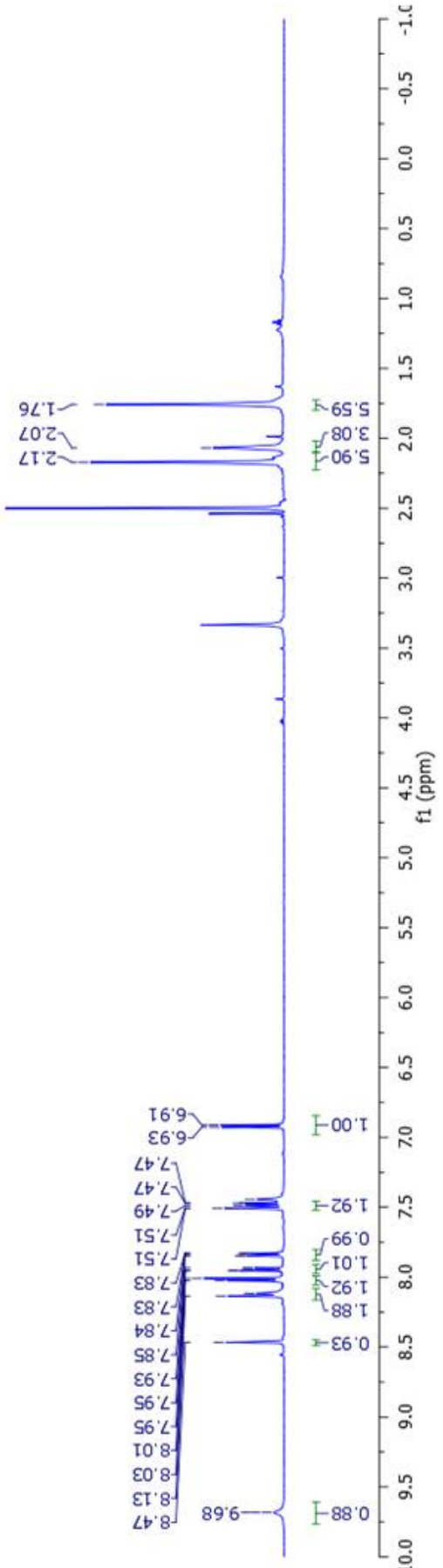

Supplementary Figure 6. ^{1}H NMR spectrum of **3** recorded in DMSO-d_6 at 500 MHz.

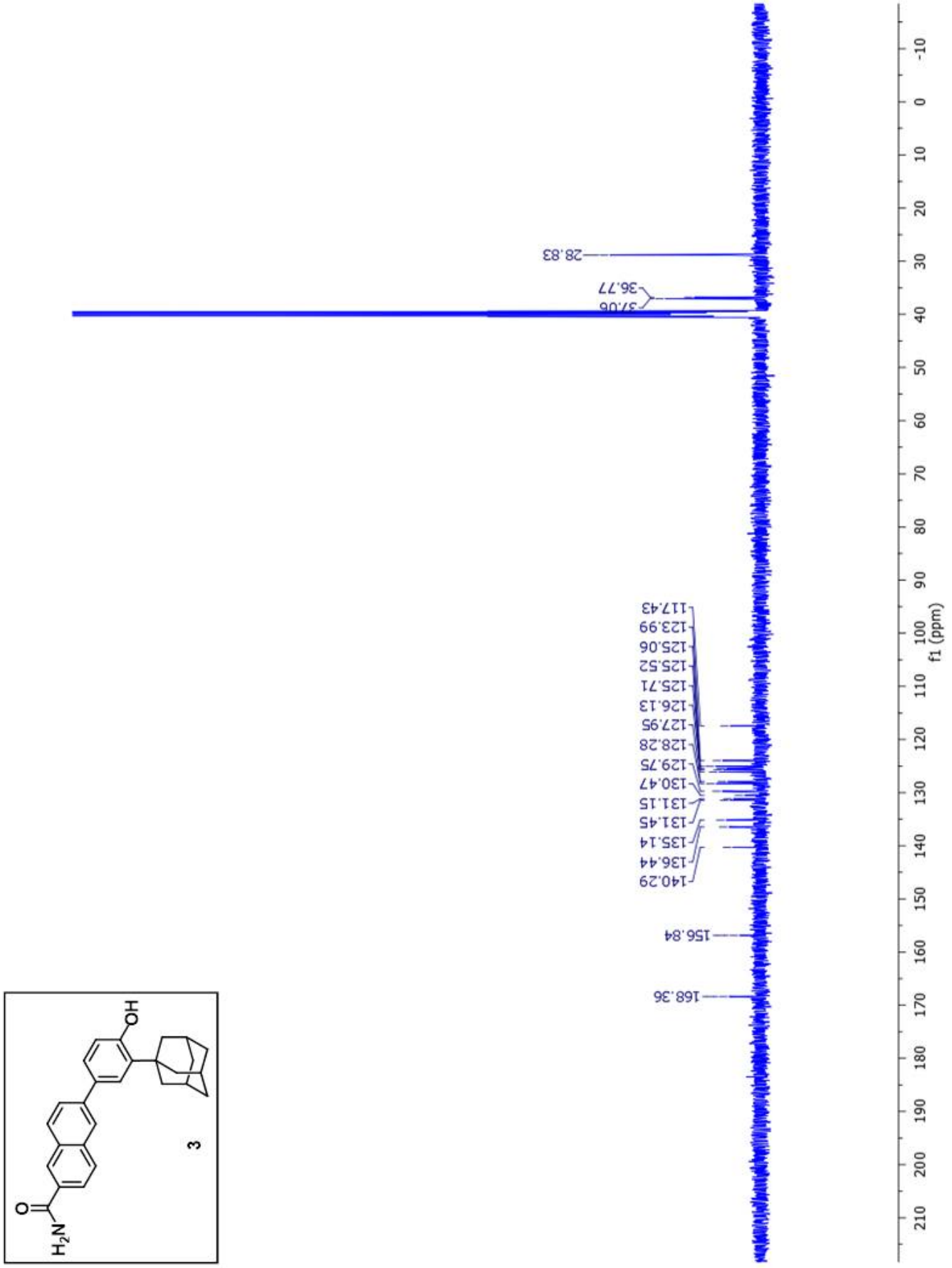

Supplementary Figure 7. ^{13}C NMR spectrum of **3** recorded in DMSO-d_6 at 125 MHz.

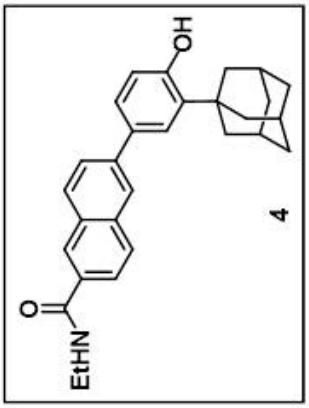

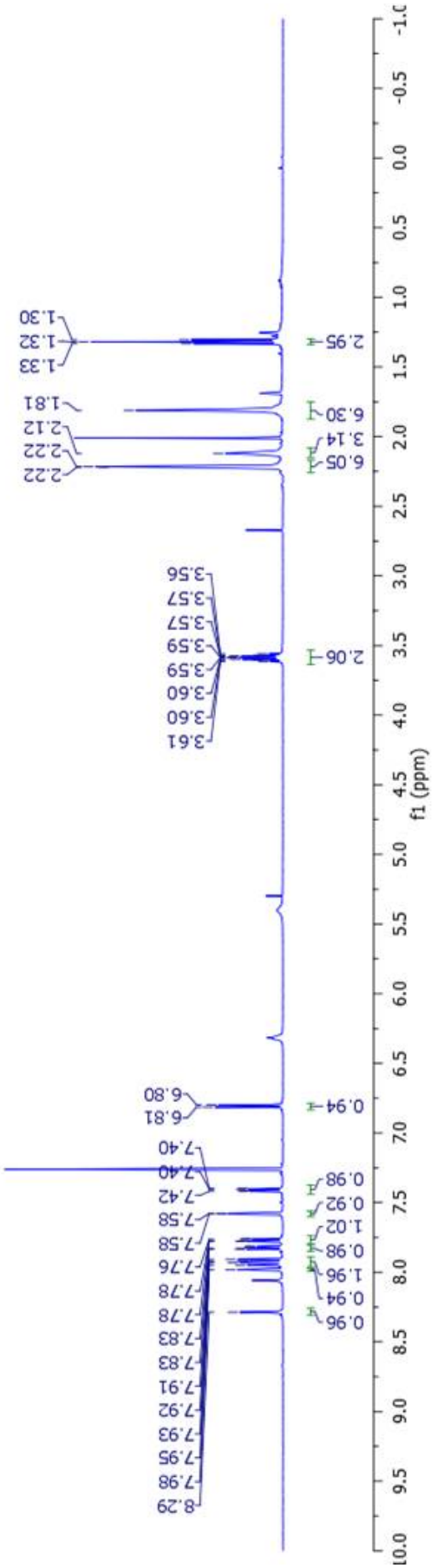

Supplementary Figure 8. ^{1}H NMR spectrum of **4** recorded in $CDCl_3$ at 500 MHz.

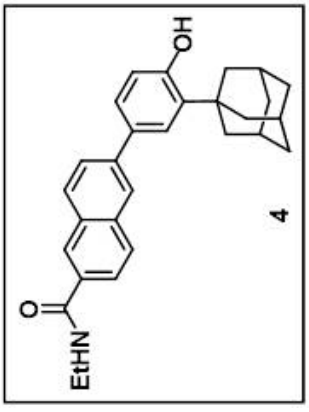

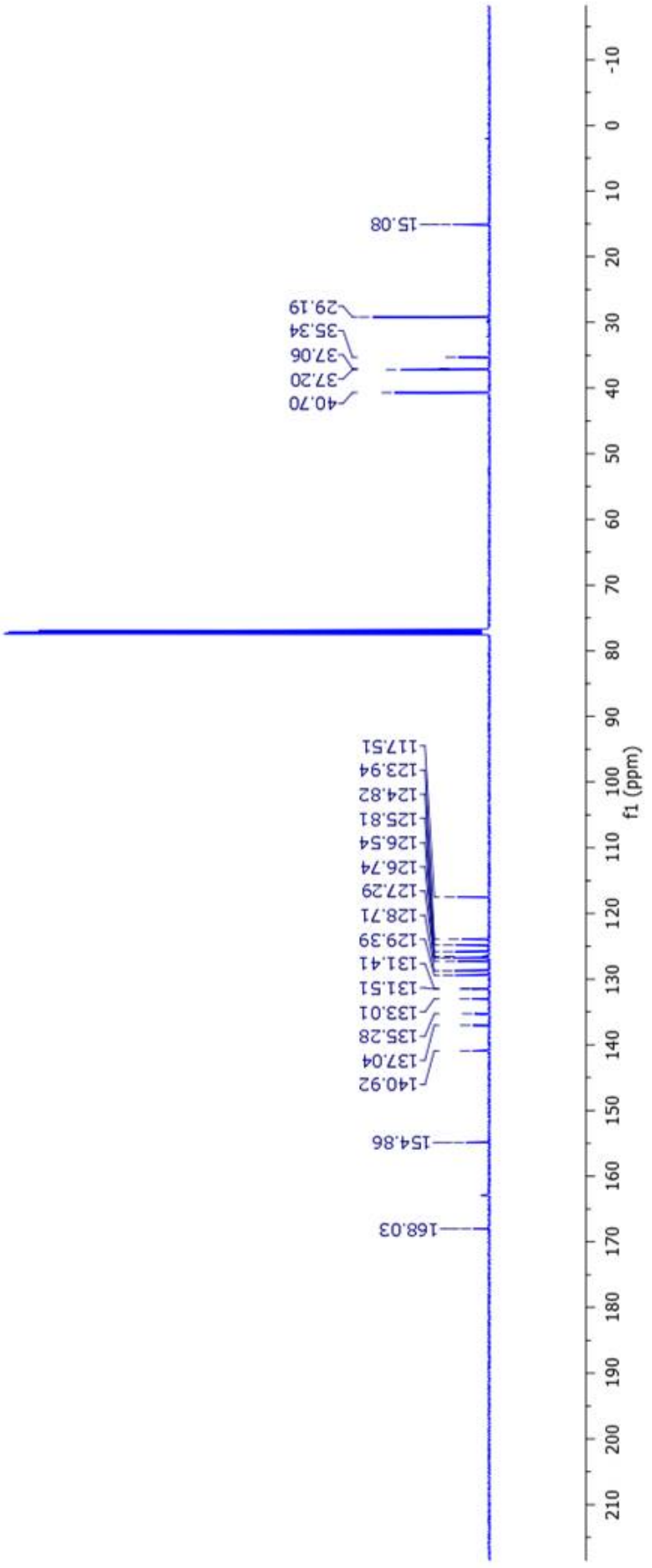

Supplementary Figure 9. ^{13}C NMR spectrum of **4** recorded in $CDCl_3$ at 125 MHz.

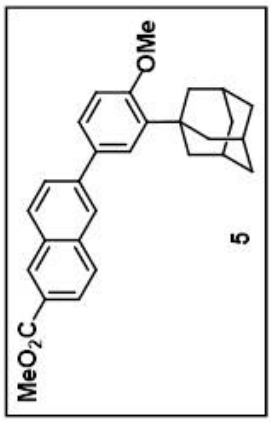

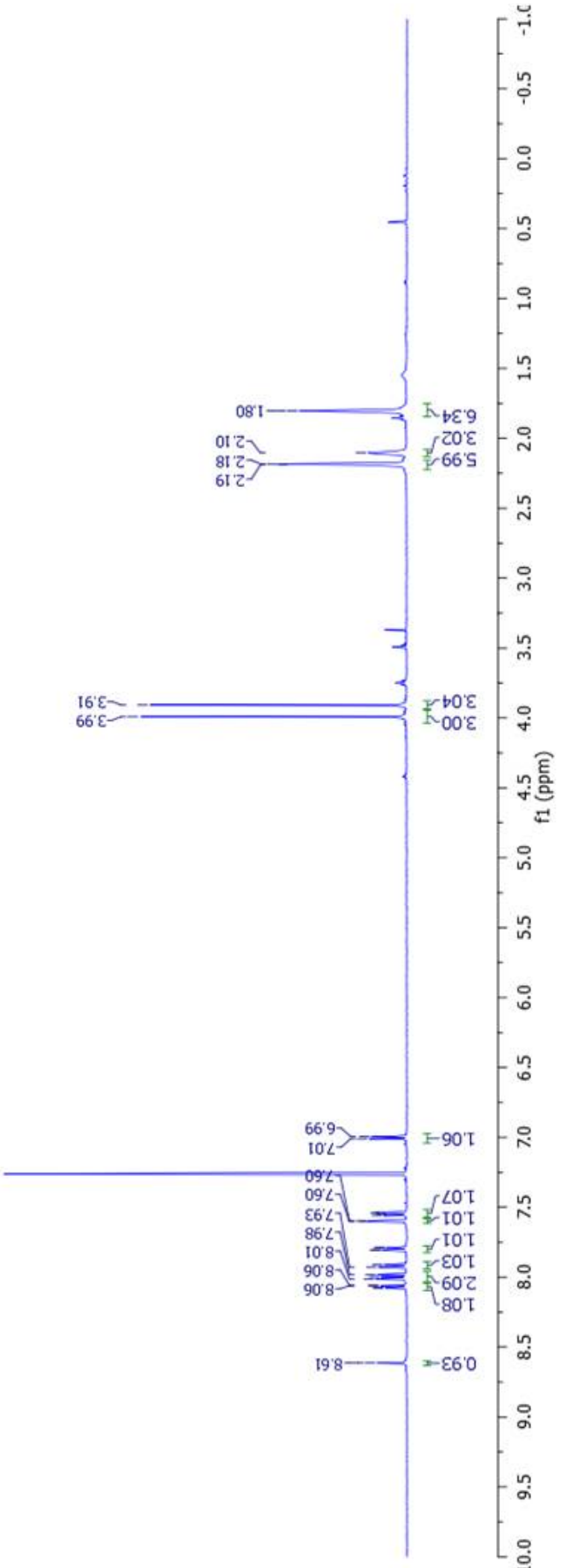

Supplementary Figure 10. ^{1}H NMR spectrum of **5** recorded in $CDCl_3$ at 500 MHz.

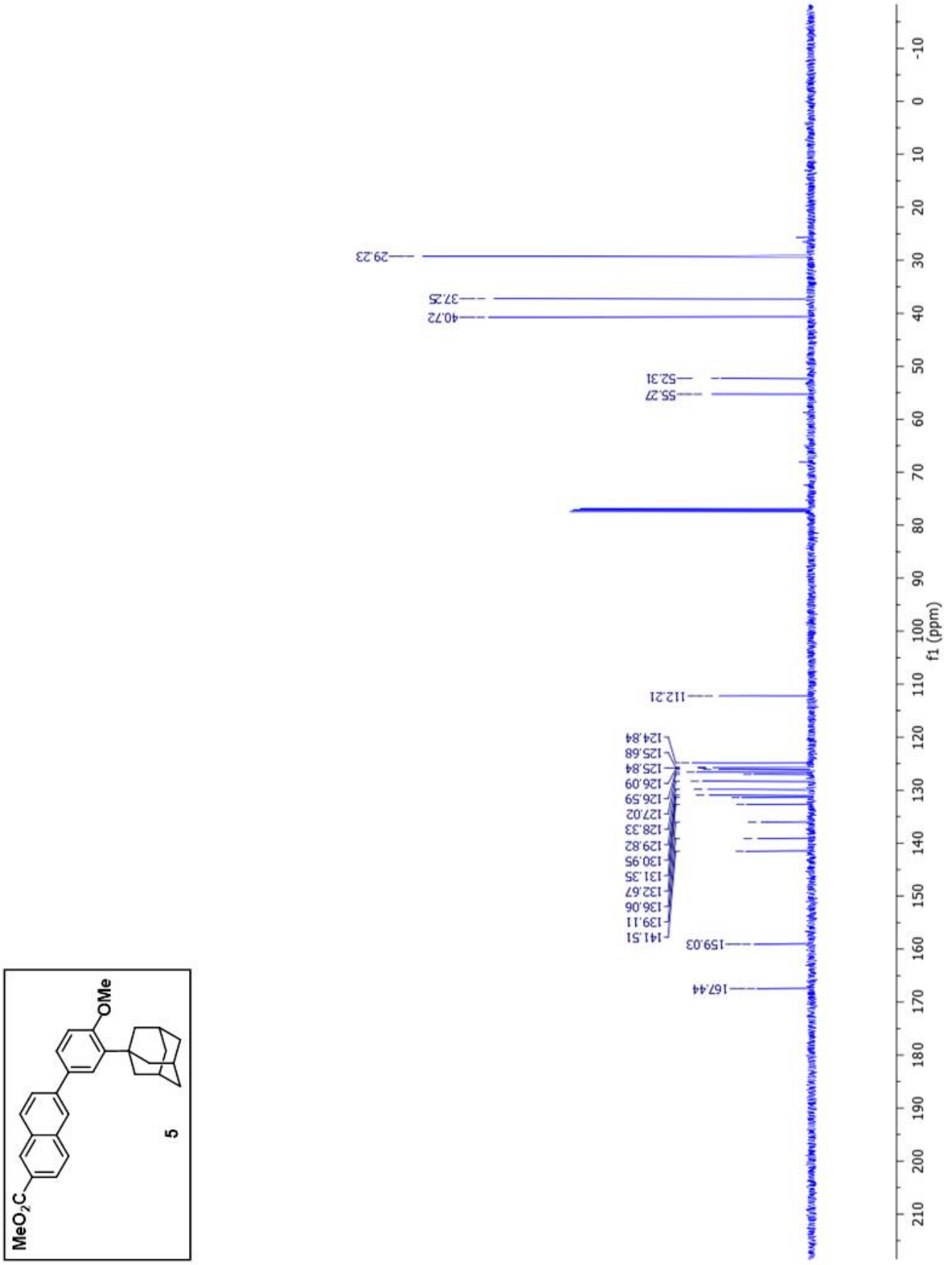

Supplementary Figure 11. ^{13}C NMR spectrum of **5** recorded in $CDCl_3$ at 125 MHz.

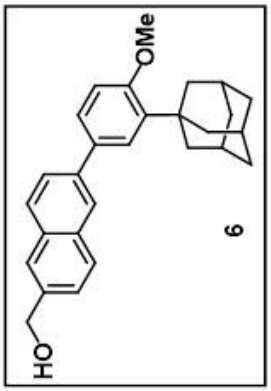

Supplementary Figure 12. ^{1}H NMR spectrum of **6** recorded in $CDCl_3$ at 500 MHz.

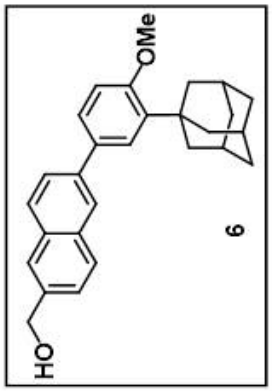

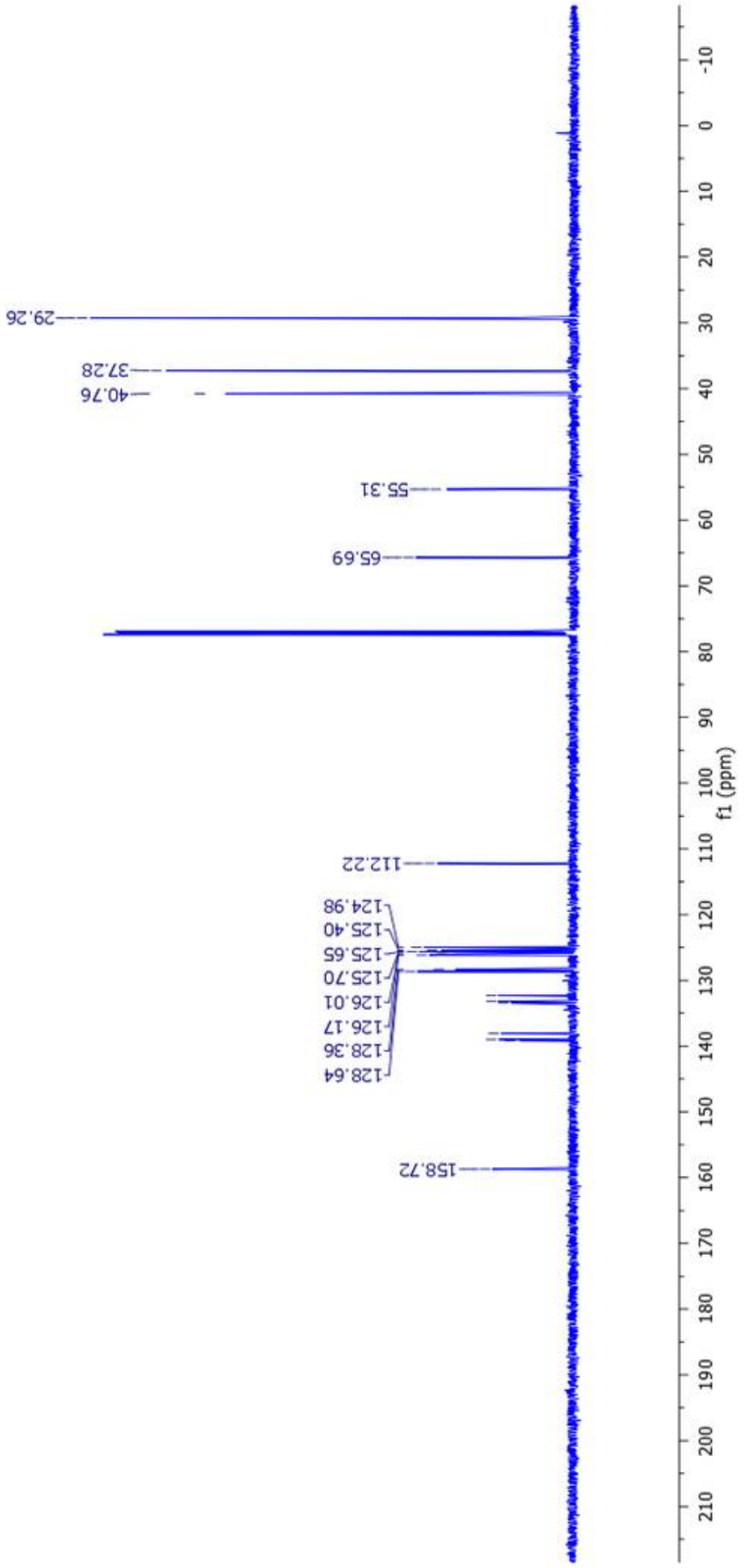

Supplementary Figure 13. ^{13}C NMR spectrum of **6** recorded in $CDCl_3$ at 125 MHz.

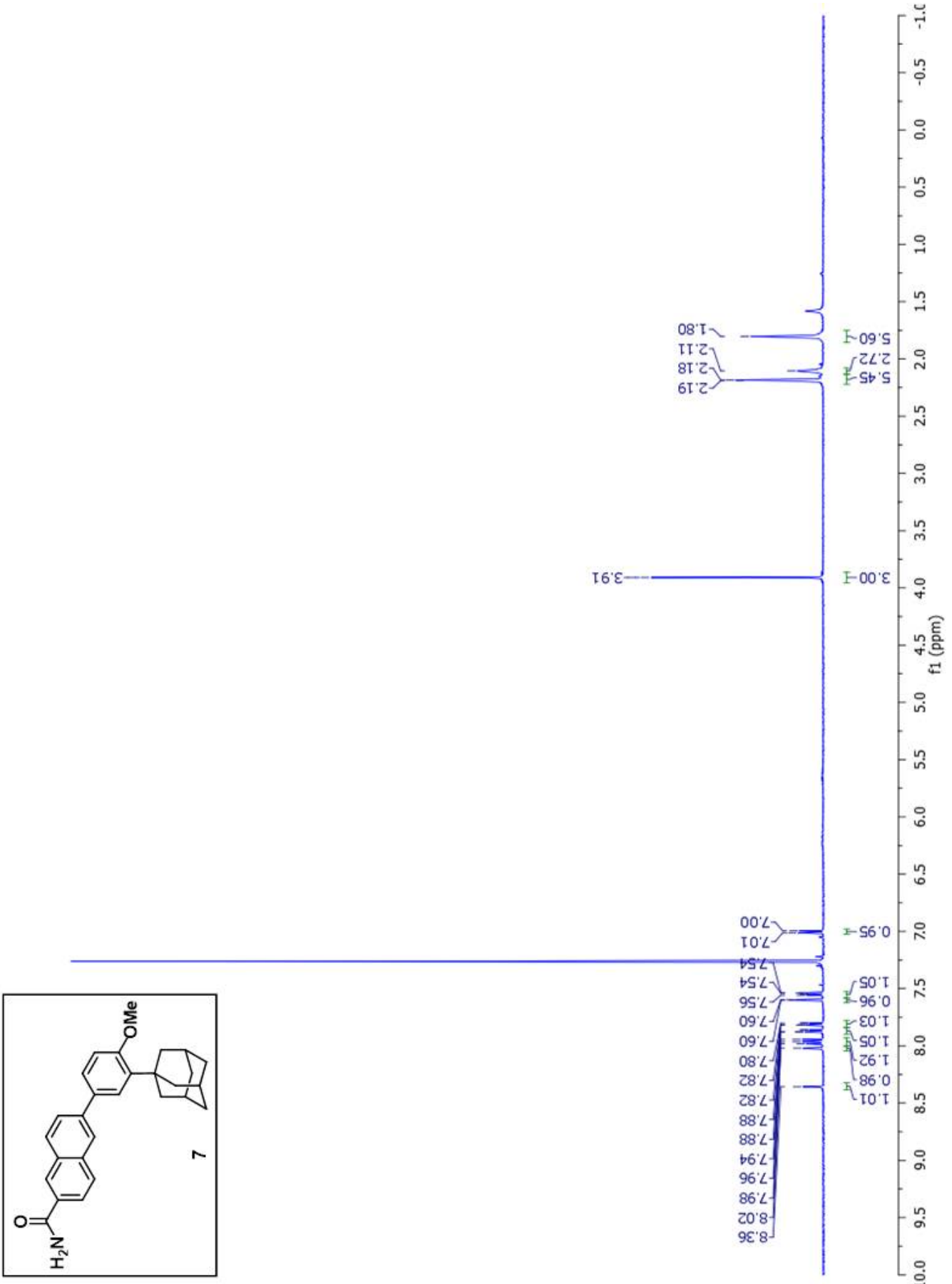

Supplementary Figure 14. ^{1}H NMR spectrum of **7** recorded in $CDCl_3$ at 500 MHz.

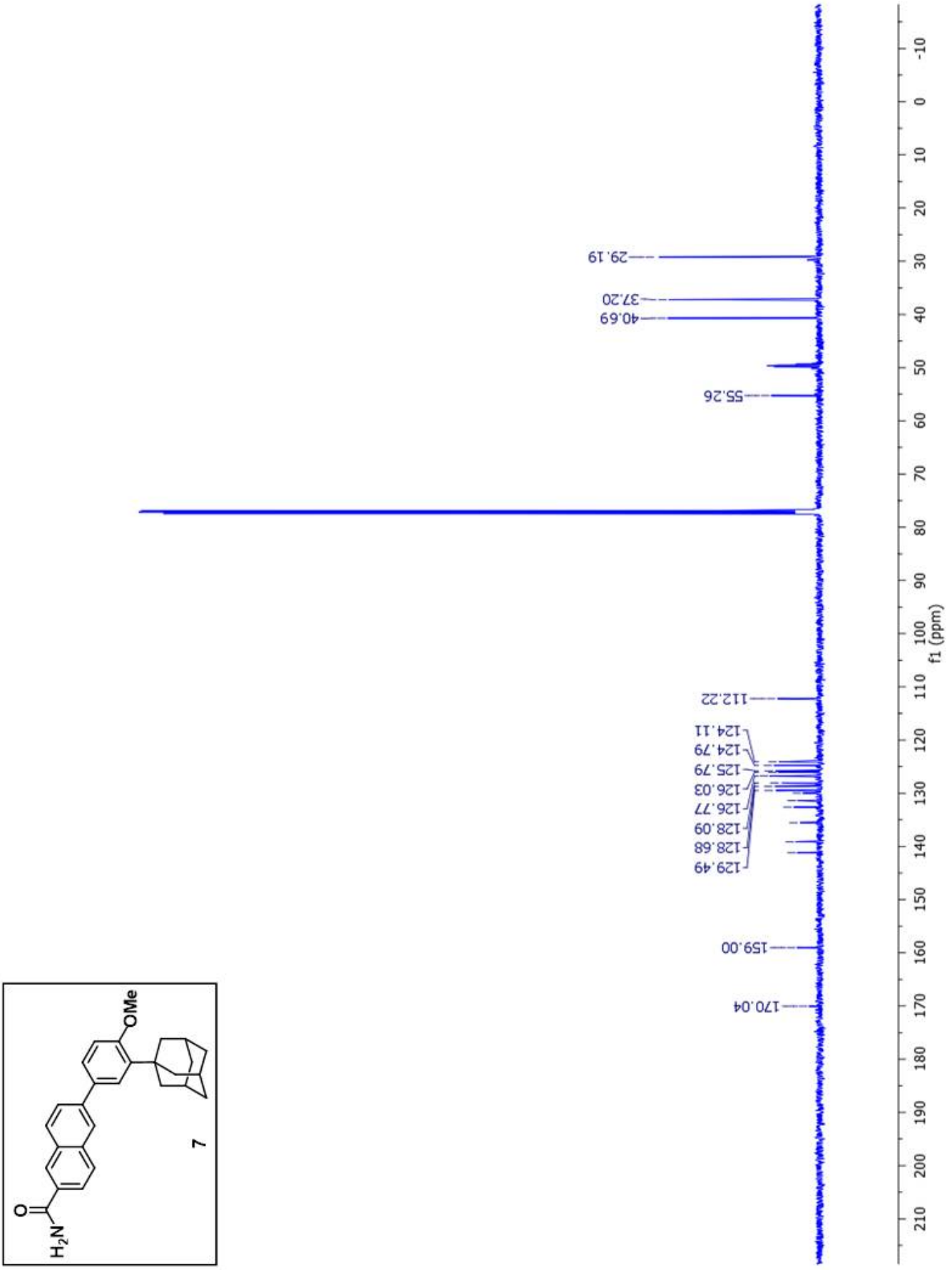

Supplementary Figure 15. ^{13}C NMR spectrum of **7** recorded in $CDCl_3$ at 125 MHz.

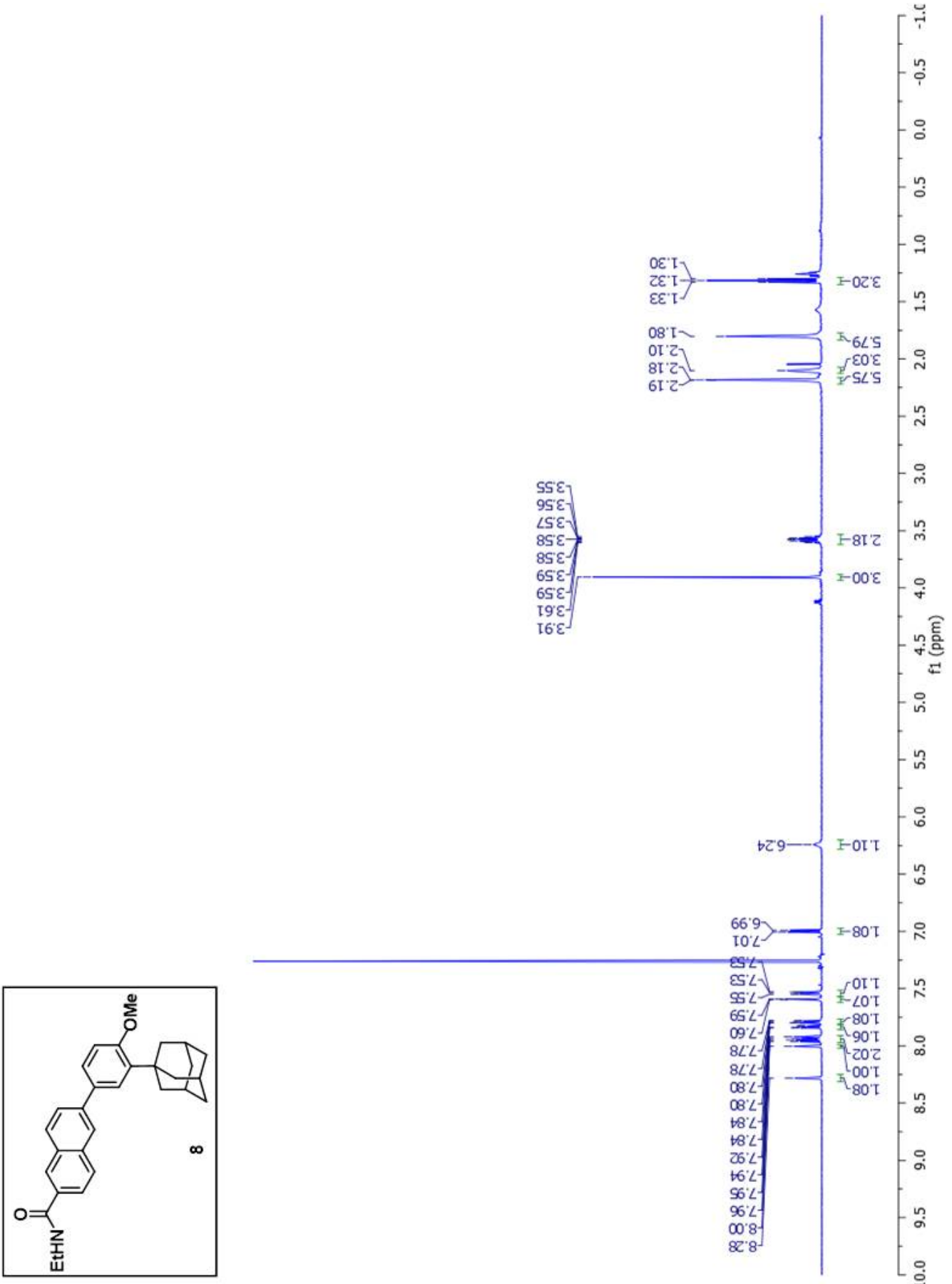

Supplementary Figure 16. ^{1}H NMR spectrum of **8** recorded in $CDCl_3$ at 500 MHz.

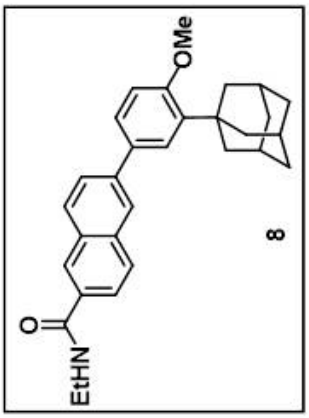

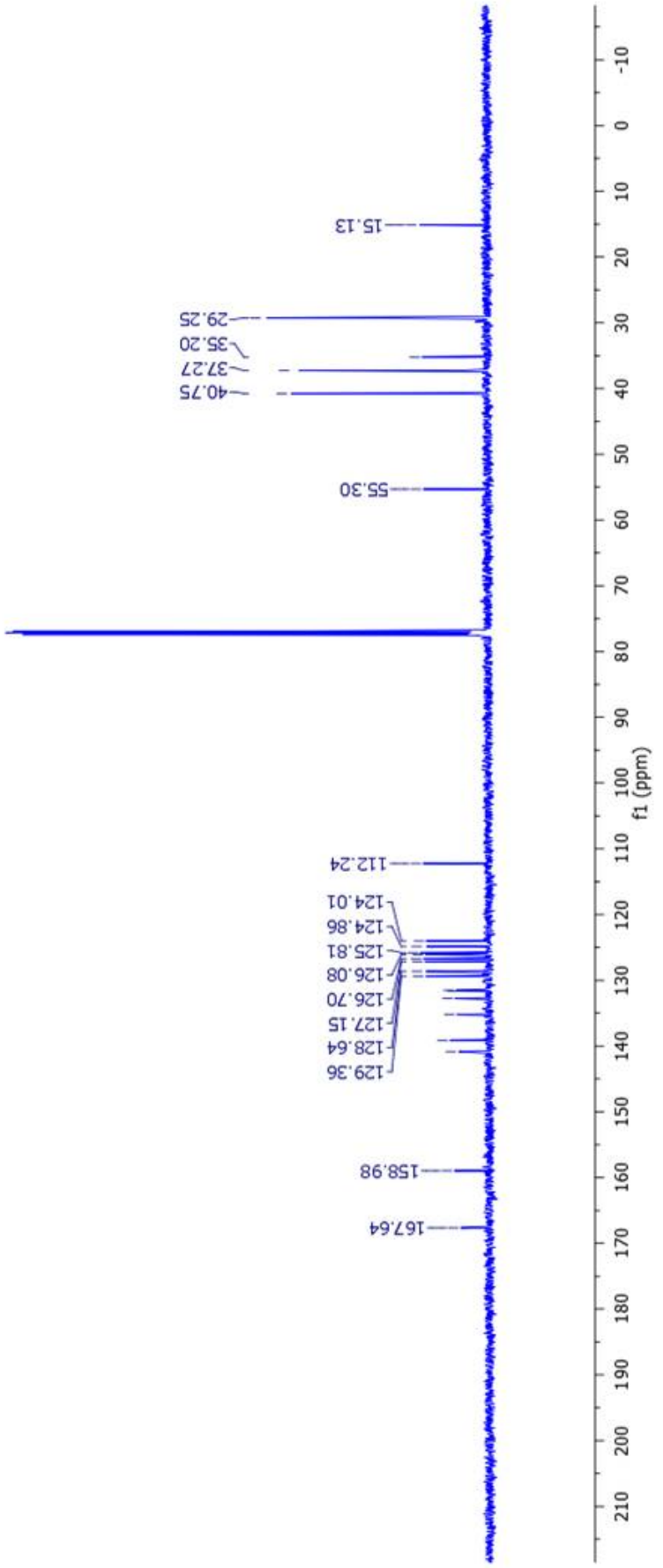

Supplementary Figure 17. ^{13}C NMR spectrum of **8** recorded in $CDCl_3$ at 125 MHz.

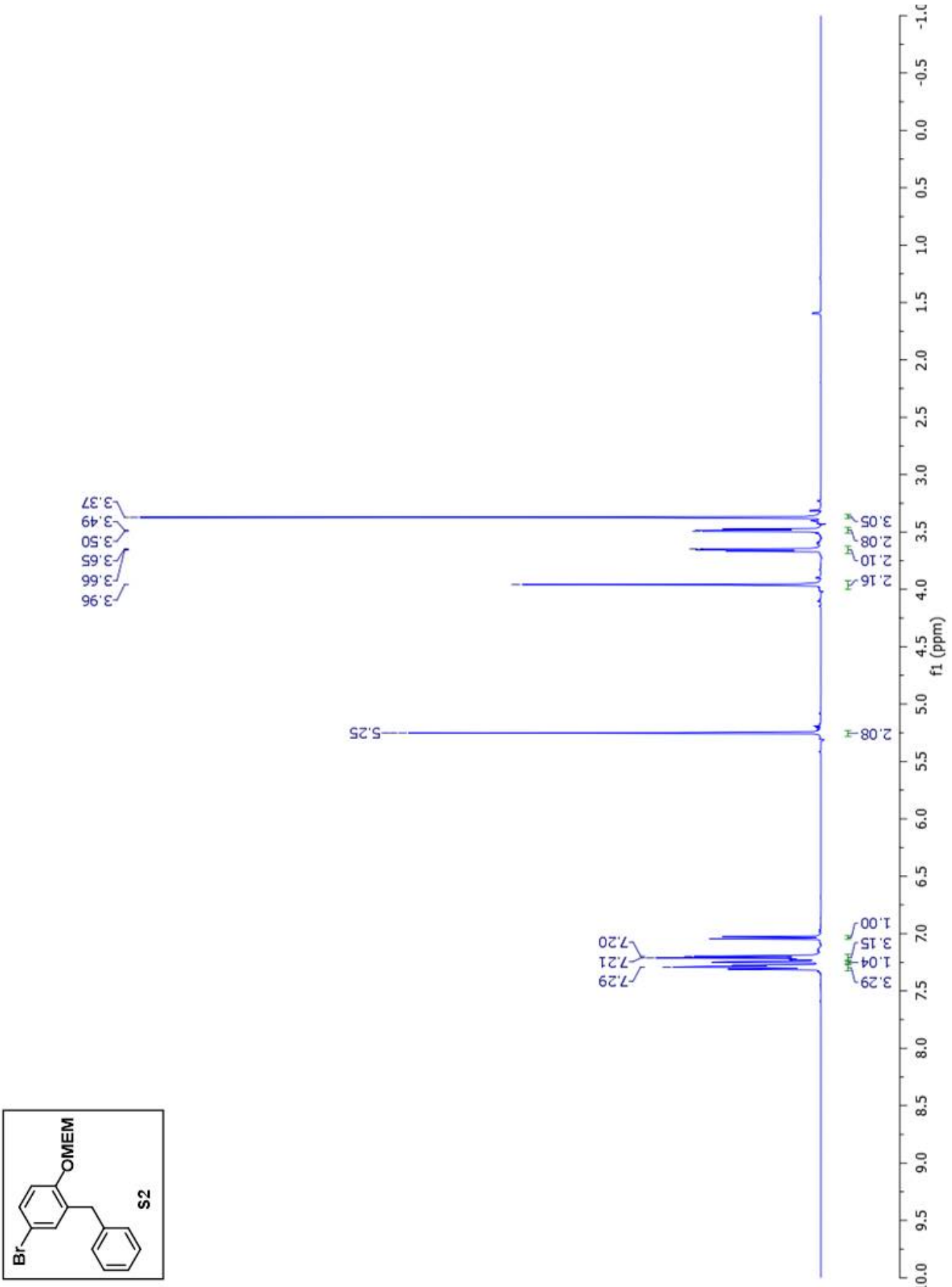

Supplementary Figure 18. ^{1}H NMR spectrum of **S2** recorded in $CDCl_3$ at 500 MHz.

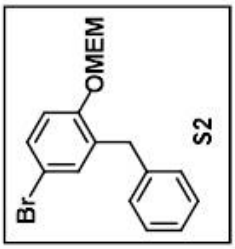

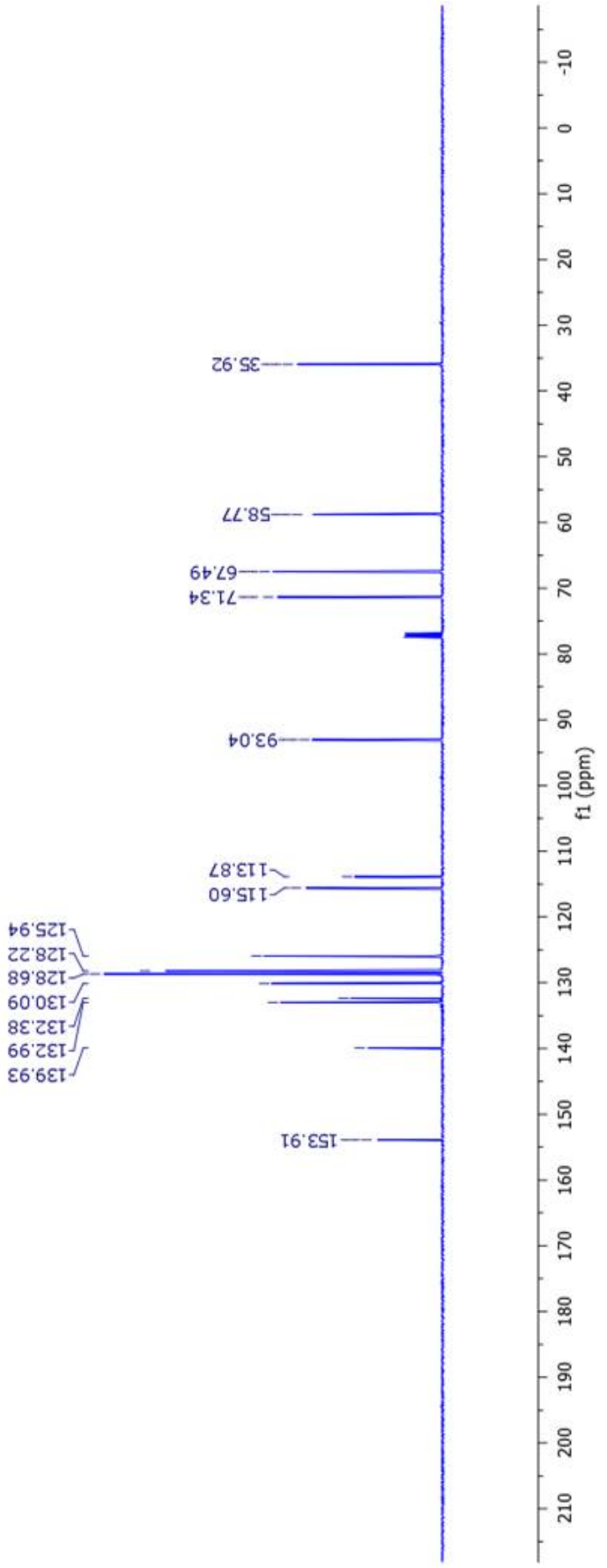

Supplementary Figure 19. ^{13}C NMR spectrum of **S2** recorded in $CDCl_3$ at 125 MHz.

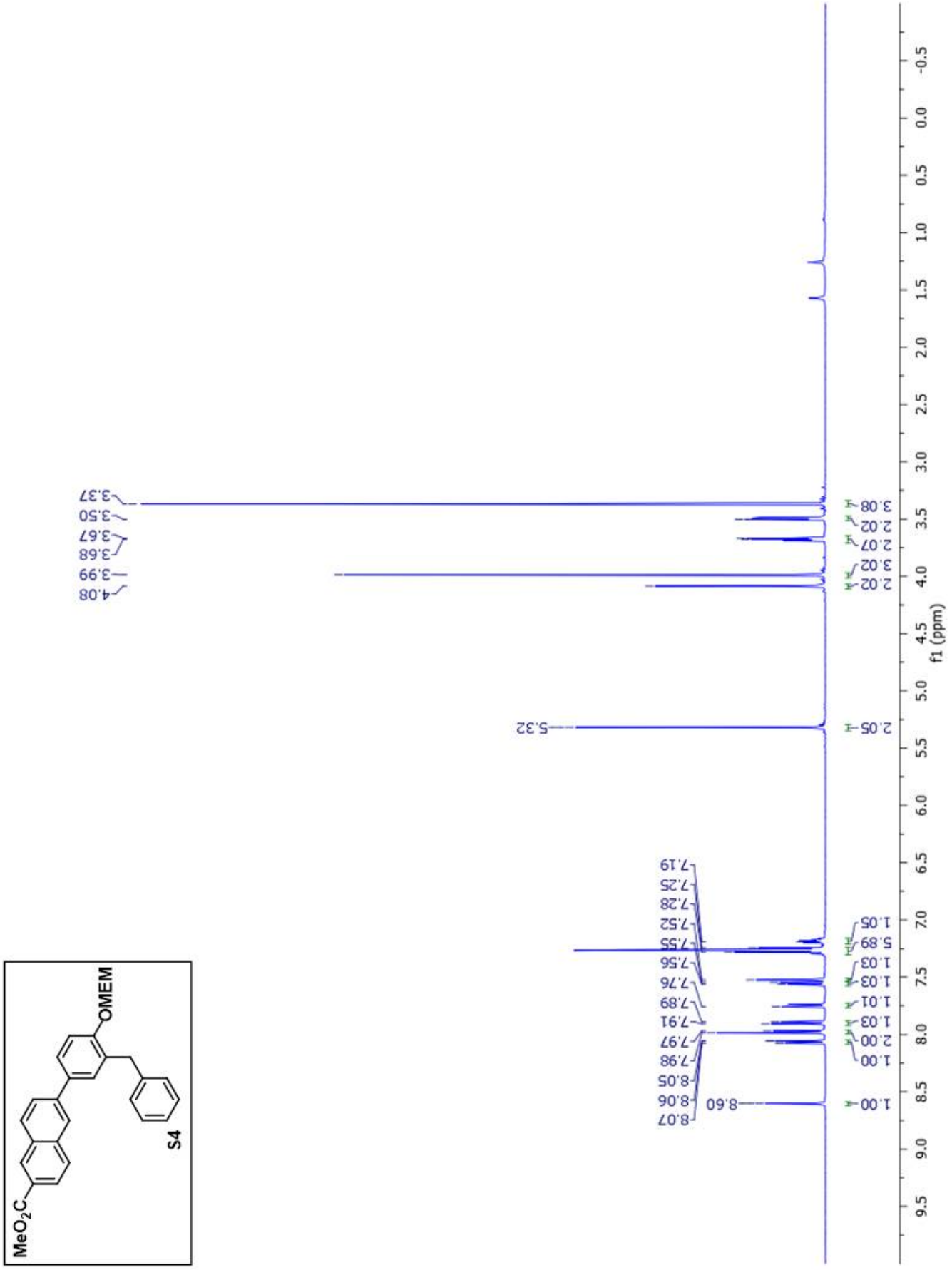

Supplementary Figure 20. ^{1}H NMR spectrum of **S4** recorded in $CDCl_3$ at 500 MHz.

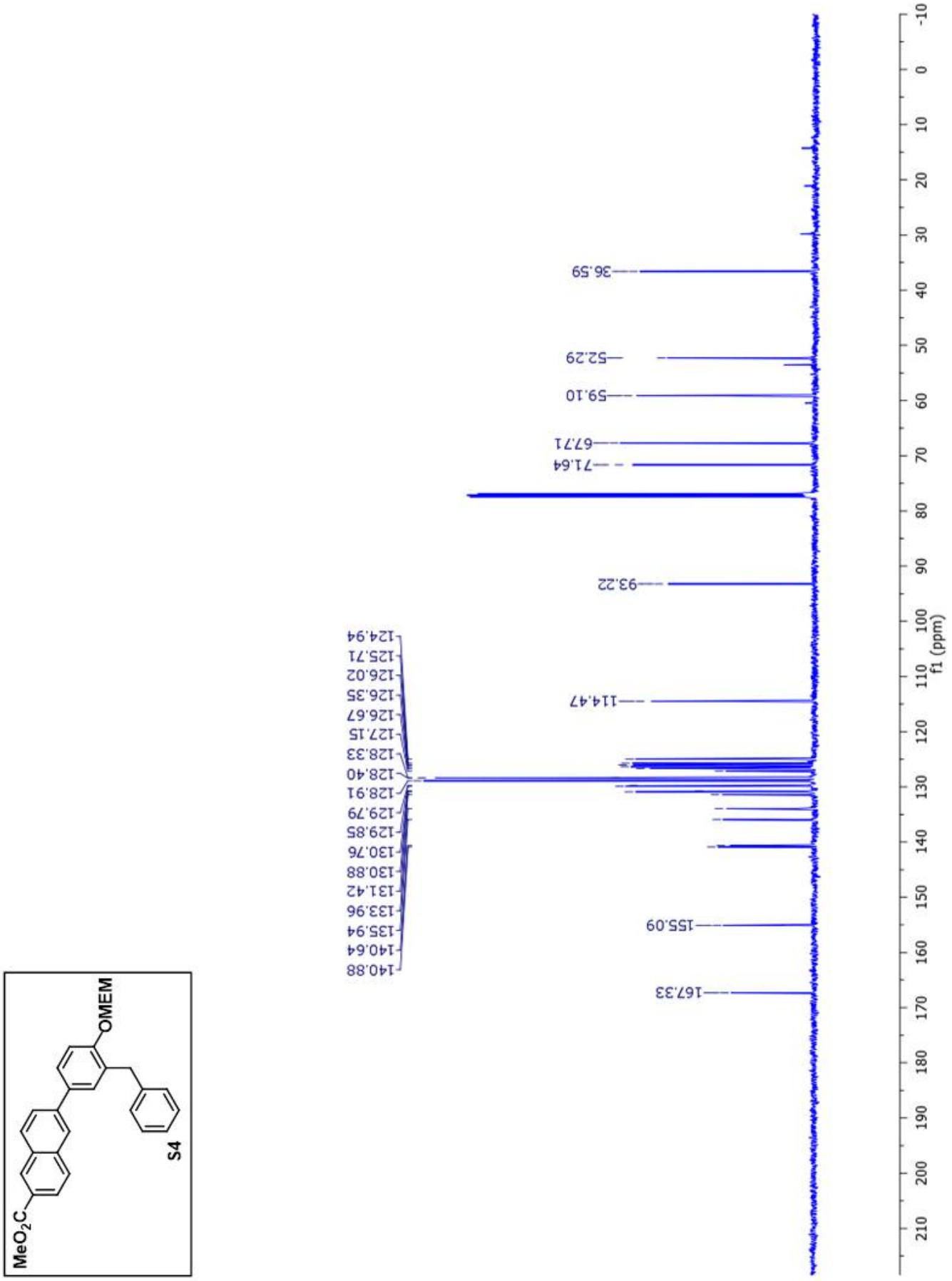

Supplementary Figure 21. ^{13}C NMR spectrum of **S4** recorded in $CDCl_3$ at 125 MHz.

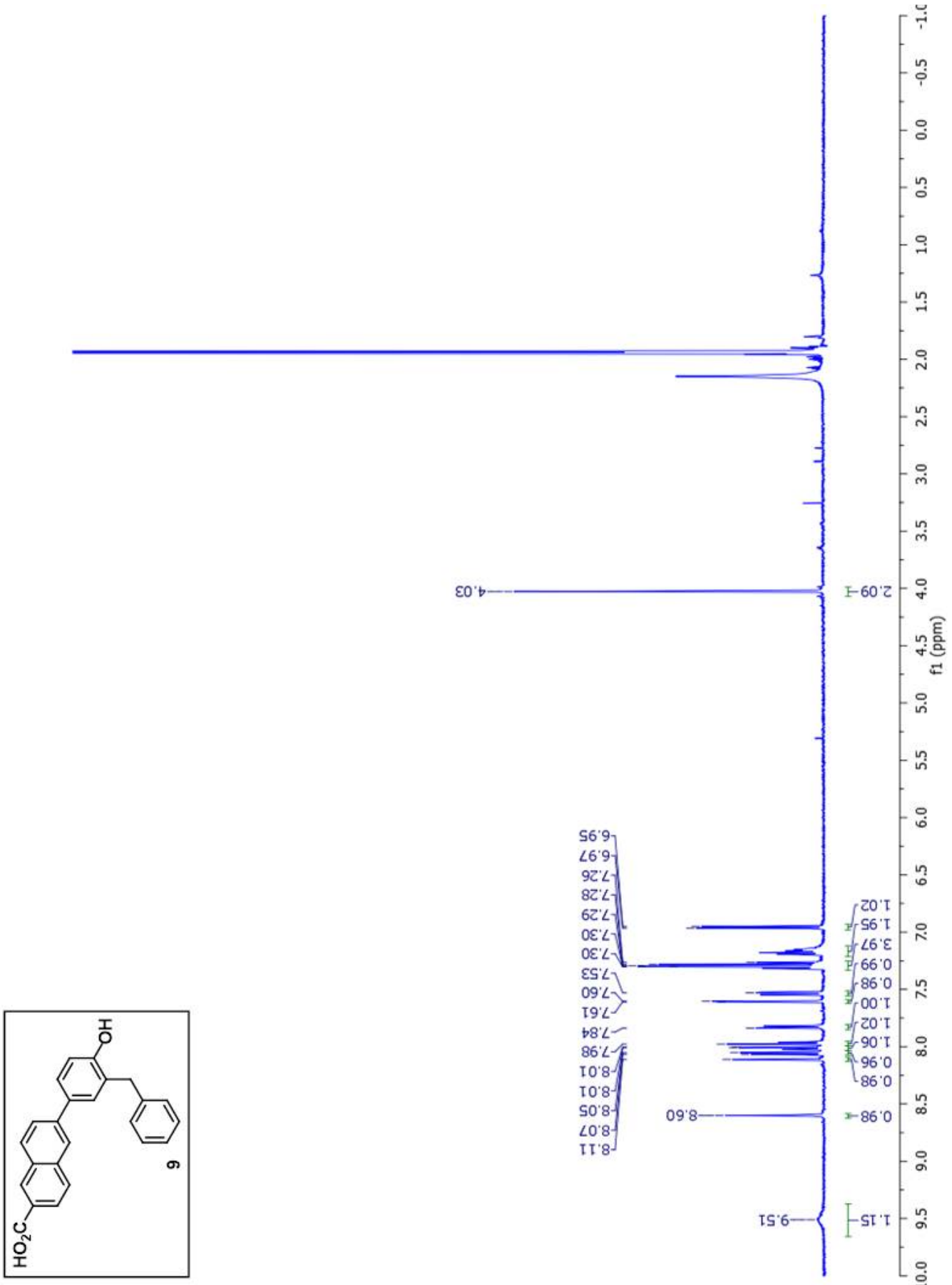

Supplementary Figure 22. ^{1}H NMR spectrum of **9** recorded in CD_3CN at 500 MHz.

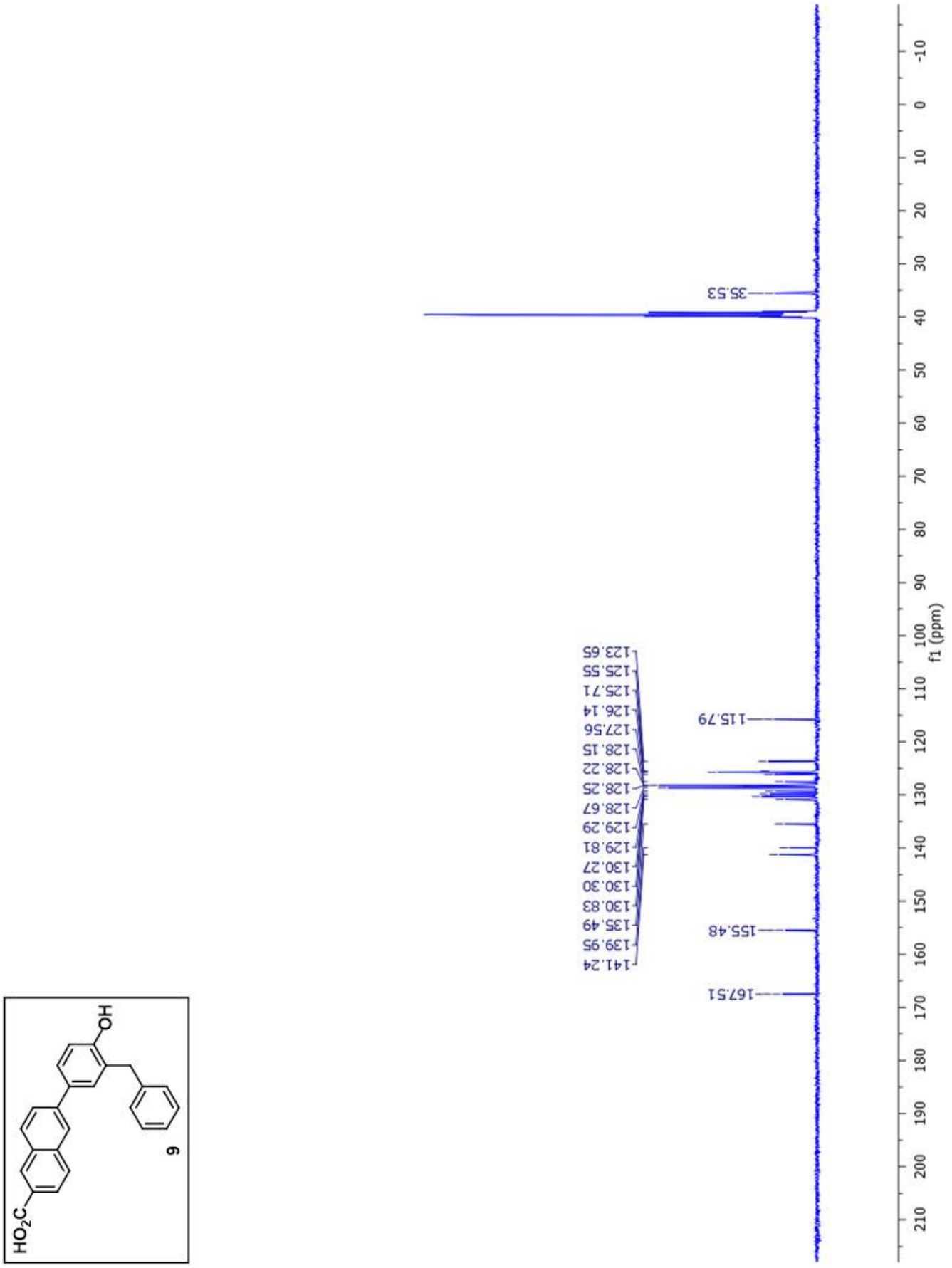

Supplementary Figure 23. ^{13}C NMR spectrum of **9** recorded in CD_3CN at 125 MHz.

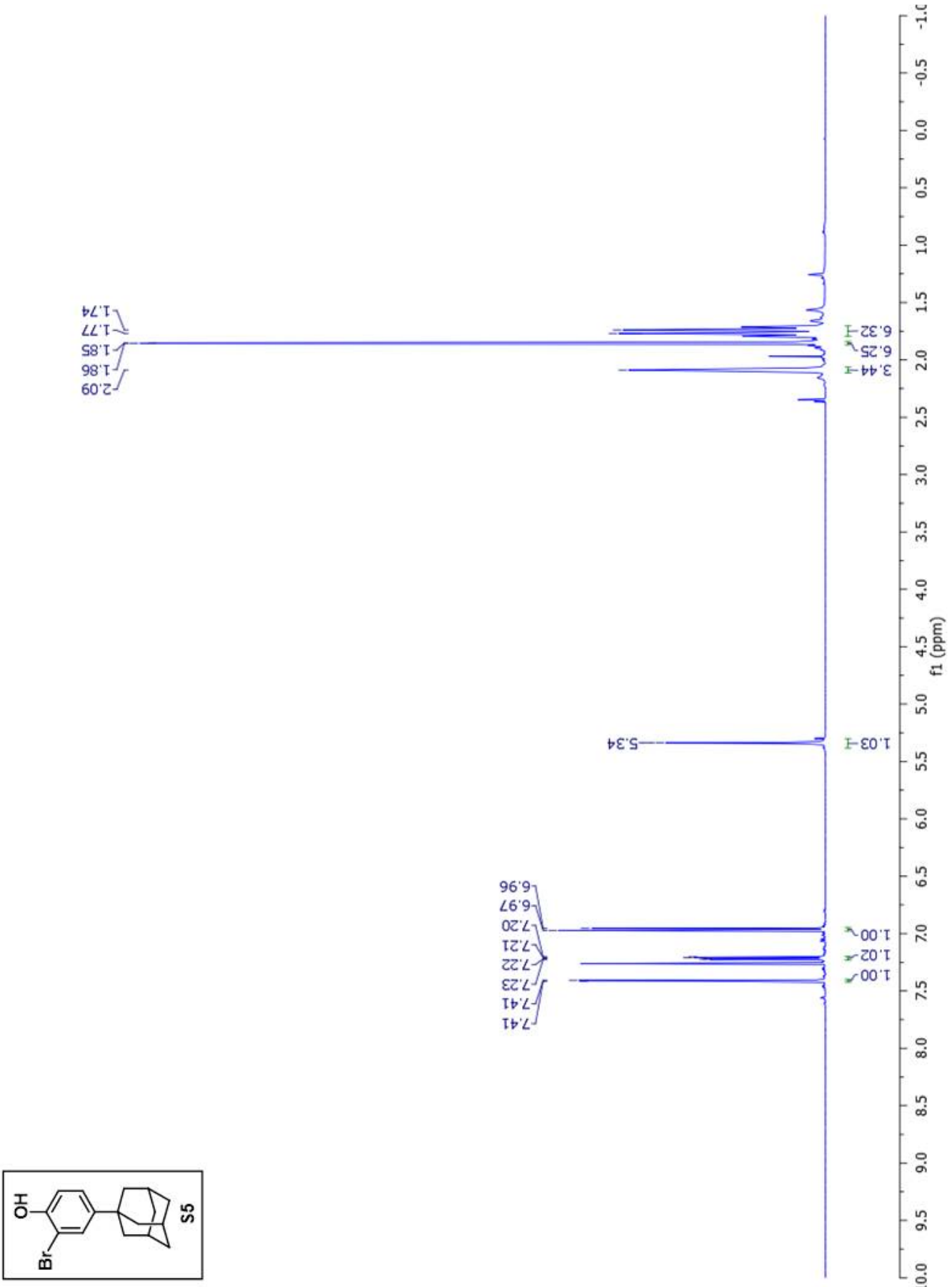

Supplementary Figure 24. ^{1}H NMR spectrum of **S5** recorded in $CDCl_3$ at 500 MHz.

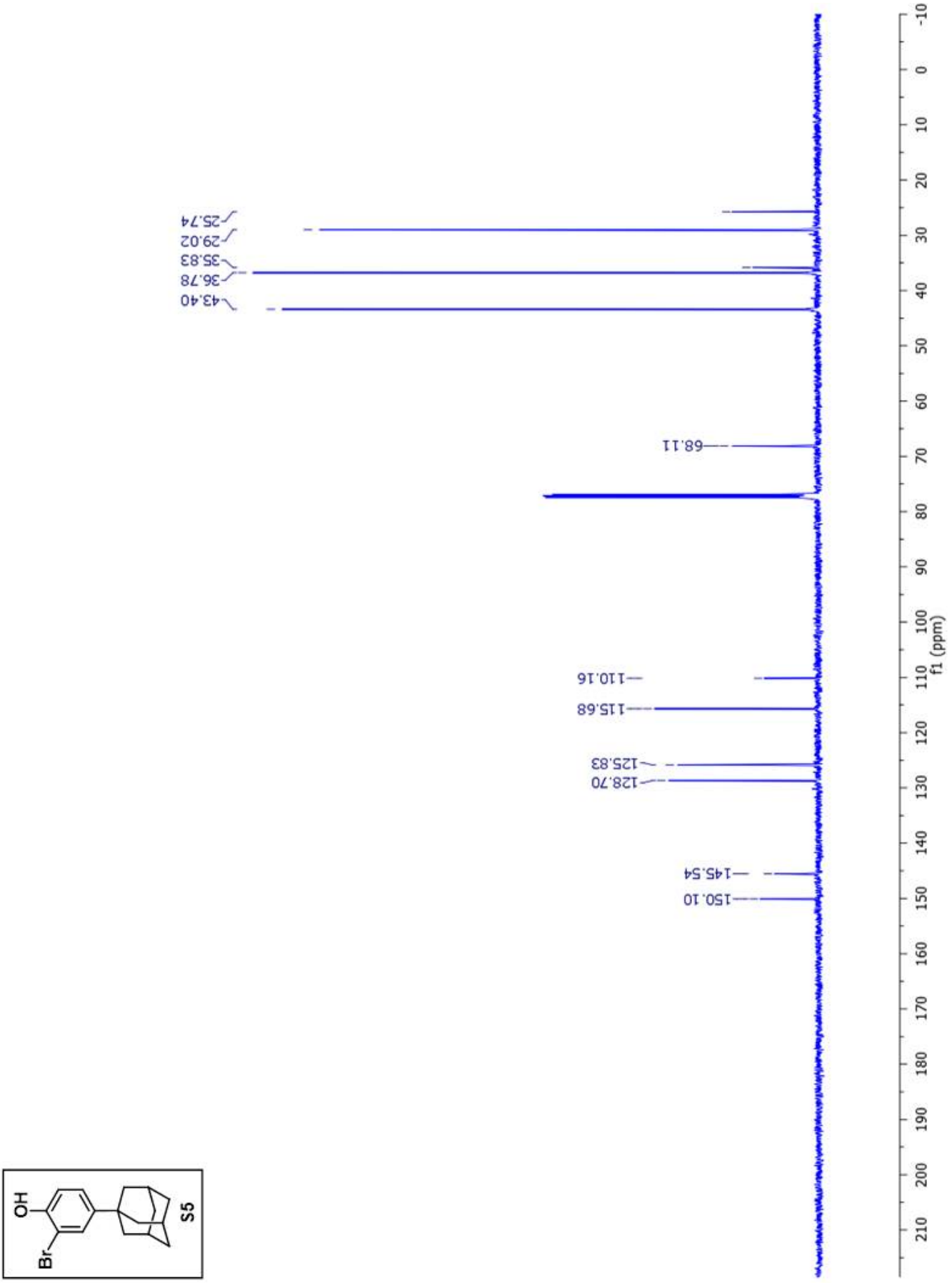

Supplementary Figure 25. ^{13}C NMR spectrum of **S5** recorded in $CDCl_3$ at 125 MHz.

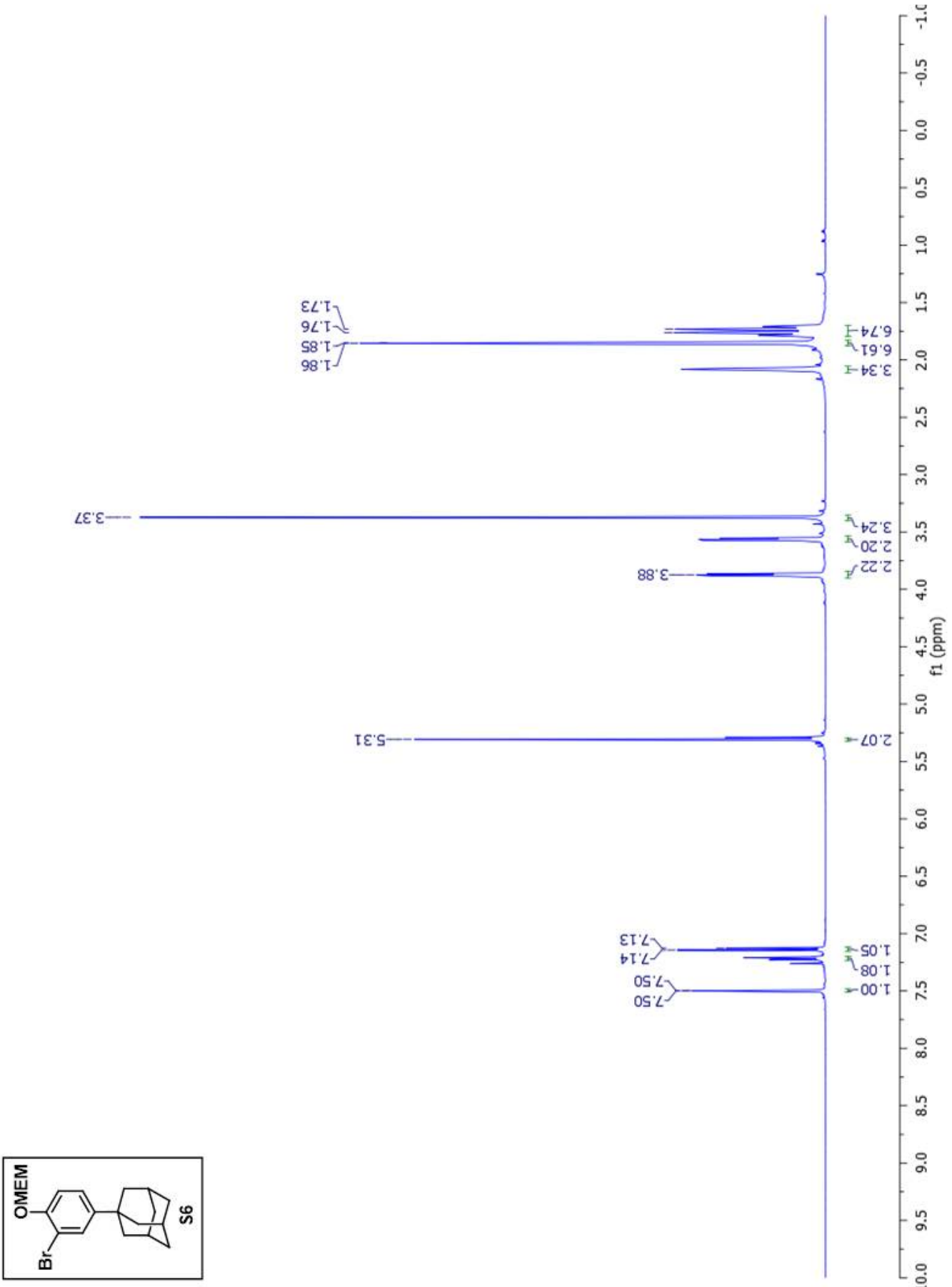

Supplementary Figure 26. ^{1}H NMR spectrum of **S6** recorded in $CDCl_3$ at 500 MHz.

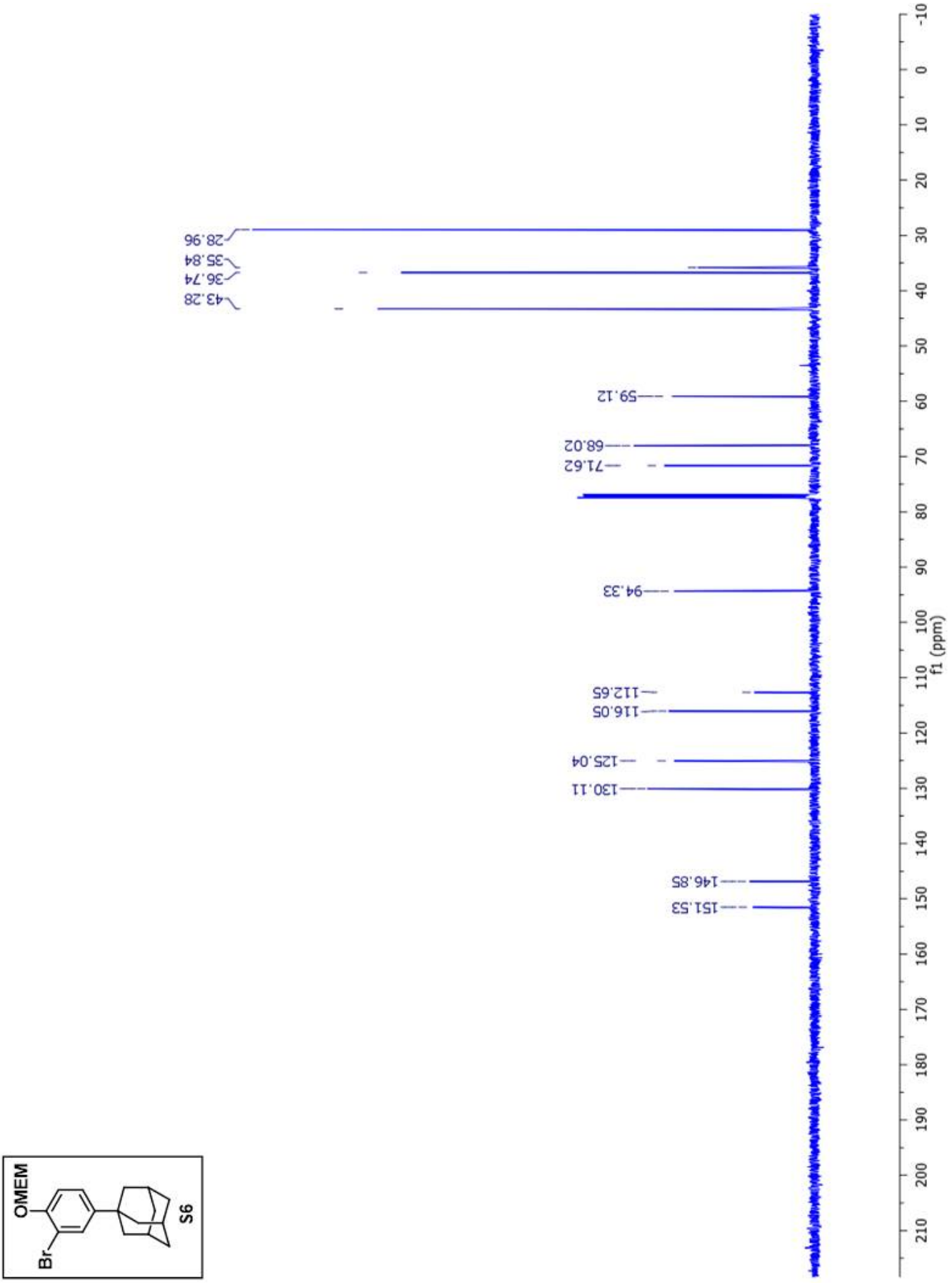

Supplementary Figure 27. ^{13}C NMR spectrum of **S6** recorded in $CDCl_3$ at 125 MHz.

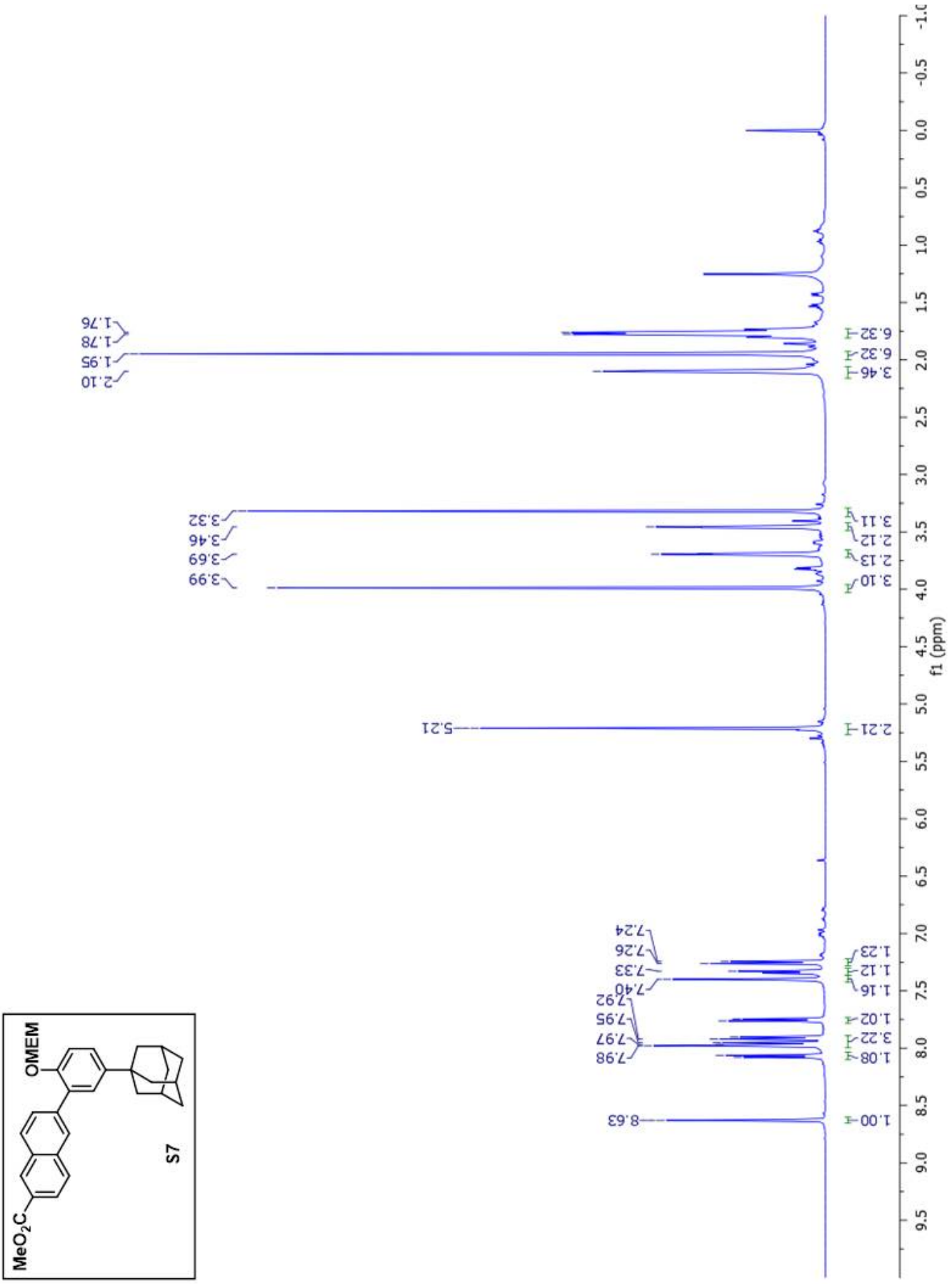

Supplementary Figure 28. ^{1}H NMR spectrum of **S7** recorded in $CDCl_3$ at 500 MHz.

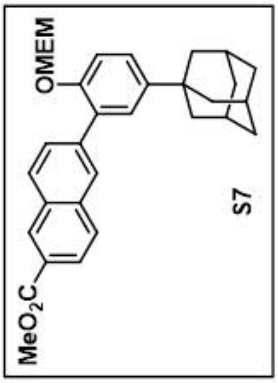

Supplementary Figure 29. ^{13}C NMR spectrum of **S7** recorded in $CDCl_3$ at 125 MHz.

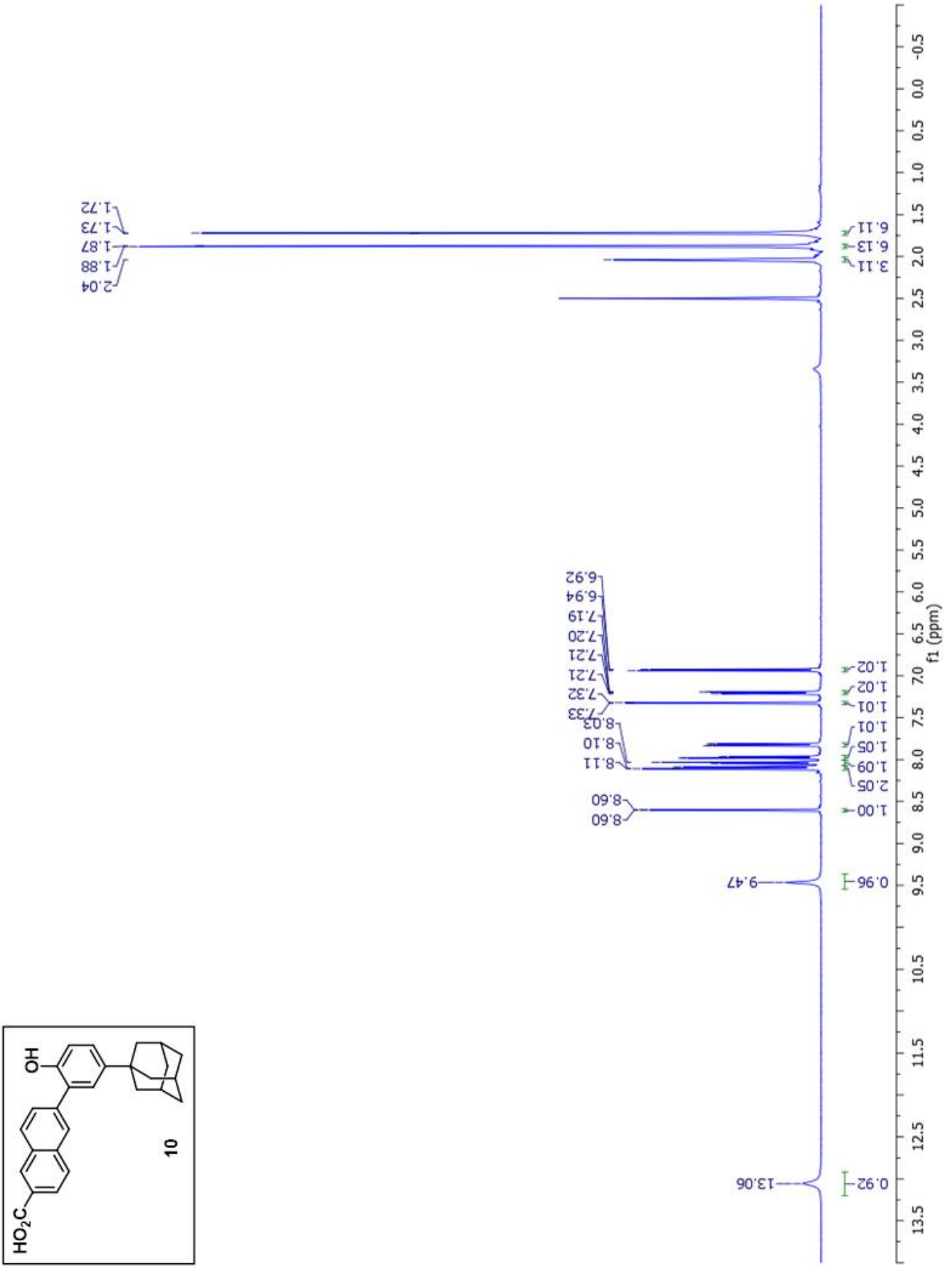

Supplementary Figure 30. ^{1}H NMR spectrum of **10** recorded in DMSO-d_6 at 500 MHz.

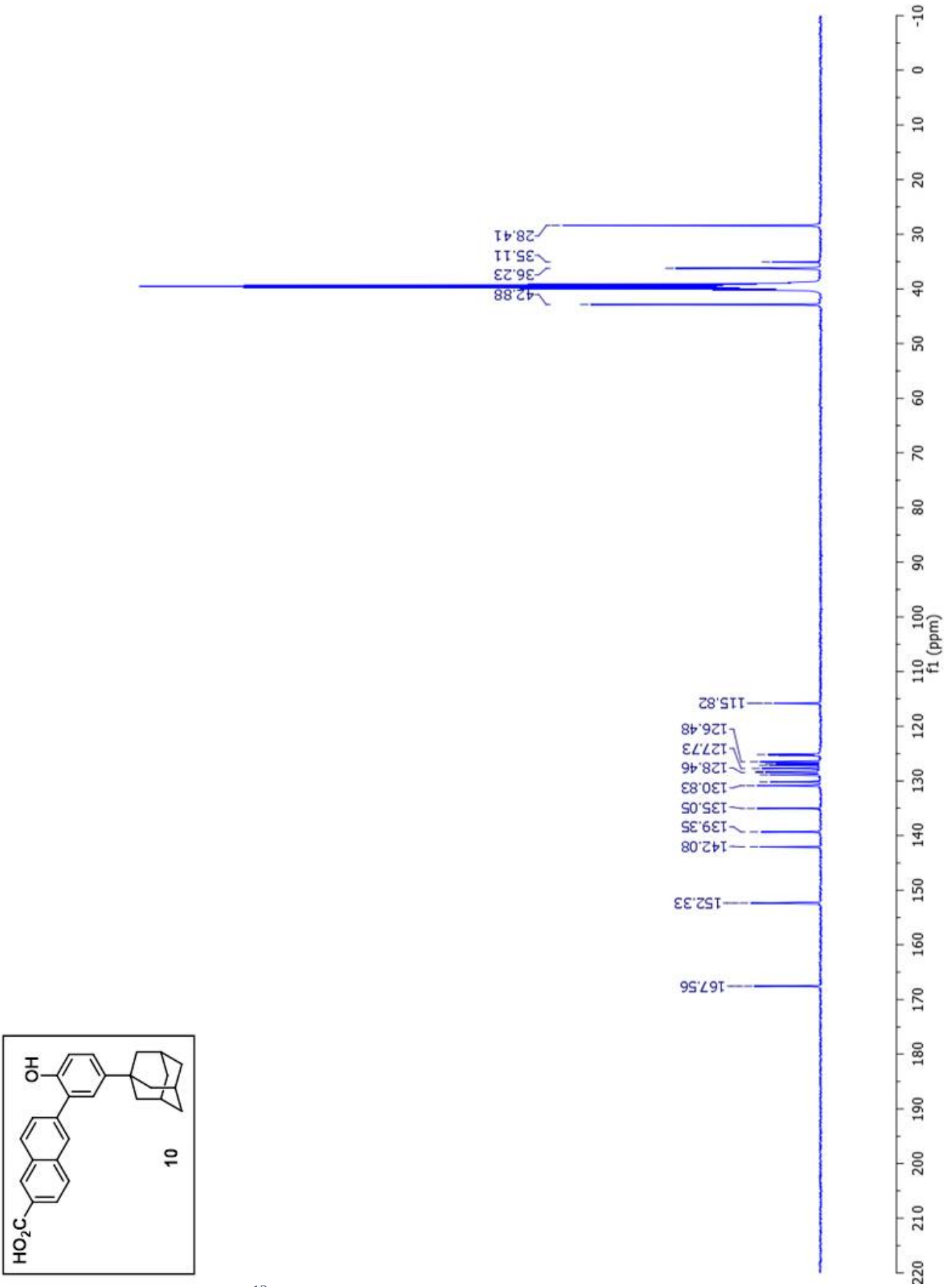

Supplementary Figure 31. ^{13}C NMR spectrum of **10** recorded in DMSO-d_6 at 125 MHz.

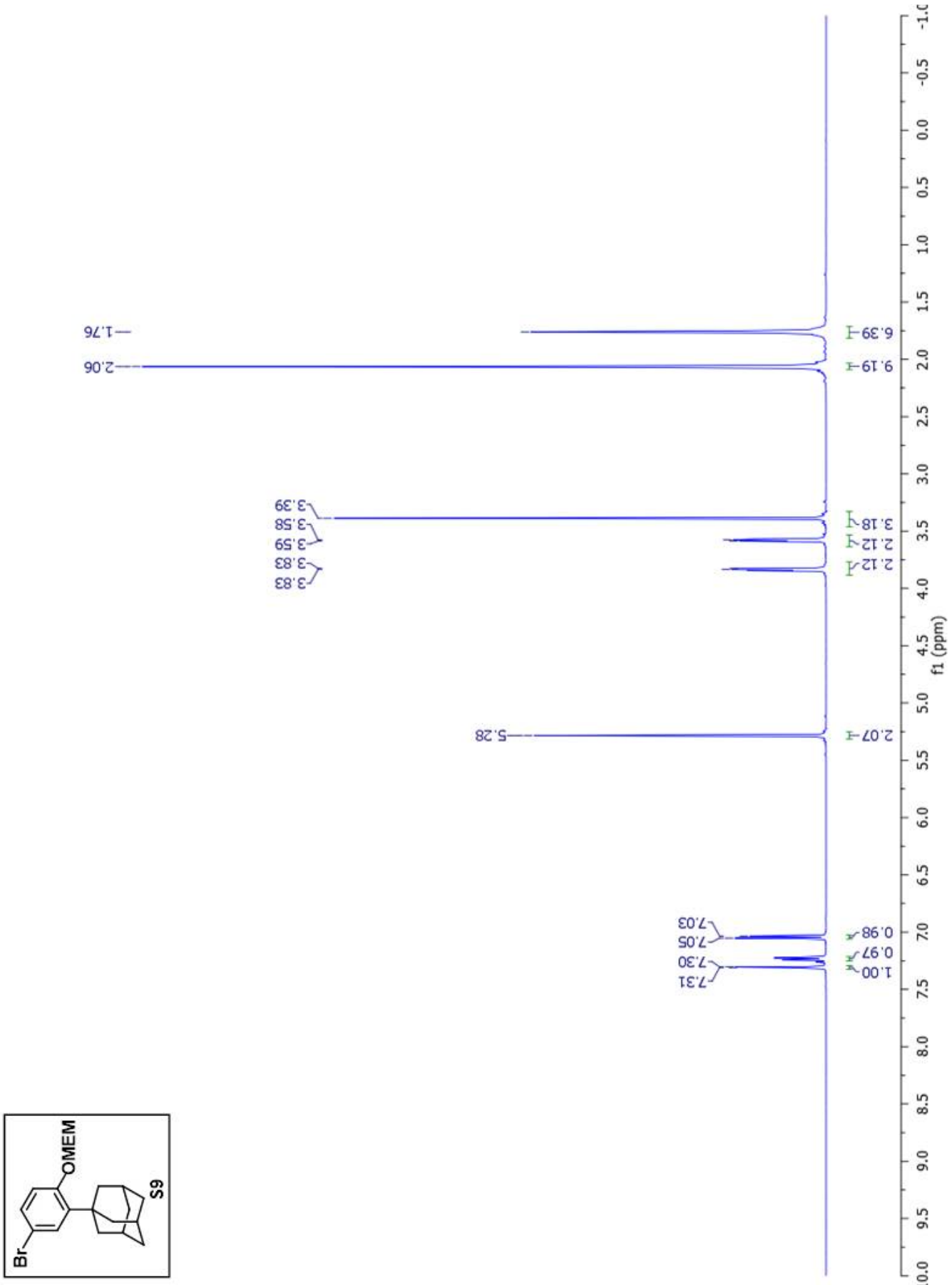

Supplementary Figure 32. ^{1}H NMR spectrum of **S9** recorded in $CDCl_3$ at 500 MHz.

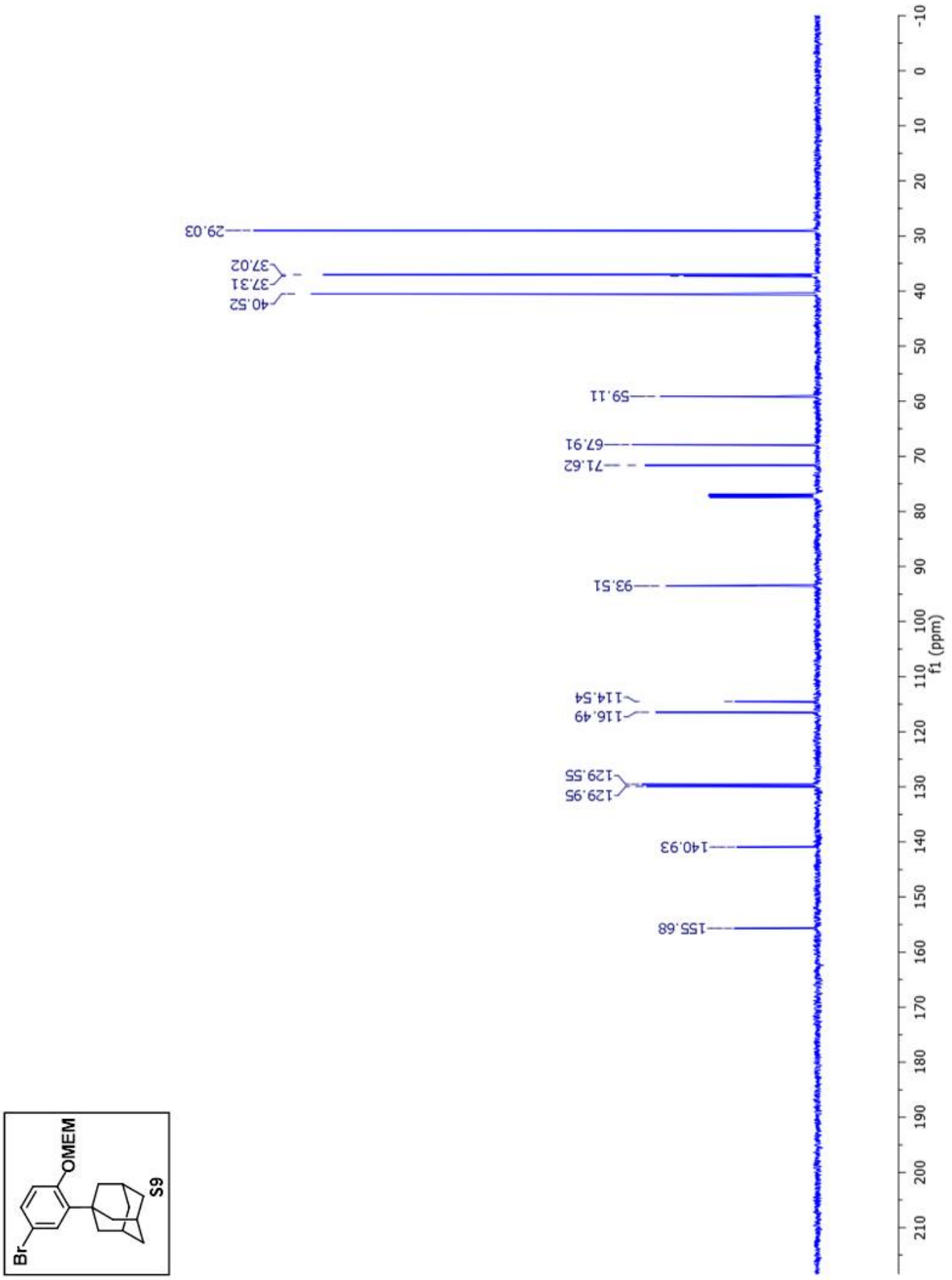

Supplementary Figure 33. ^{13}C NMR spectrum of **S9** recorded in $CDCl_3$ at 125 MHz.

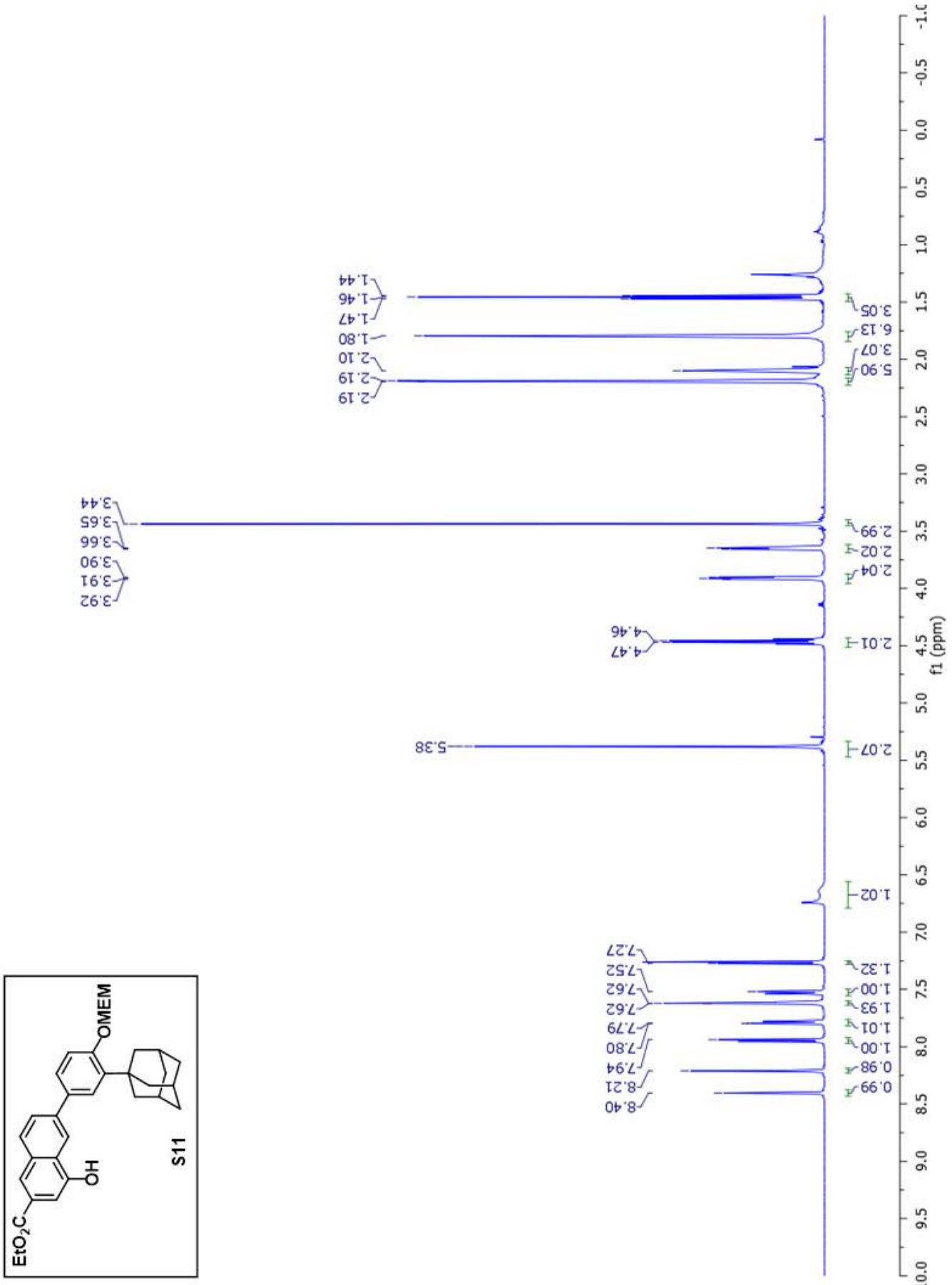

Supplementary Figure 34. ^{1}H NMR spectrum of **S11** recorded in $CDCl_3$ at 500 MHz.

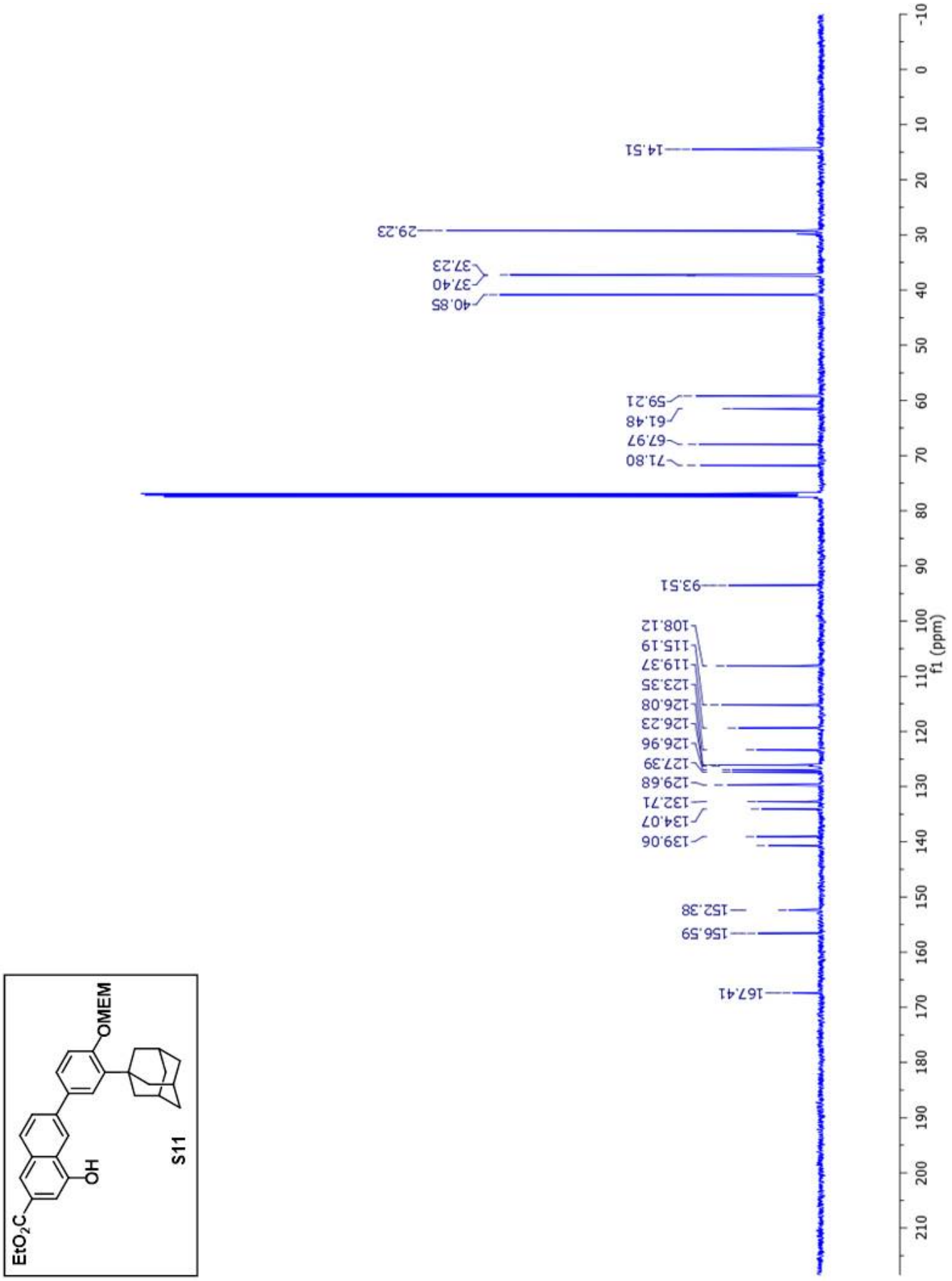

Supplementary Figure 35. ^{13}C NMR spectrum of **S11** recorded in $CDCl_3$ at 125 MHz.

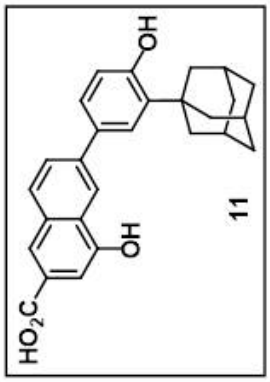

Supplementary Figure 36. ^{1}H NMR spectrum of **11** recorded in CD_3CN at 500 MHz.

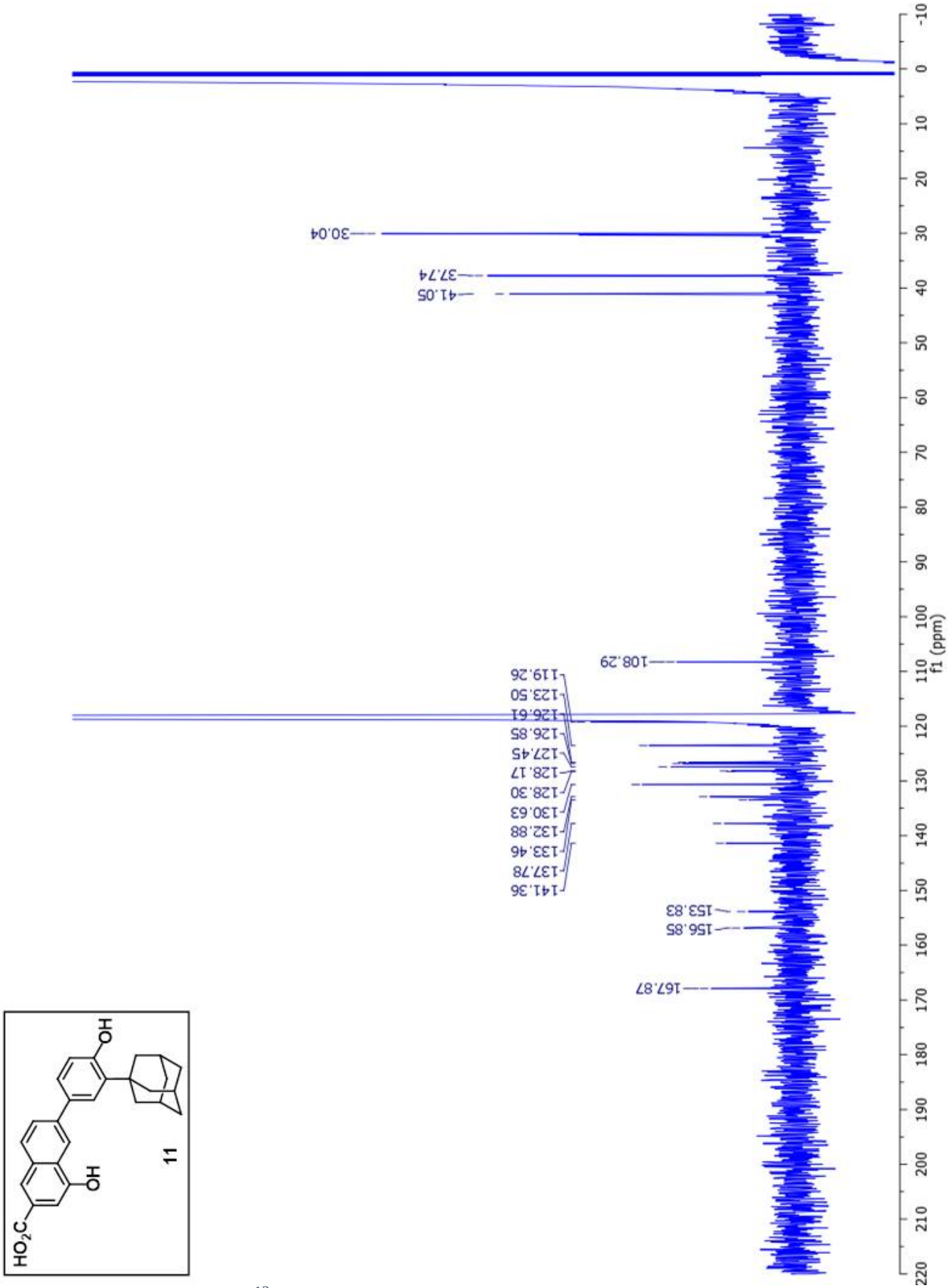

Supplementary Figure 37. ^{13}C NMR spectrum of **11** recorded in CD_3CN at 100 MHz.

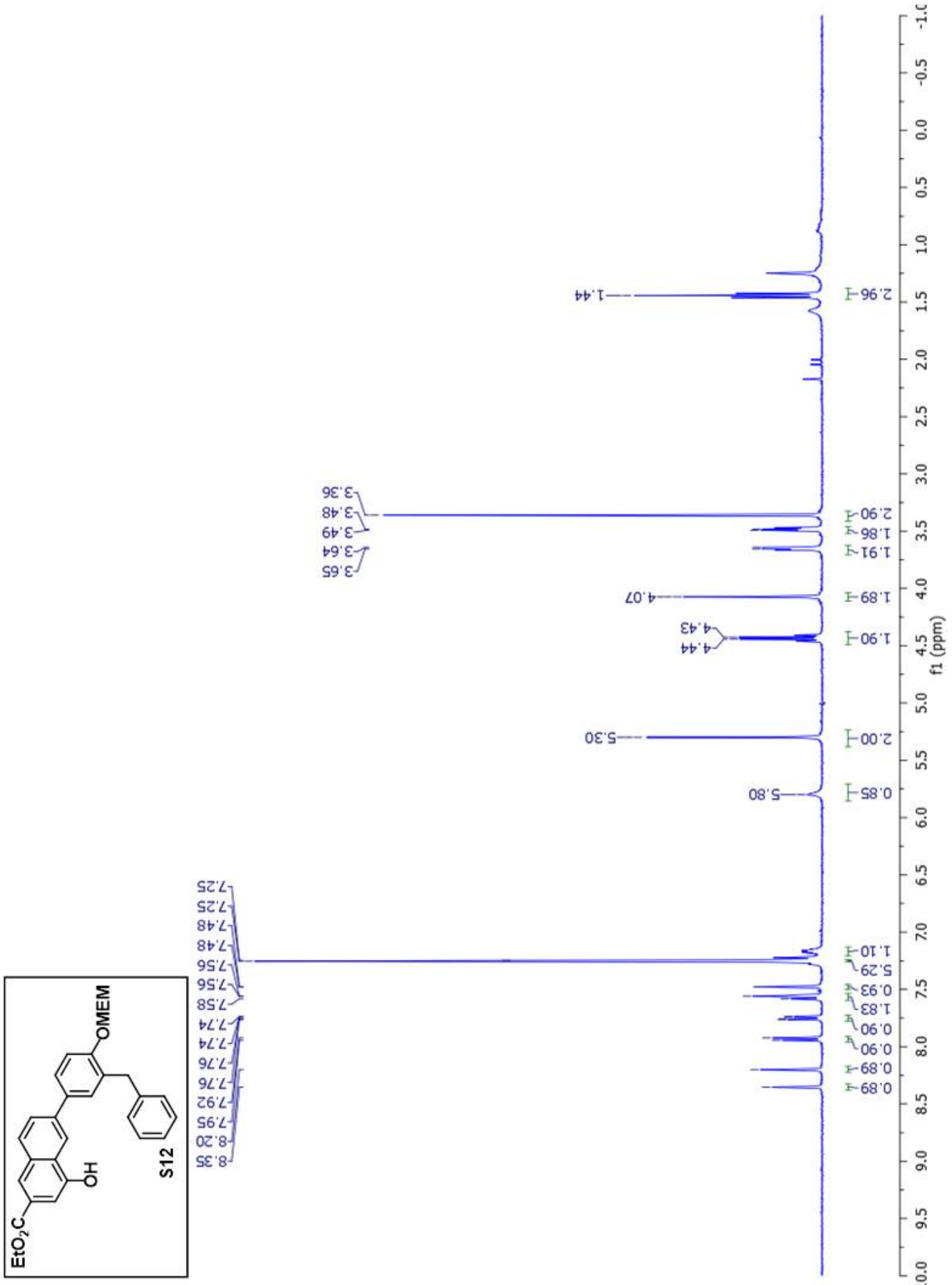

Supplementary Figure 38. ^{1}H NMR spectrum of **S12** recorded in $CDCl_3$ at 400 MHz.

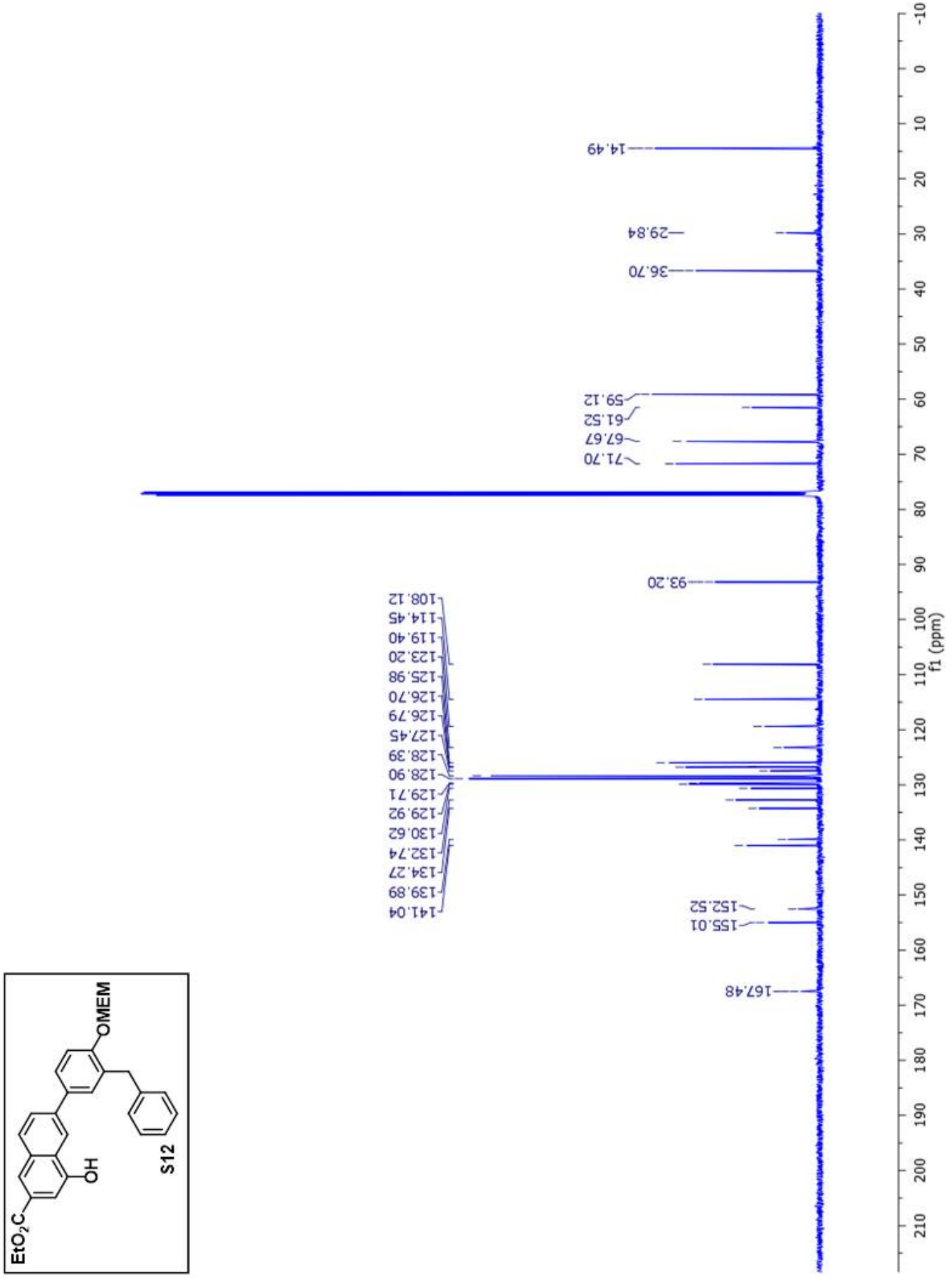

Supplementary Figure 39. ^{13}C NMR spectrum of **S12** recorded in $CDCl_3$ at 125 MHz.

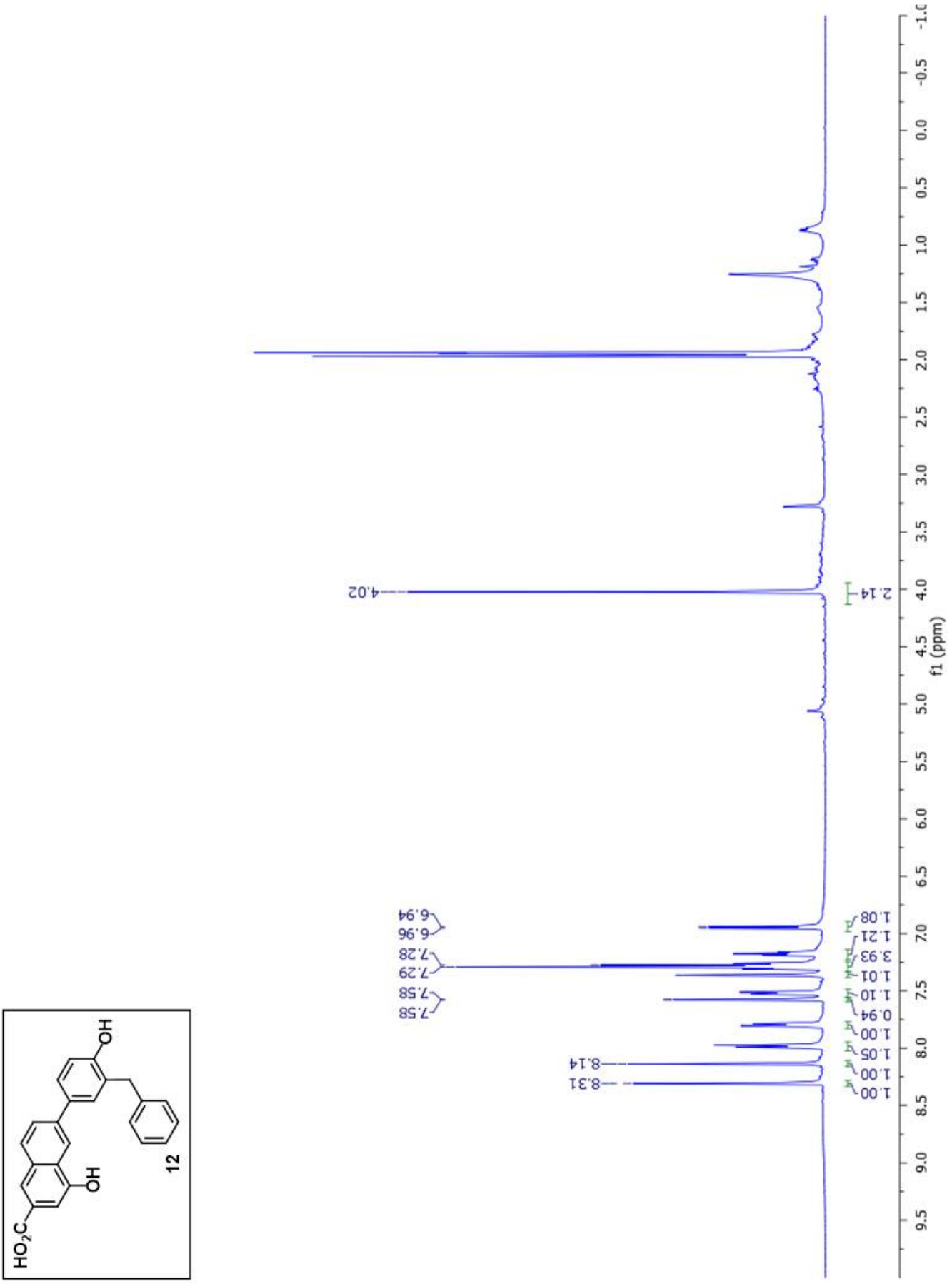

Supplementary Figure 40. ^{1}H NMR spectrum of **12** recorded in CD_3CN at 500 MHz.

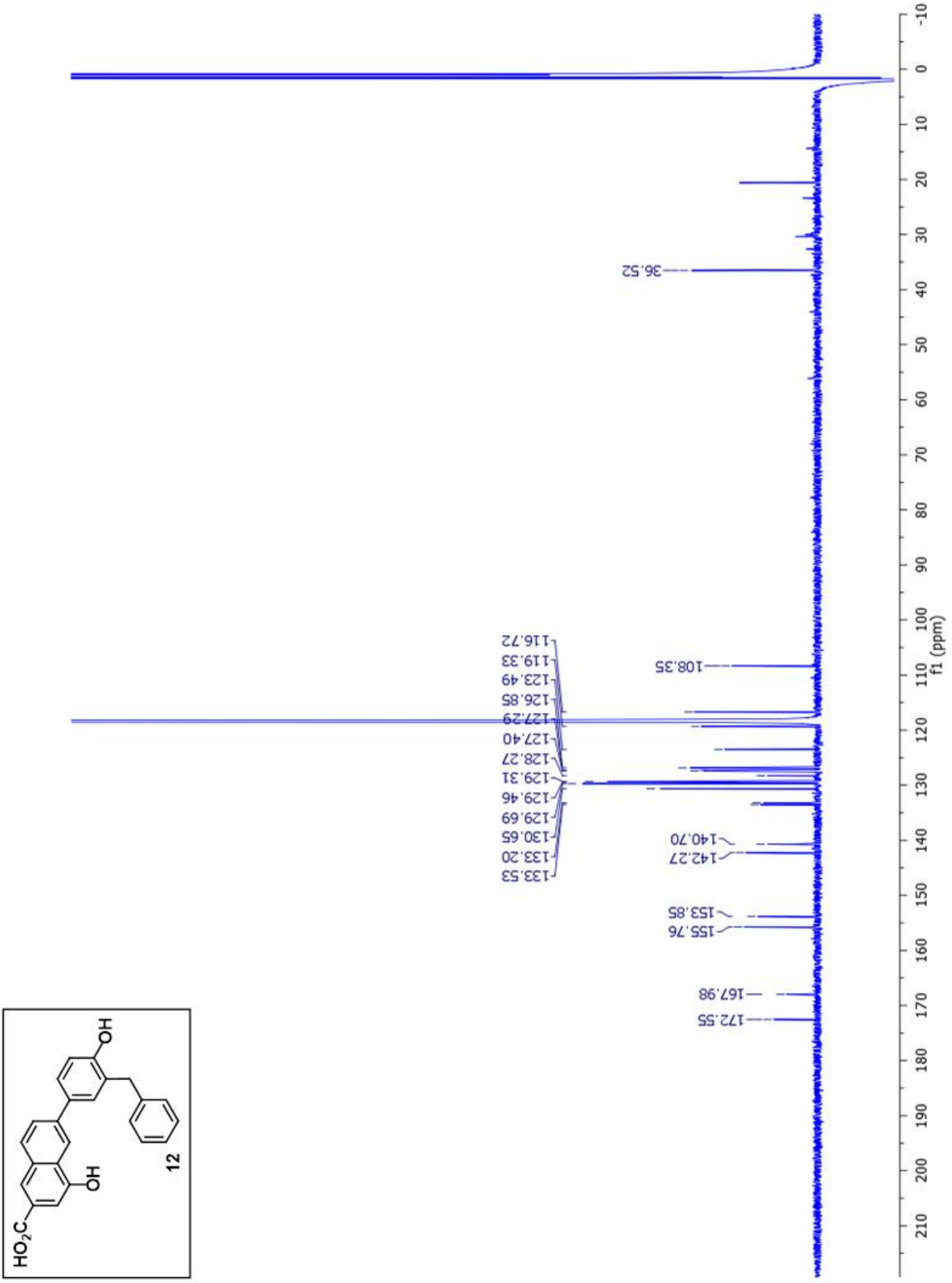

Supplementary Figure 41. ^{13}C NMR spectrum of **12** recorded in CD_3CN at 125 MHz.

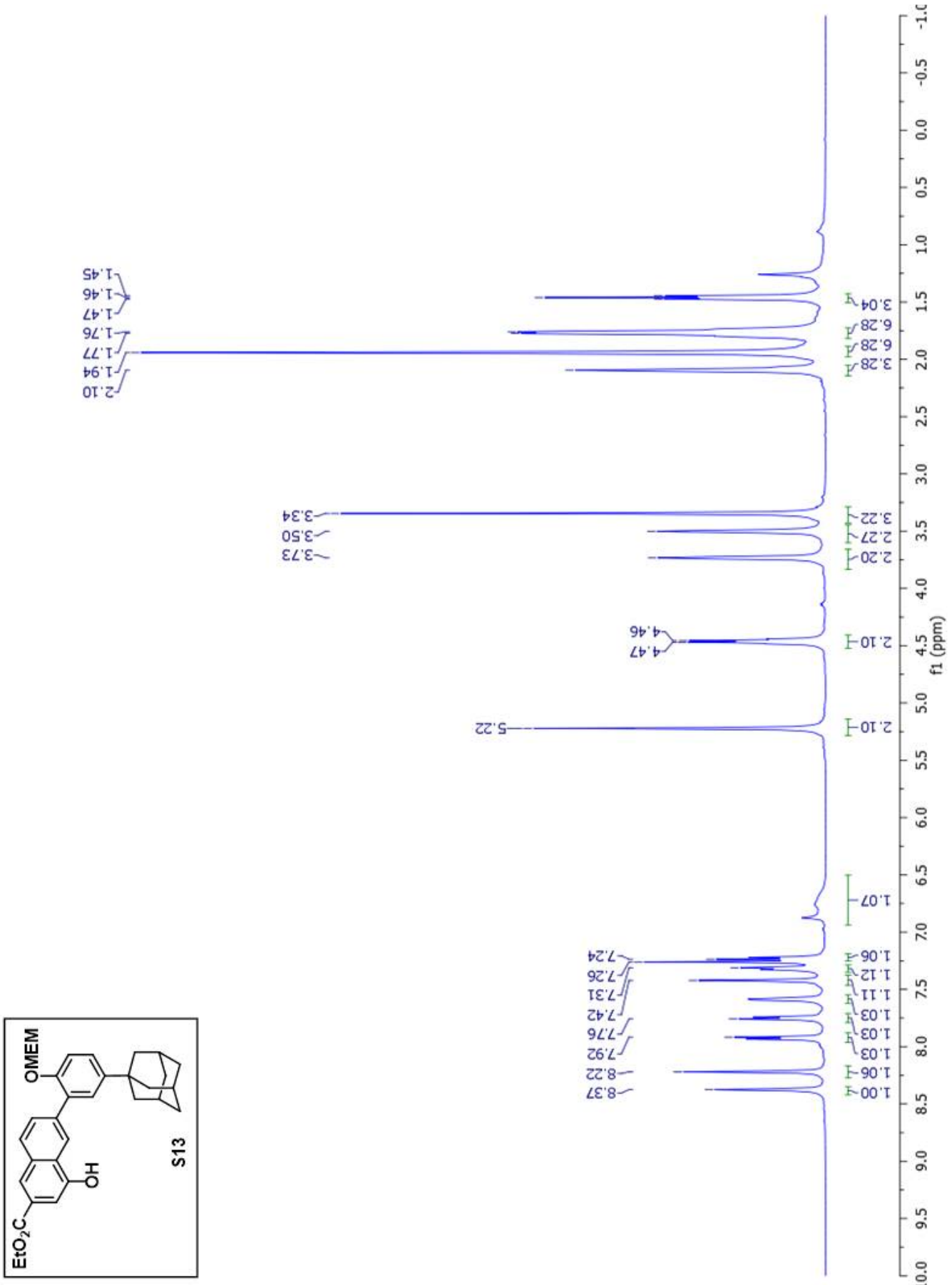

Supplementary Figure 42. ^{1}H NMR spectrum of **S13** recorded in $CDCl_3$ at 500 MHz.

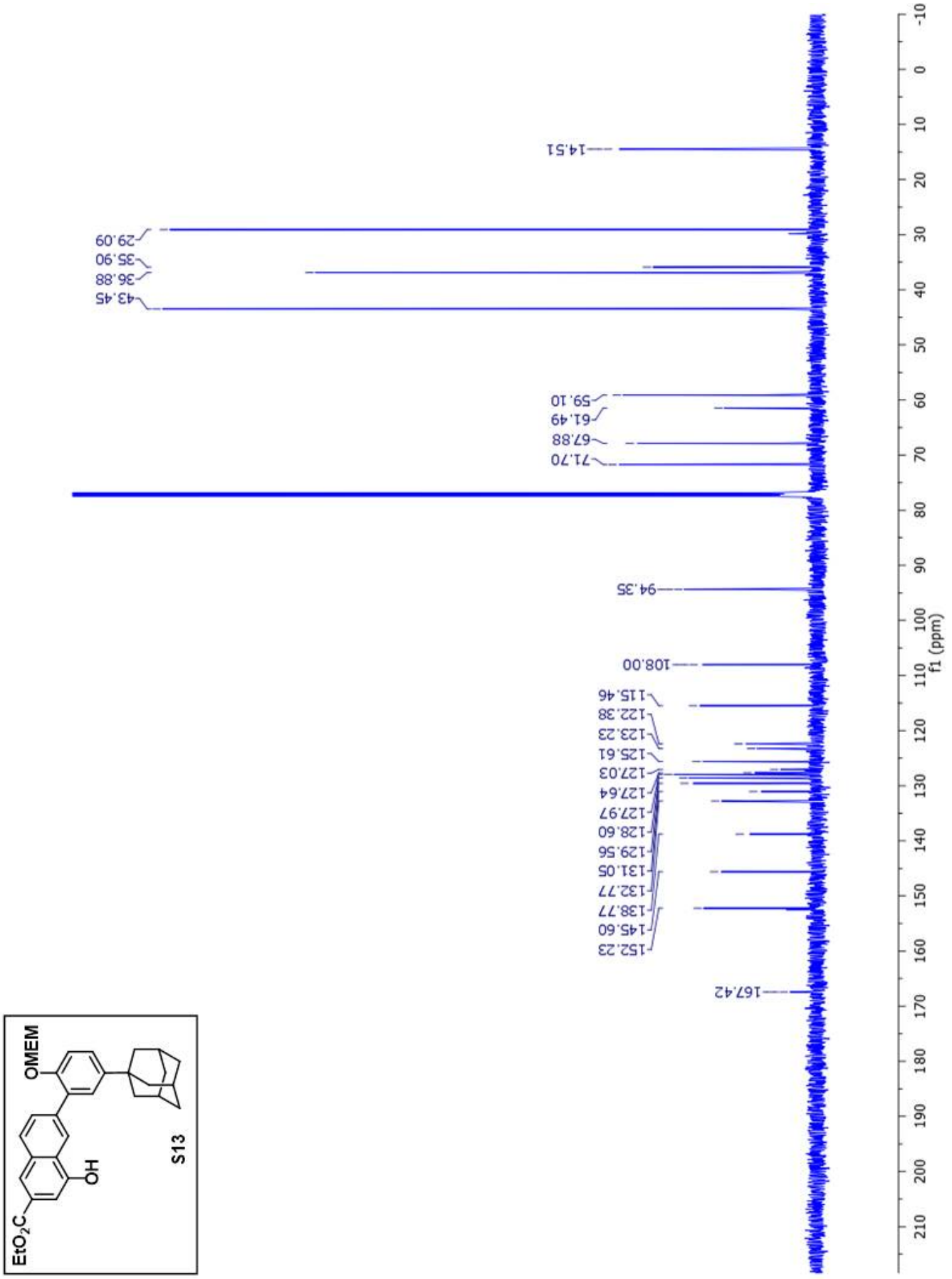

Supplementary Figure 43. ^{13}C NMR spectrum of **S13** recorded in $CDCl_3$ at 125 MHz.

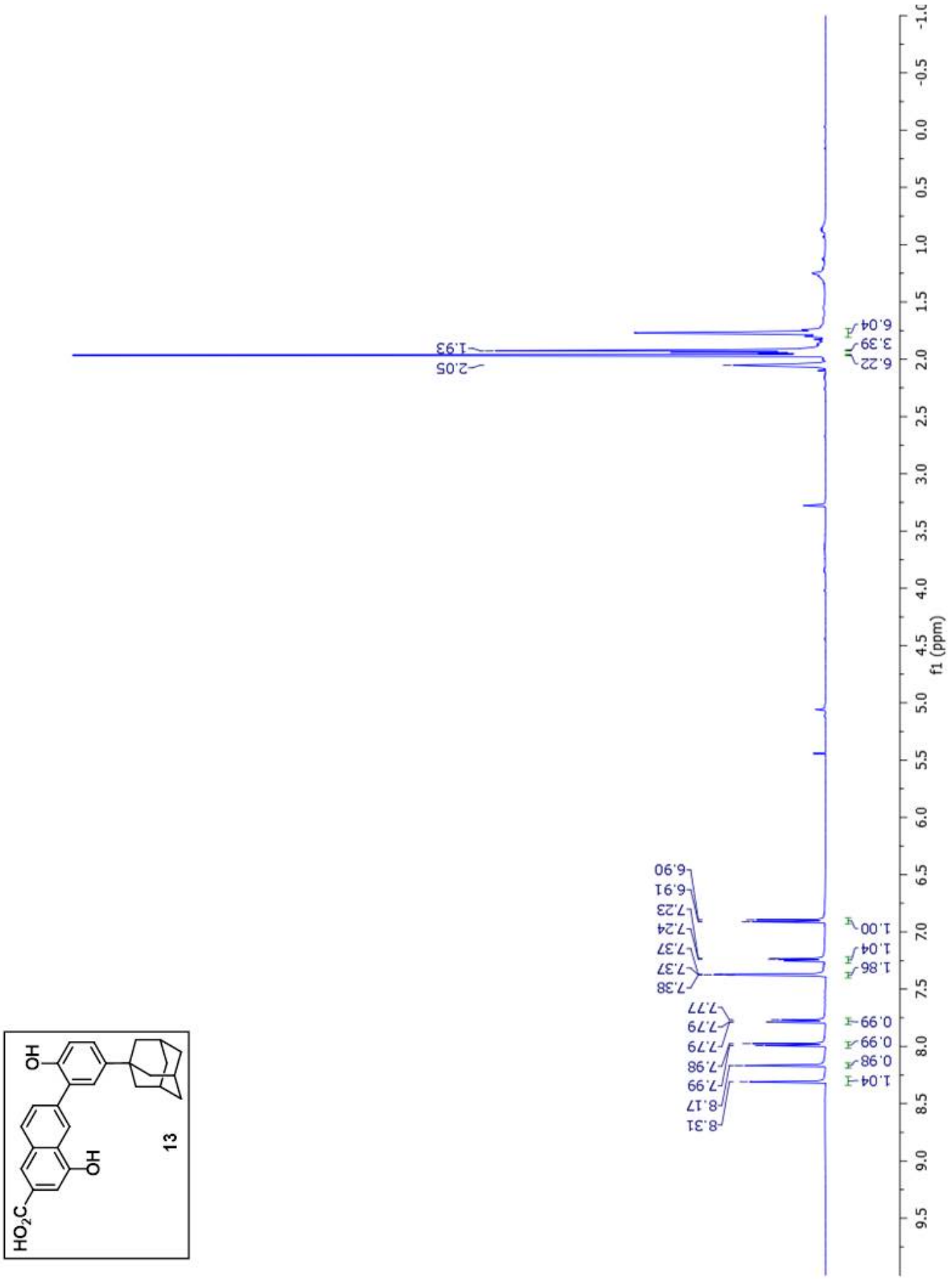

Supplementary Figure 44. ^{1}H NMR spectrum of **13** recorded in CD_3CN at 500 MHz.

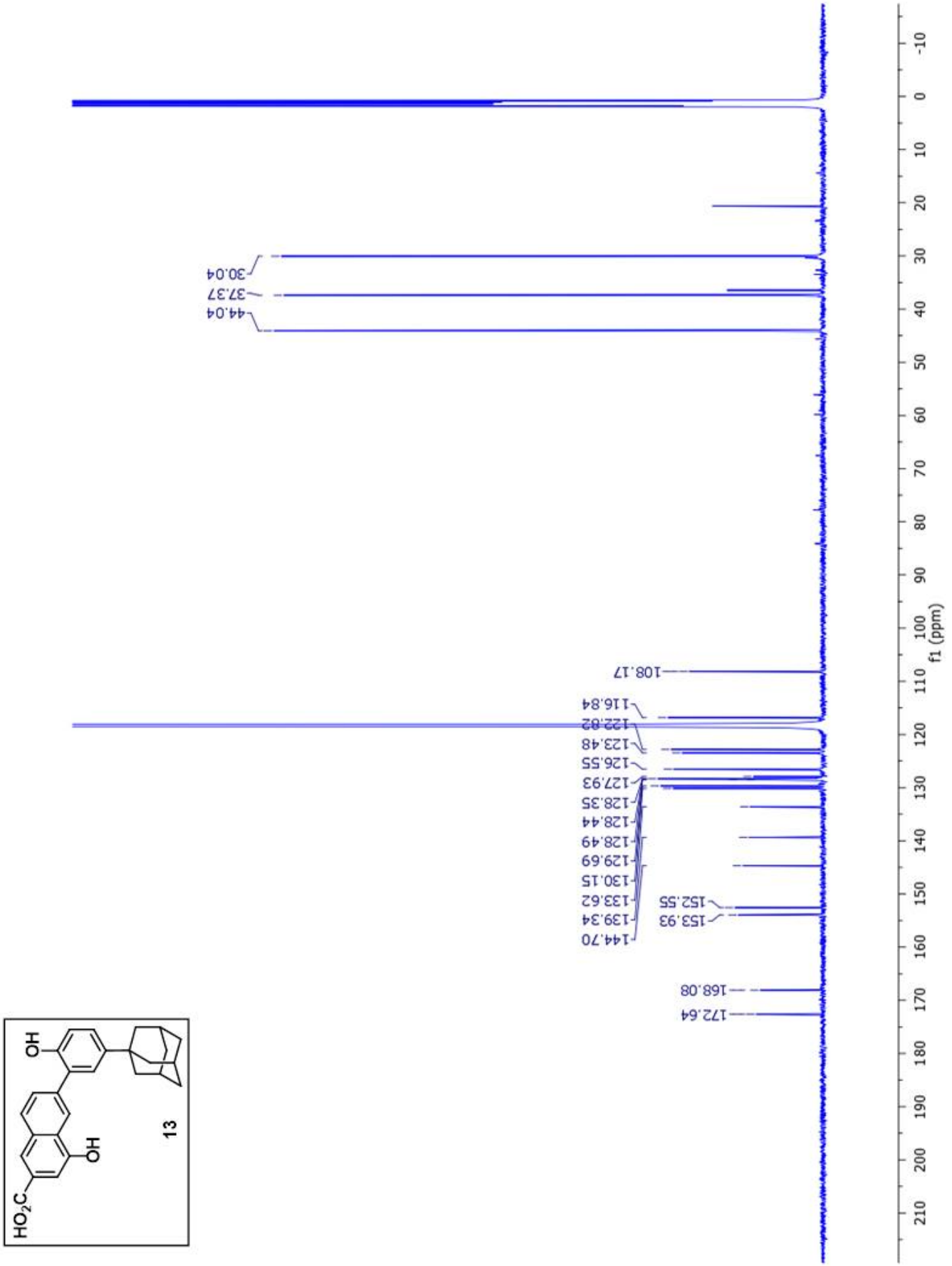

Supplementary Figure 45. ^{13}C NMR spectrum of **13** recorded in CD_3CN at 125 MHz.

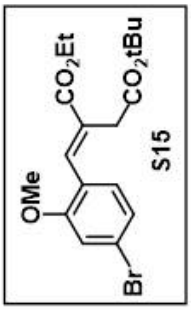

Supplementary Figure 46. ^{1}H NMR spectrum of **S15** recorded in $CDCl_3$ at 500 MHz.

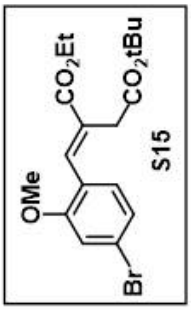

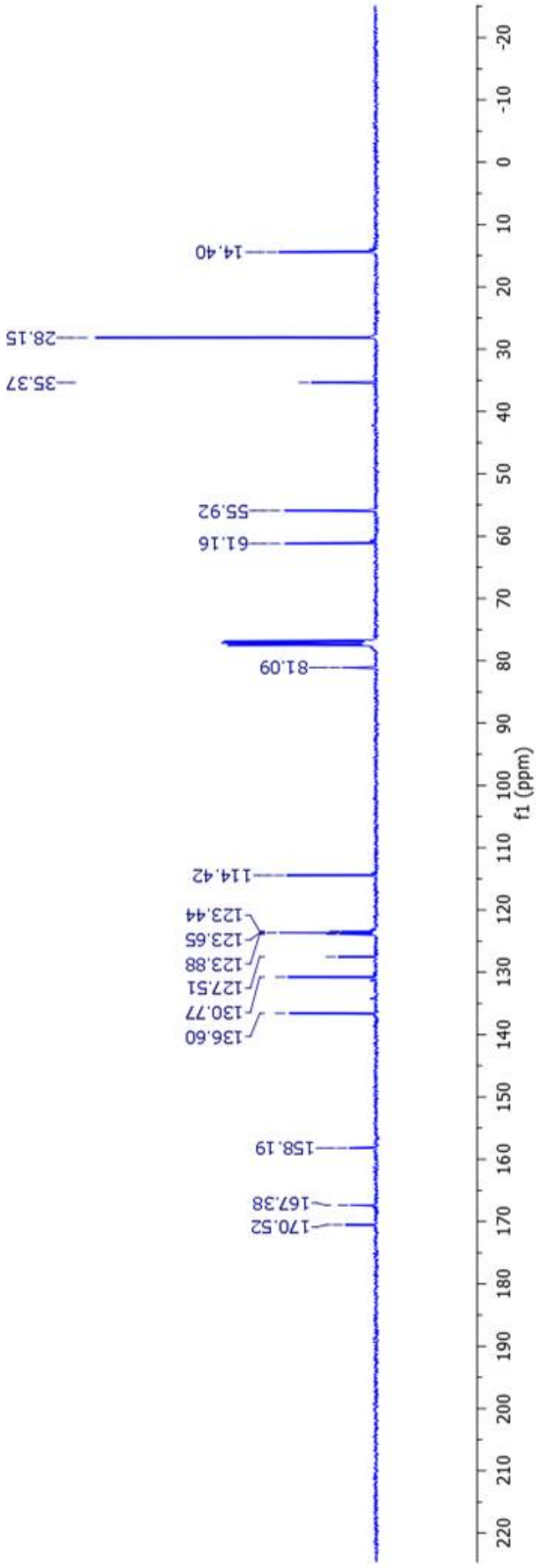

Supplementary Figure 47. ^{13}C NMR spectrum of **S15** recorded in $CDCl_3$ at 100 MHz.

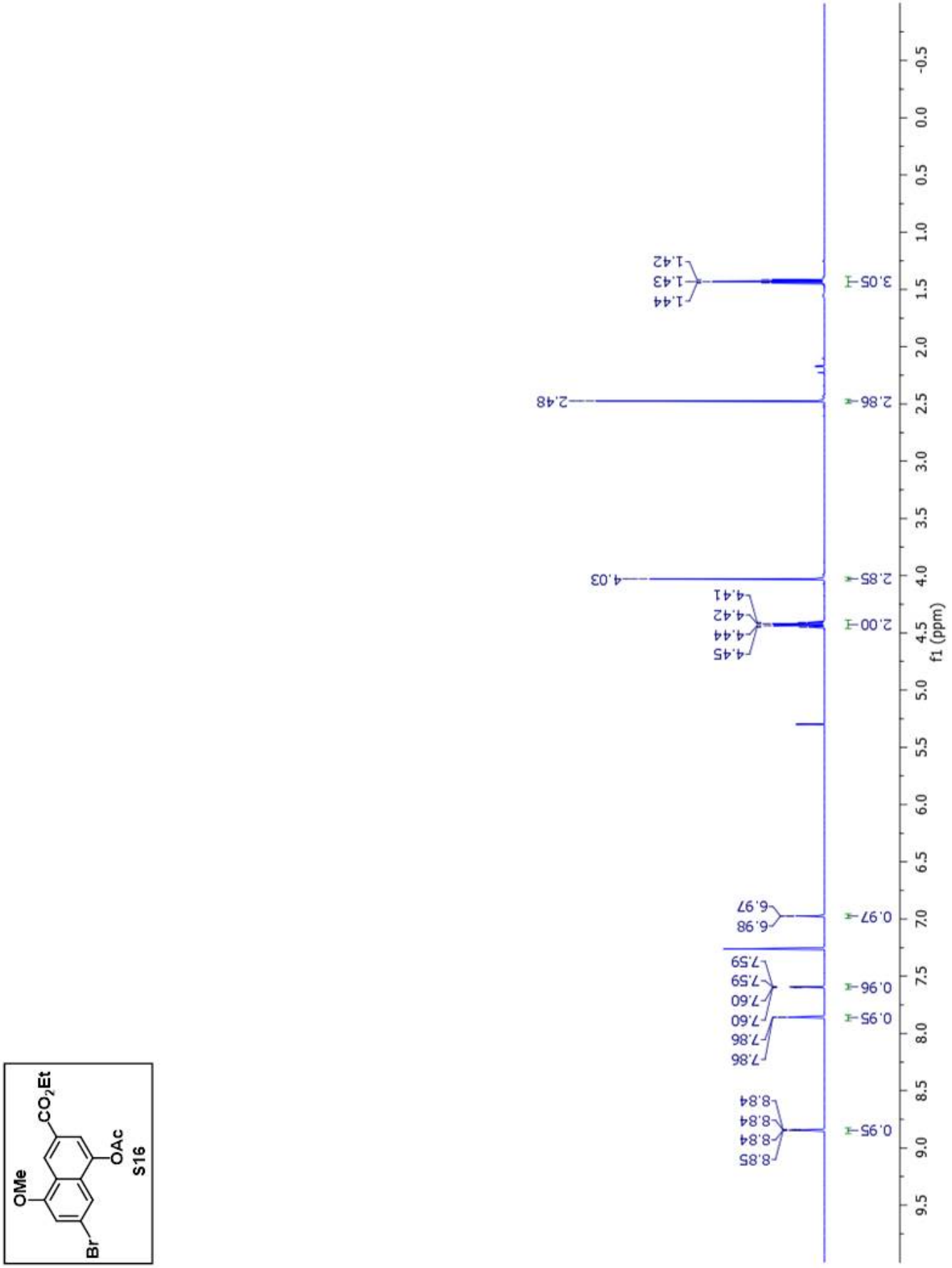

Supplementary Figure 48. ^{1}H NMR spectrum of **S16** recorded in $CDCl_3$ at 500 MHz.

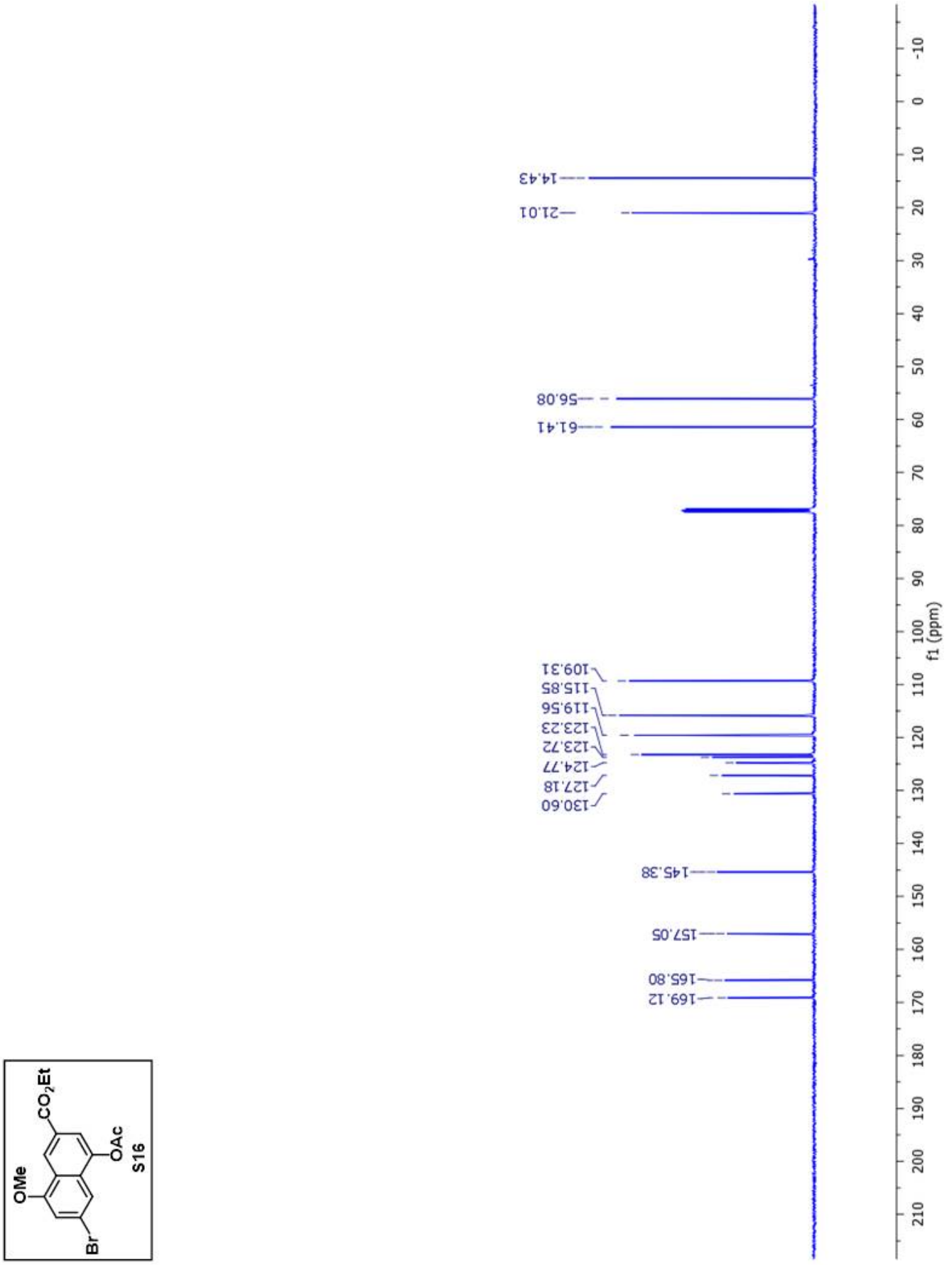

Supplementary Figure 49. ^{13}C NMR spectrum of **S16** recorded in $CDCl_3$ at 125 MHz.

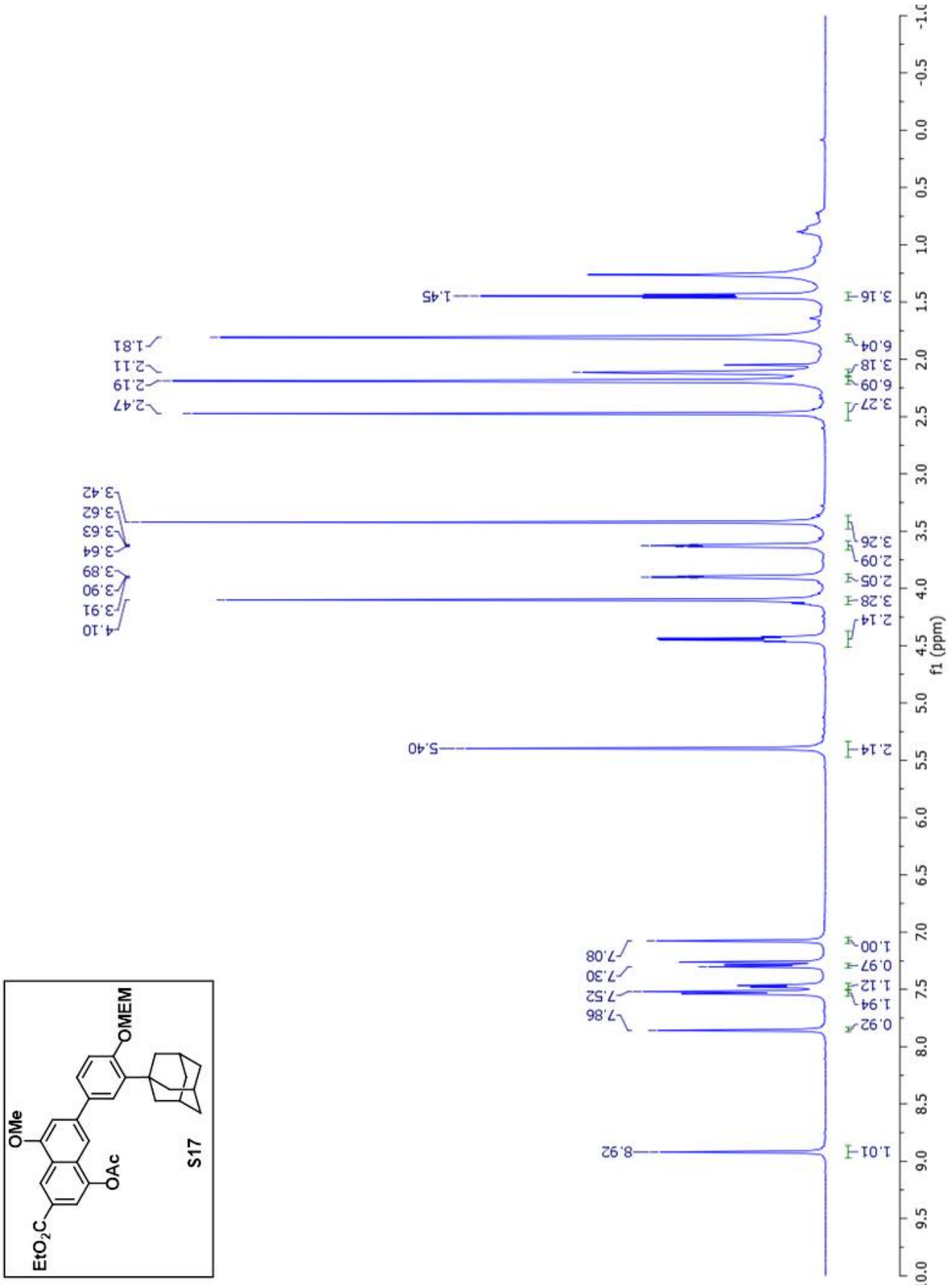

Supplementary Figure 50. ^{1}H NMR spectrum of **S17** recorded in $CDCl_3$ at 500 MHz.

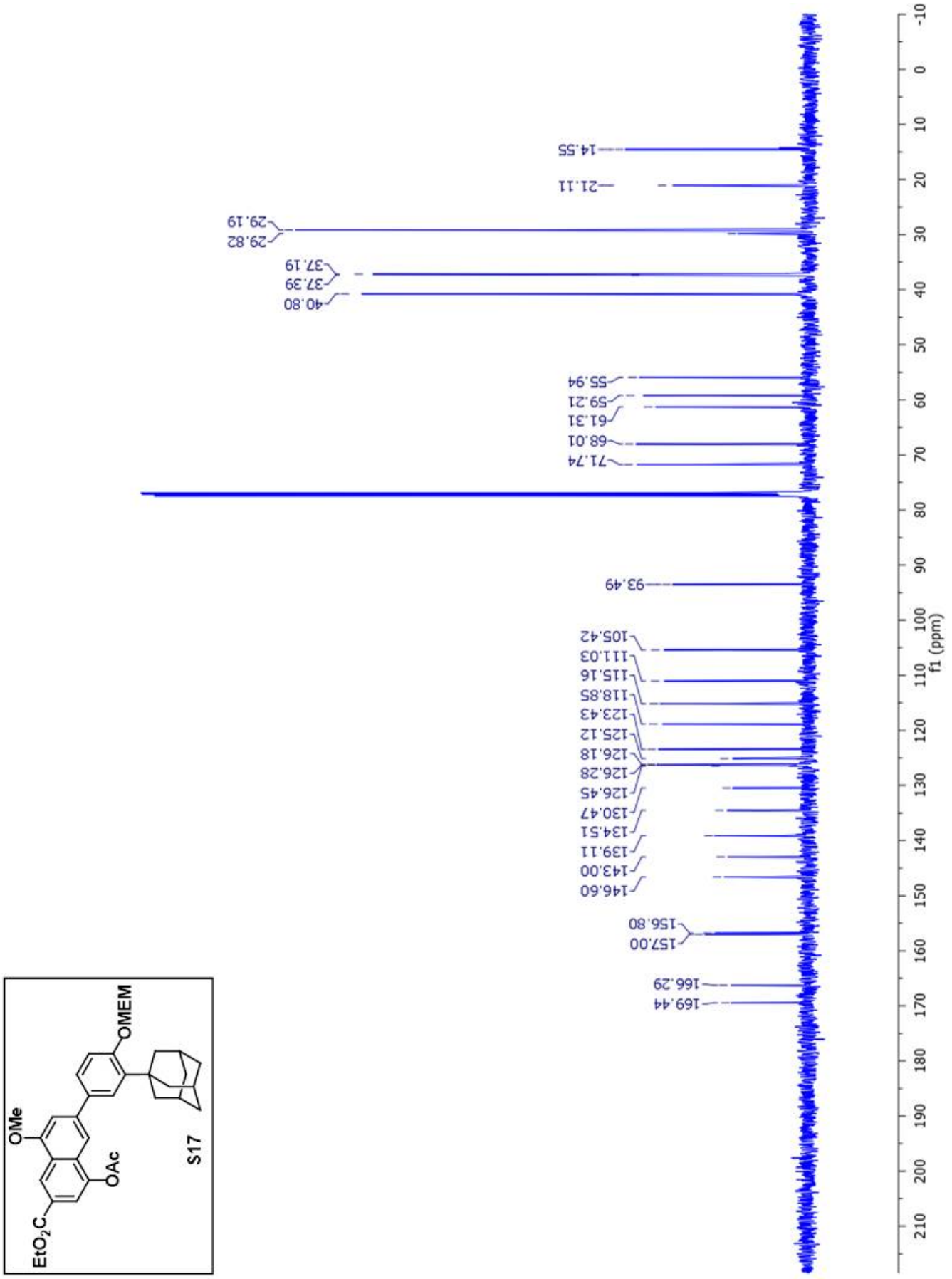

Supplementary Figure 51. ^{13}C NMR spectrum of **S17** recorded in $CDCl_3$ at 125 MHz.

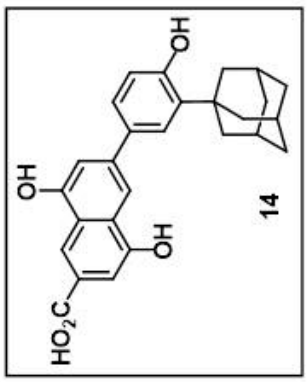

Supplementary Figure 52. ^{1}H NMR spectrum of **14** recorded in CD_3CN at 400 MHz.

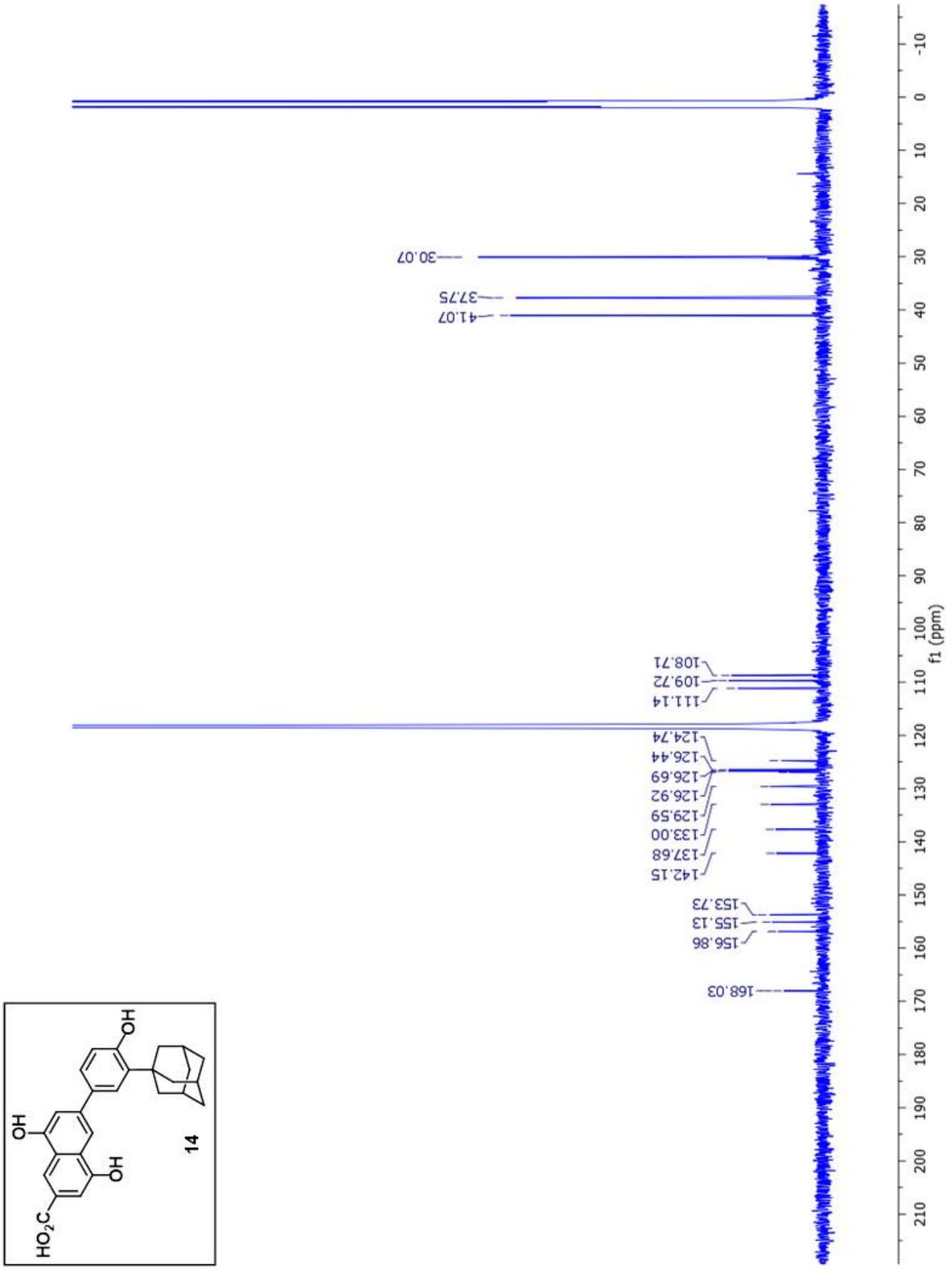

Supplementary Figure 53. ^{13}C NMR spectrum of **14** recorded in CD_3CN at 125 MHz.

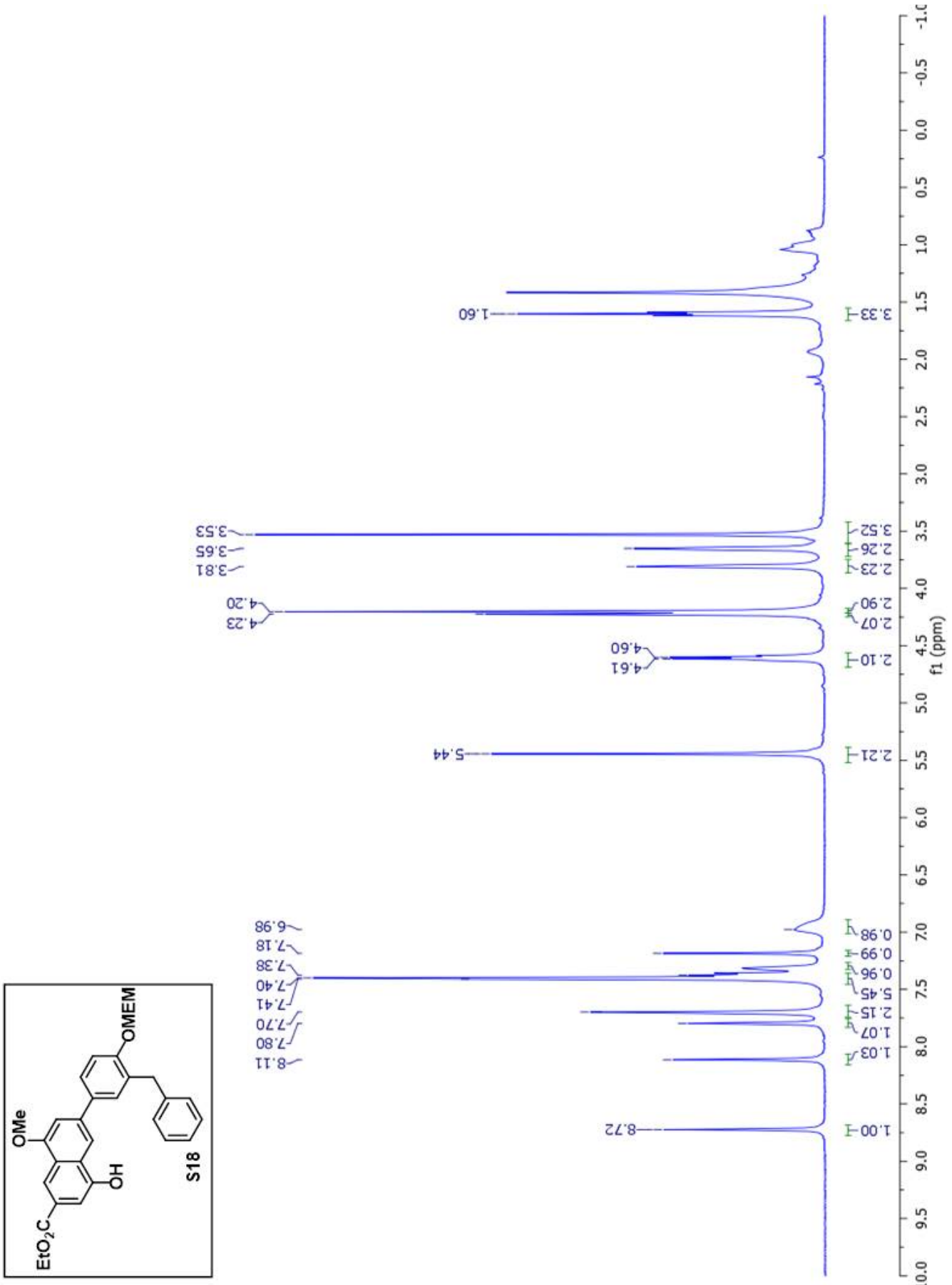

Supplementary Figure 54. ^{1}H NMR spectrum of **S18** recorded in $CDCl_3$ at 500 MHz.

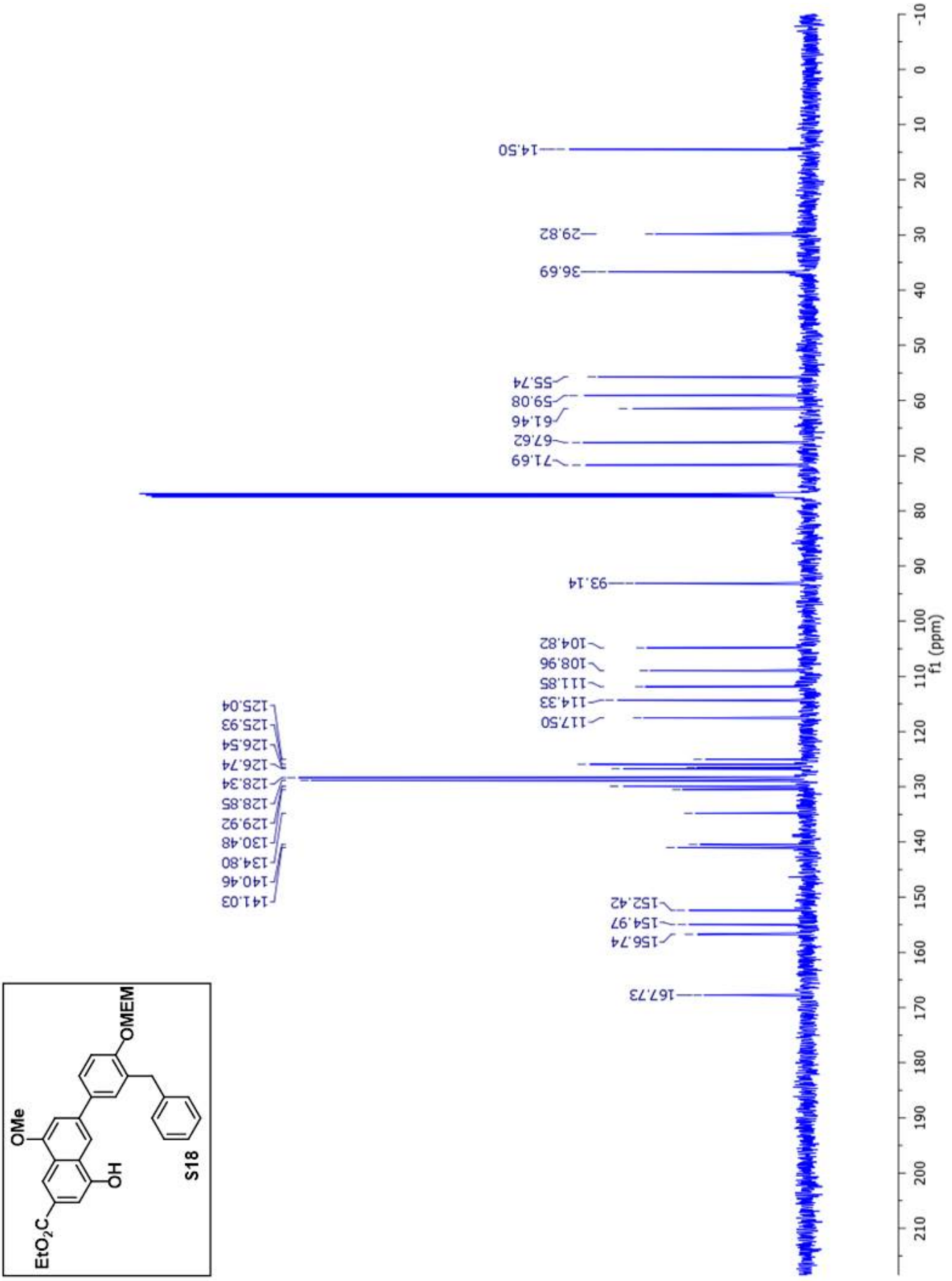

Supplementary Figure 55. ^{13}C NMR spectrum of **S18** recorded in $CDCl_3$ at 125 MHz.

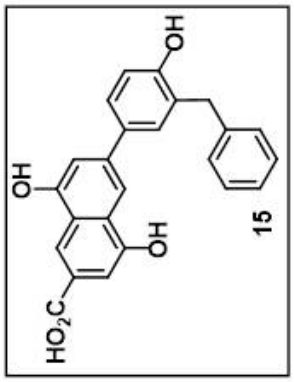

Supplementary Figure 56. ^{1}H NMR spectrum of **15** recorded in CD_3CN at 400 MHz.

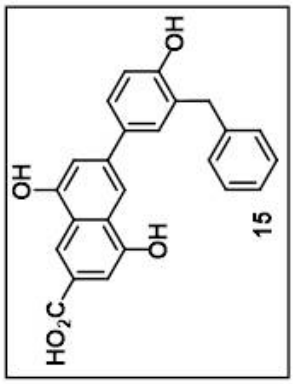

Supplementary Figure 57. ^{13}C NMR spectrum of **15** recorded in CD_3CN at 125 MHz.

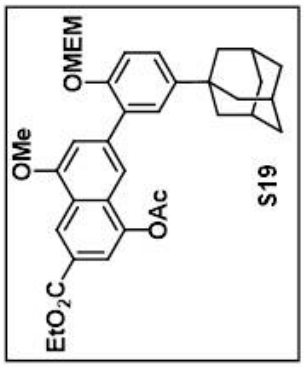

Supplementary Figure 58. ^{1}H NMR spectrum of **S19** recorded in $CDCl_3$ at 500 MHz.

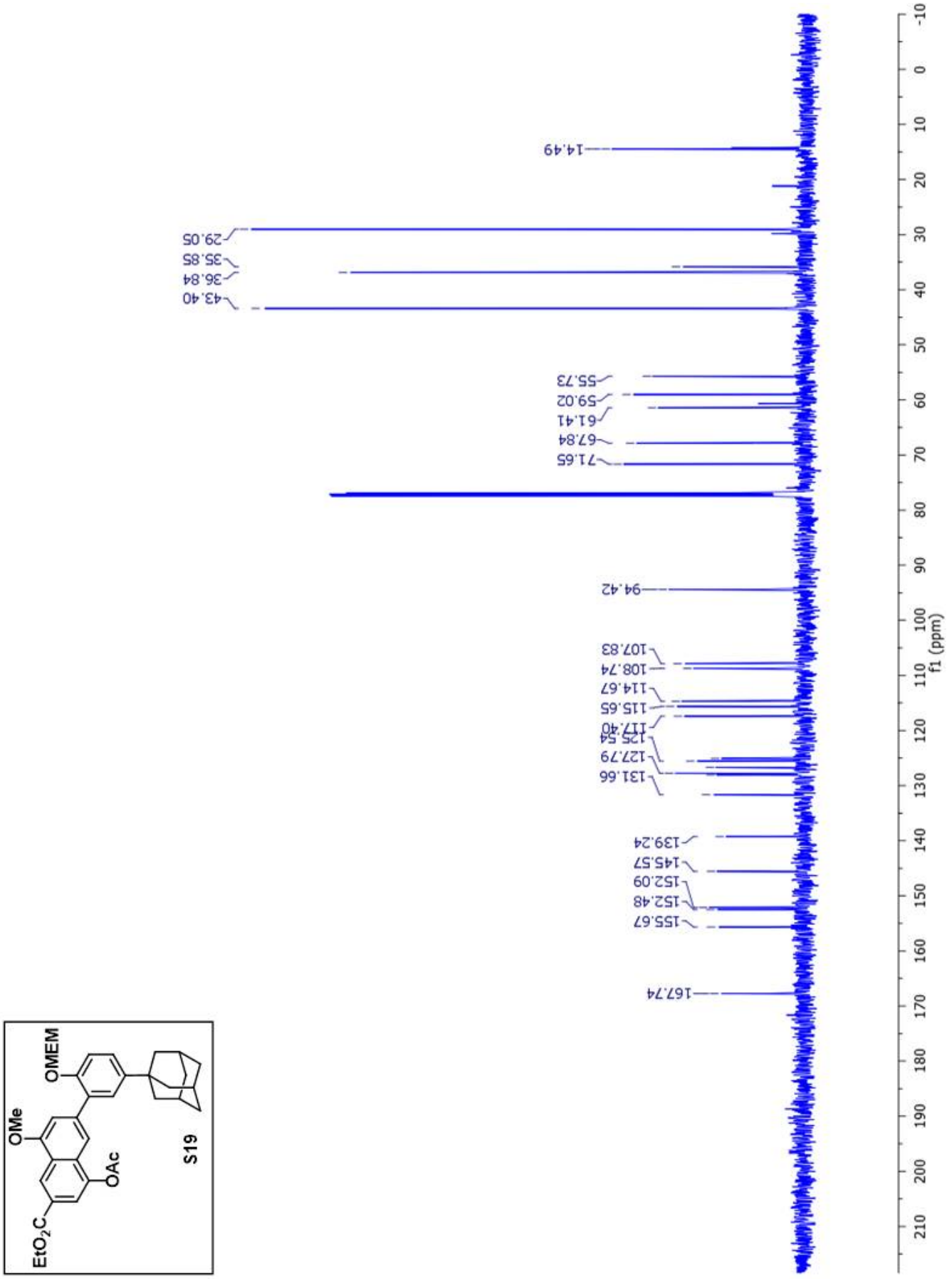

Supplementary Figure 59. ^{13}C NMR spectrum of **S19** recorded in $CDCl_3$ at 125 MHz.

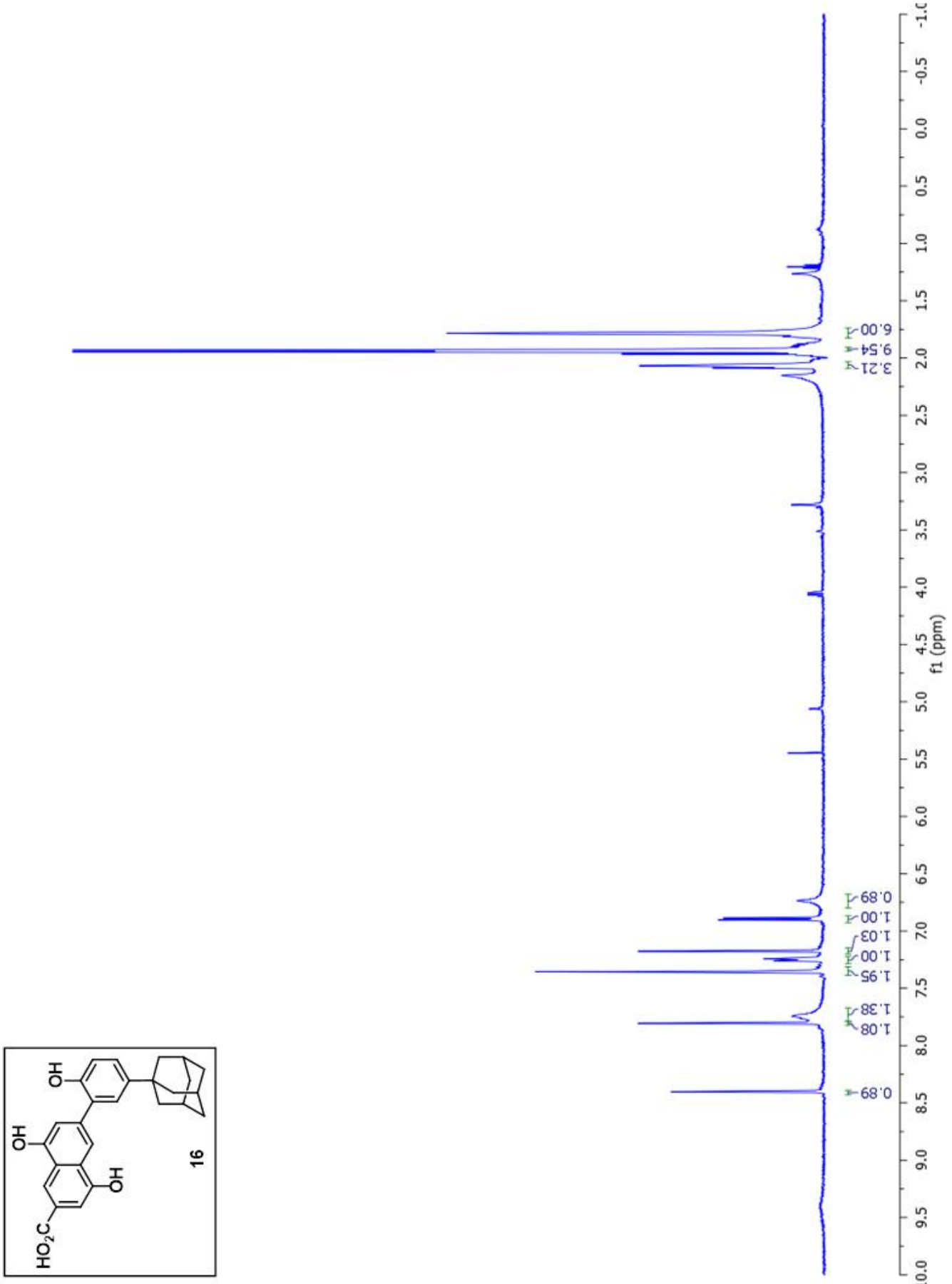

Supplementary Figure 60. ^{1}H NMR spectrum of **16** recorded in CD_3CN at 500 MHz.

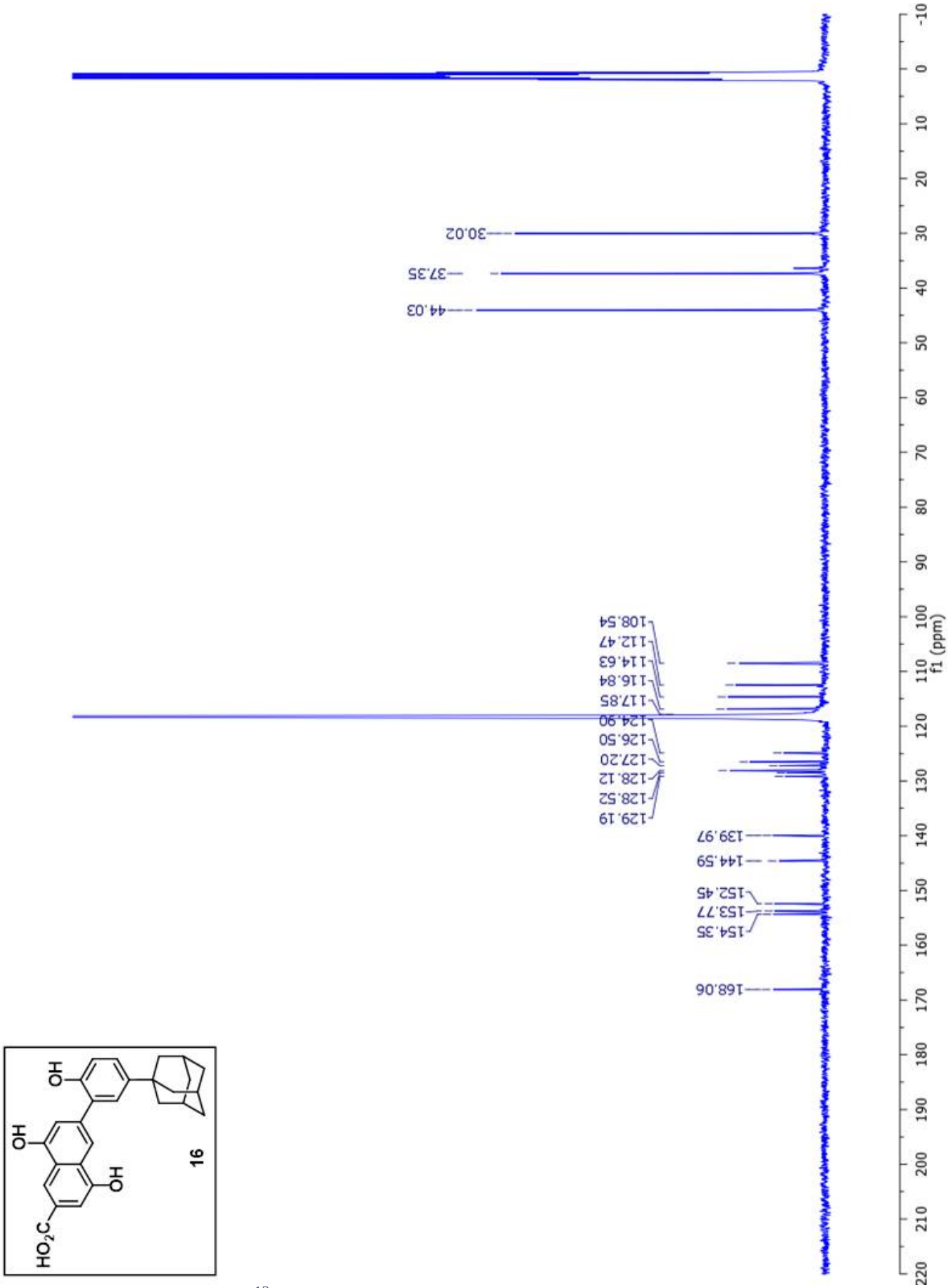

Supplementary Figure 61. ^{13}C NMR spectrum of **16** recorded in CD_3CN at 125 MHz.